Supporting Information

First Experimental Evidence for the Elusive Tetrahedral Cations $[EP_3]^+$ (E = S, Se, Te) in the Condensed Phase

Philippe Weis[a], David Christopher Röhner[a], Richard Prediger[a], Burkhard Butschke[a], Harald Scherer[a], Stefan Weber[b] and Ingo Krossing[a]*

[a] M. Sc. Philippe Weis, B.Sc. David Röhner, B.Sc. Richard Prediger, Dr. Burkhard Butschke, Dr. Harald Scherer and Prof. Dr. I. Krossing, Institut für Anorganische und Analytische Chemie and Freiburger Materialforschungszentrum (FMF), Universität Freiburg, Albertstr. 21, 79104 Freiburg, Germany.

[b] Prof. Dr. Stefan Weber Institut für Physikalische Chemie Universität Freiburg Albertstr. 21, 79104 Freiburg, Germany

* Correspondence to krossing@uni-freiburg.de.

Table of contents

1. General Information ... 1
2. Structure and Spectroscopic Characterization of all Novel ECl_3^+ Salts ... 4
3. Experimental Details ... 6
3.1. Experimental Section ... 6
3.2. Spectral Data of $ECl_3[WCA]$ ... 11
3.2.1. Spectral Data of $SeCl_3[Al(OR^F)_4]$ 1a ... 11
3.2.2. Spectral Data of $SeCl_3[F(Al(OR^F)_3)_2]$ 1b ... 15
3.2.3. Spectral Data of $SeCl_3[FAl(OR^F)_3]$ 1c ... 18
3.2.4. Spectral Data of $TeCl_3[Al(OR^F)_4]$ ... 21
3.2.5. Spectral Data of $TeCl_3[F(Al(OR^F)_3)_2]$ 2b ... 23
3.2.6. Spectral Data of $SCl_3[F(Al(OR^F)_3)_2]$ 3 ... 25
3.2.7. Complete Tables of the Vibrational Spectra of the $ECl_3[WCA]$ salts ... 27
3.3. Reactions with $Na[Nb(P_3)(ODipp)_3]$*3THF ... 30
3.4. Reactions with White Phosphorus ... 34
3.4.1. Solvent Screening ... 34
NMR spectra of the Reactions in different solvents ... 37
3.4.2. Anion screening ... 45
Typical Reactions of $ECl_3[WCA]$ with P_4 ... 51
3.4.3.1 Typical reaction with $SeCl_3[WCA]$ ($[WCA]^-$ = $[Al(OR^F)_4]^-$ and $[F(Al(OR^F)_3)_2]^-$) ... 51
3.4.3.2. Reaction on a bigger scale under optimized reaction conditions ... 55
3.4.3.3. Typical reaction with $TeCl_3[A]$ ($[A]^-$ = $[Al(OR^F)_4]^-$ and $[F(Al(OR^F)_3)_2]^-$) ... 59
3.4.3.4. Typical reaction with $SCl_3[F(Al(OR^F)_3)_2]$ ... 64
3.5. Other tested Reactions ... 67
4. Details to the Quantum Chemical Calculations ... 73
4.1. Calculated MO Diagrams ... 73
4.2. Aim Analyses and Laplacian of the Electron Density ... 73
4.3. Calculated NMR parameters ... 75
4.4. Summary of the ab initio Reaction Enthalpies and Free Reaction Energies ... 77
4.5. Summary of the Calculated FIAs ... 78
4.5. Calculated Structures ... 79
References ... 87

1. General Information

General conditions: All manipulations were performed by using standard grease free Schlenk or dry box techniques and an argon atmosphere. Reactions were carried out in two bulb-glass vessels incorporating a fine sintered glass G4 frit with two J. Young valves and a Teflon coated stirring bar if not mentioned otherwise. SO_2 and CD_2Cl_2, *o*-dfb and 1,2,3,4-tfb were dried with CaH_2 and distilled afterwards. Sulfur and P_4 were sublimed before use, $SeCl_4$, TlF, Cl_2 (2.8 N) and $TeCl_4$ were bought and used as received. $SeCl_3[F(Al(OR^F)_3)_2]$ (**1b**) was synthesized according to the literature.[1] $Ag[Al(OR^F)_4]$, $Ag[FAl(OR^F)_3]$, $Ag[F(Al(OR^F)_3)_2]$ and $TeCl_3[Al(OR^F)_4]$ (**2a**) were synthesized according to the literature.[2] $Tl[Al(OR^F)_4]$ was synthesized according to the literature procedure for $Tl[Al(O\mathit{hfip})_4]$ (-*hfip* = $C(H)(CF_3)_2$).[3] $Ag[Al(OR^F)_4]$ is commercially available at www.iolitec.de.

NMR Spectroscopy: NMR samples were prepared in 5 mm thick walled NMR tubes with J. Young valves. All spectra were recorded on a Bruker Avance DPX 200, a Bruker Avance III HD 300, a Bruker Avance II WB 400 or a Bruker Avance III HD 600 spectrometer in CD_2Cl_2, CH_2Cl_2, *o*-dfb, 1,2,3,4-tfb or SO_2 at room temperature. The spectra were calibrated relative to the residual solvent signals with respect to TMS.[4] All other nuclei were adjusted accordingly using the Ξ table.[5] Spectra recorded in SO_2 were referenced against the chemical shift of the $[Al(OR^F)_4]^-$ anion in CD_2Cl_2. All graphical representations were created using TopSpin (V3.2).

Vibrational Spectroscopy: FT-Raman spectra were recorded on a Bruker VERTEX 70 spectrometer equipped with a RAM II module (1064 nm Nd-YAG laser) with a cooled Ge detector. The samples were measured in flame-sealed glass pipettes in the range of 4000-50 cm^{-1} with a resolution of 3 cm^{-1} at room temperature. The data were processed with the Bruker OPUS 7.5 software package. All spectra are shown without further manipulations. ATR-IR spectra were recorded on a Bruker ALPHA with a QuickSnap Platinum ATR sampling module inside the glovebox. The data were processed with the Bruker OPUS 7.5 software package. Unless otherwise stated, the spectra were recorded in the range of 4000-400 cm^{-1} with a resolution of 2 cm^{-1} at RT. All IR and Raman spectra were normalized to 1 and intensities are given as follows, vw = very weak (< 0.2), w = weak (< 0.4), m = medium (< 0.6), s = strong (< 0.8), vs = very strong (≥ 0.8).

Mass spectra: Mass spectra were recorded on a Thermo-Fischer Scientific LTQ XL linear ion-trap mass-spectrometer equipped with an electrospray-ionization (ESI) source. Millimolar solutions of the sample dissolved in *o*-dfb were introduced through a fused-silica capillary to the ESI source via a syringe pump (ca. 5 µL min^{-1}). Nitrogen was used as a Sheath, Sweep, and Auxiliary Gas at flow rates adjusted to 5, 0, and 0, respectively (given in arbitrary units). The Source Voltage was set to 3.5 kV. The Tube Lens and the Capillary Voltage were adjusted to 200 V and 36 V, respectively. The Capillary Temperature

was 275 °C. The identity of the ions was confirmed by comparison of the accumulated spectra with the expected isotope patterns complemented by collision-induced dissociation (CID) experiments. In the CID experiments, helium served as the collision gas. The collision energy was adjusted between 0 and 30. Note that this value is denoted as Normalized Collision Energy and not further quantified in terms of a specific unit. We refrain therefore from a more detailed discussion of absolute collision energies.

Single-Crystal X-ray Diffraction: Single crystal X-ray crystallographic data were collected on a Bruker SMART APEXII Quazar with a CCD area detector and an INCOATEC 1st gen. Mo Microsource. The structures were solved with SHELXT[6] and refined by using SHELXL[7], ShelXle[8], and DSR.[9] Disorders were handled according to the SHELX-2018 manual with SIMU, RIGU, SADI, SAME and PART instructions. Graphics of the crystal structures were produced with OLEX 2.1.[10] A summary of all crystal structures is given in the ESI in Table S 1.

CCDC-1898379 (**1a**), 1860640 (**1b**) 1898390 (**1c**), 1898381 (**3**) and 1898381 ($Tl[Al(OR^F)_4]$) contain the supplementary crystallographic data for the compounds of this paper. These data can be obtained free of charge from the Cambridge Crystallographic Data Centre via www.ccdc.cam.ac.uk/data_request/cif.

Computational details: All computations were performed by using the program packages TURBOMOLE 7.1[11] and ORCA 4.1.[12] All investigated molecular structures were optimized using the functional B3-LYP[13] (with RI approximation[14]) and together with the basis set def-TZVPP.[15,16] A fine integration grid (m4) and the default SCF convergence criteria (10^{-6} a.u.) were used. The vibrational frequencies of all assessed species were computed with the implemented module AOFORCE[17] and checked for minima (no imaginary frequencies). COSMO[18] energies were optimized at BP86/def2-TZVPP level and with ε_r = 8.93 (CH_2Cl_2), 13.38 (*o*-dfb) and 16.3 (SO_2).[19] The MO diagrams and the NBO[20], PABOON[21] and AIM[22] charges were obtained at the B3-LYP/def2-TZVPP level. The structures were then further optimized at the (RIJ)MP2/def2-QZVPP level and used for further calculations. MP2[23] and CCSD(T)[16,24] calculations were performed using Turbomole. For the CBS extrapolation, the basis set aug-cc-pVnZ[25] was used for fluorine, aug-cc-pV(n+d)Z[26], was used for chlorine, sulfur and phosphorus, aug-cc-pVnZ-PP[27] for selenium and bromine and aug-cc-pwCVnZ-PP[28] was used for tellurium and iodine. The molecules were calculated with a frozen core approximation (F = 1; P, S, Cl = 5; Se, Br = 9; Te, I = 4).[29] The contour plots of the Laplacians of the electron density was done based on the MP2/def2-QZVPP calculations and the obtained wfn files were evaluated using MultiWFN3.6.[30] NMR shifts were calculated with ORCA 4.1 with the GIAO[31] method with (RIJ)B3-LYP(DKH2[32])/cc-pVQZ[33] single point calculations with a fully decontracted basis set and were based on the previously obtained geometries on the (RIJ)MP2/def2-QZVPP level.

Table S 1 Summary of the crystallographic details of **1a**, **1b**, **1c**, **3** and Tl[Al(OR^F)$_4$].

	1a	**1b**[1]	**1c**	**3**	**Tl[Al(OR^F)$_4$]**
CCDC Number	1898379	1860640	1898380	1898381	1898382
Empirical formula	$C_{96}Al_6Cl_{18}F_{216}O_{24}Se_6$	$C_{24}Al_2Cl_3F_{55}O_6Se$	$C_{12}AlCl_3F_{28}O_3Se$	$C_{24}Al_2Cl_3F_{55}O_6S$	$C_{16}AlF_{36}O_4Tl$
Formula weight	6914.23	1668.51	936.41	1621.55	1171.51
crystal size [mm^3]	0.05 × 0.04 × 0.02	0.40 × 0.20 × 0.20	0.25 × 0.15 × 0.05	0.50 × 0.40 × 0.20	0.18 × 0.16 × 0.10
crystal system	Monoclinic	Triclinic	Orthorhombic	Triclinic	Triclinic
space group	*P*1*n*1	$P\bar{1}$	*Pca*2$_1$	$P\bar{1}$	*P*1
a [Å]	16.5135(7)	13.016(1)	17.320(1)	12.9940(6)	9.6336(2)
b [Å]	31.955(2)	13.814(1)	14.869(1)	13.8170(7)	10.4764(3)
c [Å]	19.1323(9)	13.853(1)	10.2605(7)	13.8774(7)	16.8374(4)
α [°]	90	84.326(2)	90	84.132(2)	81.433(2)
β [°]	105.965(1)	81.663(2)	90	73.214(2)	73.486(1)
γ [°]	90	73.928(2)	90	81.787(2)	63.371(1)
V [nm^3]	9706.6(8)	2363.6(4)	2642.3(3)	2356.0(2)	1455.95(6)
Z	2 (Z' = 6)	2	4	2	2
ρ_{calcd} [g*cm^{-3}]	2.366	2.344	2.354	2.286	2.672
μ [mm^{-1}]	1.673	1.261	1.976	0.537	5.838
abs correction	Multi-scan	Multi-scan	Multi-scan	Multi-scan	Multi-scan
F(000)	6600	1596	1284	1560	1092
index range	-21 ≤ h ≤ 21, -40 ≤ k ≤ 40, -24 ≤ l ≤ 23	-17 ≤ h ≤ 17, -18 ≤ k ≤ 18, -18 ≤ l ≤ 18	-25 ≤ h ≤ 22, -19 ≤ k ≤ 19, -14 ≤ l ≤ 13	-18 ≤ h ≤ 20, -20 ≤ k ≤ 21, 0 ≤ l ≤ 20	-14 ≤ h ≤ 13, -15 ≤ k ≤ 14, -23 ≤ l ≤ 20
max 2ϑ [°]	54.168	58.332	61.982	67.914	64.512
T [K]	100(2)	100(2)	100(2)	100(2)	100(2)
diffractometer type	Bruker Smart Apex II Quazar	Bruker Smart Apex II	Bruker Smart Apex II Quazar	Bruker Smart Apex II Quazar	Bruker Smart Apex II Quazar
Radiation	MoKα (λ = 0.71073)	MoKα (λ = 0.71073)	MoKα (λ = 0.71073)	MoKα (λ = 0.71073)	MoKα (λ = 0.71073)
Reflections collected	230879	78160	62818	23976	23627
unique reflns [I > 2σ]	40927	12672	7252	15040	12615
data/restraints/parameter	40927/95750/3461	12672/7840/914	7252/1/434	15040/16012/1172	12615/12837/1155
GOOF	1.006	1.053	1.054	1.078	1.028
final R$_1$ [I > 2σ]	0.0435	0.0390	0.0275	0.0644	0.0305
final wR$_2$ [I > 2σ]	0.1051	0.1076	0.0660	19.05	0.0725
largest residual peak [e Å^{-3}]	1.86	1.15	0.69	1.12	1.95
largest residual hole [e Å^{-3}]	-0.59	-0.68	-0.34	-0.79	-1.66

2. Structure and Spectroscopic Characterization of all Novel ECl_3^+ Salts

The structures of several of these salts could be determined (Figure S 1). All structures contain the desired $[ECl_3]^+$ cation and the corresponding anion. It is notable that **1a** crystallizes in a commensurate superstructure showing six crystallographically independent cations and anions in the asymmetric unit. The bigger anion $[F(Al(OR^F)_3)_2]^-$ did not pose this problem in **1b** but has shown some disorder in the cation and the anion. These problems arise because of the weakly coordinating nature of the anions.[34] The basic $[FAl(OR^F)_3]^-$ anion was able to circumvent these problems by coordinating weakly to the $[SeCl_3]^+$ cation and thus eliminating disorder in the structure of **1c**. The determined crystal structure of $SCl_3[F(Al(OR^F)_3)_2]$ adopts the same structure type than **1b** and shows only slight differences in the lattice parameters and a small fraction of disorder in the cation.

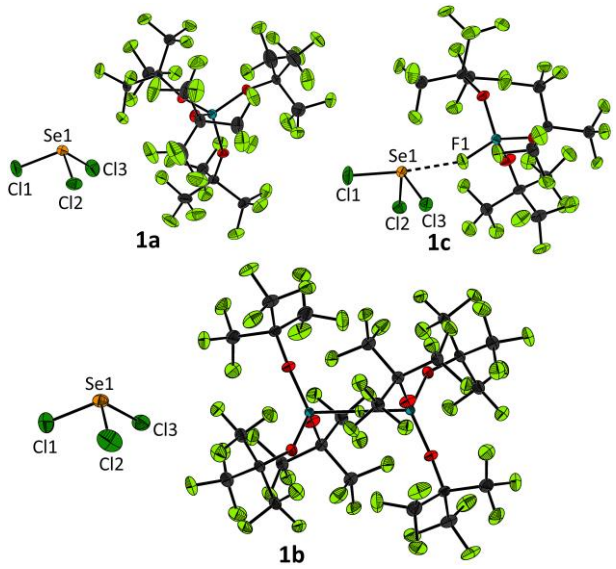

Figure S 1 View of the molecular structures of **1a**, **1b**, **1c** at 100 K. All thermal ellipsoids are shown at 50 % probability. As 3 is isostructural to **1b**, only the structure of **1b** is shown. Selected bond lengths [pm] and angles [°]: For **1a**: $d(Se–Cl)_{range}$ 207.8(2) – 210.3(2), $d(Se–Cl)_{average}$ 209.0; ∡(Cl–Se–Cl)$_{range}$ 99.7(1) – 101.8(1), ∡(Cl–Se–Cl)$_{average}$ 100.9.* For **1b**: Se1–Cl1 209.1(1), Se1–Cl2 208.2(1), Se1–Cl3 208.2(1); Cl1–Se1–Cl2 100.9(1), Cl2–Se1–Cl3 101.5(1), Cl1–Se1–Cl3 100.3(1). For **1c**: Se1–Cl1 211.6(1), Se1–Cl2 209.2(1), Se1–Cl3 209.7(1), Se1–F1 240.3(2); Cl1–Se1–Cl2 99.0(1), Cl2–Se1–Cl3 100.7(1), Cl1–Se1–Cl3 99.0(1). For **3**†: S1–Cl1 195.3(1), S1–Cl2 195.7(1), S1–Cl3 194.6(1); Cl1–S1–Cl1 103.0(1), Cl2–S1–Cl3 104.1(1), Cl1–S1–Cl3 103.4(1).

The bond lengths and angles of the $[ECl_3]^+$ cations in the crystal structures correspond to the calculated structures and the known crystal structures of other $ECl_3[A]$ salts. The only notable difference is in **1c**

* Due to the commensurate superstructure of **1a** six slightly different $[SeCl_3]^+$ cations are present in the asymmetric unit. Hence, the given d(Se–Cl) and ∡(Cl–Se–Cl) are the ranges and the average value.

† The cation in **3** is disordered over two positions. The given bond lengths are of the cation with the highest occupancy of 93 %.

where the Se1–Cl1 bond is elongated due to the coordination of the terminal fluorine atom of the $[FAl(OR^F)_3]^-$ anion to the $[SeCl_3]^+$ cation, showing structural changes towards the seesaw structure of gaseous $SeCl_4$.

The vibrational spectra of all $ECl_3[WCA]$ salts (given in chapter 3.2) are accordance with the findings from the scXRD data, due to the weakly coordinating character of the $[Al(OR^F)_4]^-$ and $[F(Al(OR^F)_3)_2]^-$ anions, the vibrational spectra of **1a**, **1b**, **2a**, **2b** and **3** are in accordance with known spectra of the hexafluoroantimonate salts with slight shifts towards the expected gas phase spectra.[2,35]

Table S 2 Comparison of the Raman and IR bands of the $[ECl_3]^+$ cations in powdered samples. Full spectra and tables containing the anion bands are given below in subchapter 3.8.

1a Raman	1a IR	1b Raman	1b IR	1c Raman	1c IR	2b Raman	2b IR	3 Raman	3 IR	Assignment
167 (vs)	—	162 (vs)	—	173 (m)	—	141 (vs)	—	206 (vs)	—	$\delta_{asy.}(ECl_3)$ (E)
206 (m)	—	206 (w)	—	207 (w)	—	168 (m)	—	279 (m)	—	$\delta_{sy.}(ECl_3)$ (A_1)
430 (sh)	428 (m)	434 (sh)	429 (s)	418 (sh)	416 (w)	410 (m)	406 (m)	548 (w)	546 (w)	$\nu_{asy.}(ECl_3)$ (E)
443 (vs)	—	444 (s)	—	437 (vs)	—	420 (vs)	419 (m)	524 (m)	523 (vw)	$\nu_{sy.}(ECl_3)$ (E)

w: weak, m: medium, s: strong, sh: shoulder, v: very. ν = stretching mode, δ = bending mode. sy. corresponds to the non-degenerate A_1 bands and asy. corresponds to the degenerate E bands.

The coordinating nature of the basic $[FAl(OR^F)_3]^-$ anion is also reflected in the vibrational spectra of **1c** which deviates from the vibrations of **1a** and **1b** due to the coordination of the anion, which is clearly shown by the stretching modes of $[SeCl_3]^+$ that are slightly redshifted compared to the non-coordinated $[SeCl_3]^+$ cations in **1a** and **1b**. The Raman spectra of **2b** show, that this material is always obtained with some residual $TeCl_4$ as it was also the case in the previously described synthesis of **2a**.[2]

The NMR spectra of all $ECl_3[WCA]$ salts (given in chapter 3.2) only show the typical resonances of the intact anions as well as the ^{77}Se resonance of the $[SeCl_3]^+$ cation at 1393.1 ppm (**1a**), 1383.9 ppm (**1b**), and 1406.7 ppm (**1c**), respectively. The ^{125}Te chemical shift of the $[TeCl_3]^+$ cation of **2a** and **2b** in CD_2Cl_2 at room temperature is roughly 1970 ppm. Again, the basic $[FAl(OR^F)_3]^-$ is not innocent towards the $[SeCl_3]^+$ cation also in solution. The ^{19}F chemical shift of the terminal fluorine atom of the $[FAl(OR^F)_3]^-$ anion is strongly shifted to −145.0 ppm in **1c**, instead of the usually observed shift around−185 to −200 ppm ppm for the free anion. This is in accordance with observations for $NO[FAl(OR^F)_3]$ and suggests a coordination of the $[SeCl_3]^+$ cation to the anion even in solution.[34]

3. Experimental Details

3.1. Experimental Section

Preparation of 1a: $Ag[Al(OR^F)_4]$ (3.00 g, 2.79 mmol, 1.00 eq.) and $SeCl_4$ (616 mg, 2.79 mmol, 1.00 eq.) were weighed into one bulb of a two bulb vessel separated by a glass frit. CH_2Cl_2 (12 ml) was condensed onto the solids and the mixture was stirred for 20 h at room temperature which resulted in a bright yellow solution over a precipitate of AgCl. The solution was then filtered through the glass frit and the solvent was removed under vacuum. **1a** was obtained as a fine yellow powder (3.12 g, 2.70 mmol, 97 %). Crystals suitable for scXRD were obtained by dissolving the obtained powder in little CH_2Cl_2, followed by slow cooling to 6 °C until big yellow blocks formed. **NMR:** ^{19}F-NMR (376.54 MHz, CD_2Cl_2, RT) δ = −75.7 (s, 36 F $[Al(OC(C\mathbf{F}_3)_3)_4]^-$) ppm. ^{27}Al-NMR (104.27 MHz, CD_2Cl_2, RT) δ = 34.6 (s, 1 Al, $[\mathbf{Al}(OC(CF_3)_3)_4]^-$) ppm. ^{77}Se-NMR (76.32 MHz, CD_2Cl_2, RT) δ = 1393.1 (s., 1 Se, $[\mathbf{Se}Cl_3]^+$) ppm. **ATR-IR (Diamond):** $\tilde{\nu}$ [cm^{-1}] = 429 (s), 442 (m), 536 (m), 560 (w), 571 (vw), 725 (vs), 755 (vw), 832 (w), 873 (vw), 965 (vs), 1020 (vw), 1170 (s), 1207 (vs), 1240 (s), 1264 (m), 1296 (w), 1352 (vw). **FT-Raman:** $\tilde{\nu}$ [cm^{-1}] = 168 (vs), 206 (w), 234 (vw), 289 (vw), 323 (w), 330 (vw), 354 (vw), 368 (vw), 407 (vw), 434 (w), 444 (s), 538 (vw), 562 (vw), 572 (vw), 745 (w), 799 (w), 1002 (vw), 1246 (vw), 1282 (vw), 1291 (vw), 1310 (vw).

Preparation of 1c: $Ag[FAl(OR^F)_3]$ (461 mg, 0.54 mmol, 1 eq.) and $SeCl_4$ (119 mg, 0.54 mmol, 1 eq.) were weighed into one bulb of a two bulb vessel separated by a glass frit. CH_2Cl_2 (5 ml) was condensed onto the solids and the mixture was stirred for 20 h at room temperature which resulted in a bright yellow solution over a precipitate of AgCl. The solution was then filtered through the glass frit and the solvent was removed under vacuum. **1c** was obtained as a fine yellow powder (358 mg, 0.38 mmol, 72 %). Crystals suitable for scXRD were obtained by dissolving the obtained powder in little CH_2Cl_2, followed by slow cooling to 6 °C until big yellow blocks formed. **NMR**: ^{19}F-NMR (376.5 MHz, CH_2Cl_2, RT): δ = −75.8 (d, 27 F, $[FAl(OC(C\mathbf{F}_3)_3)_3]^-$, ^5J(F; F) = 1.6 Hz), −144.9 (br, 1 F, $[\mathbf{F}Al(OC(CF_3)_3)_3]^-$) ppm. ^{27}Al-NMR (104.3 MHz, CH_2Cl_2, RT): δ = 38.8 (br, 1 Al, $[F\mathbf{Al}(OC(CF_3)_3)_3]^-$) ppm. ^{77}Se-NMR (76.3 MHz, CH_2Cl_2, RT) δ = 1406.7 (s, $[\mathbf{Se}Cl_3]^+$) ppm. **ATR-IR (Diamond):** $\tilde{\nu}$ [cm^{-1}] = 416 (w), 447 (w), 536 (w), 565 (vw), 680 (w), 725 (vs), 752 (vw), 811 (vw), 842 (vw), 866 (vw), 965 (vs), 1176 (m), 1209 (vs), 1237 (s), 1262 (m), 1297 (vw), 1352 (vw). **FT-Raman:** $\tilde{\nu}$ [cm^{-1}] = 173 (s), 207 (w), 256 (vw), 287 (w), 306 (vw), 324 (w), 367 (vw), 418 (sh), 437 (vs), 480 (vw), 538 (vw), 570 (vw), 683 (vw), 706 (w), 725 (vw), 753 (m), 811 (w), 978 (vw),

1247 (vw), 1275 (vw), 1305 (vw), 1362 (vw).

Preparation of 2b: $Ag[F(Al(OR^F)_3)_2]$ (250 mg, 0.16 mmol, 1 eq.) and $TeCl_4$ (42 mg, 0.16 mmol, 1.00 eq.) were weighed into one bulb of a two bulb vessel separated by a glass frit. SO_2 (4 ml) was condensed onto the solids and the mixture was stirred for 20 h at room temperature which resulted in a colorless solution over a precipitate of AgCl. The solution was then filtered through the glass frit and the solvent was removed under vacuum. **2b** was obtained as a fine off white powder (193 mg, 0.11 mmol, 71 %). Crystals suitable for scXRD of this compound could not be obtained, as only polycrystalline material was obtained upon slow cooling of a concentrated solution to 6 °C. **NMR**: ^{19}F-NMR (282.5 MHz, CD_2Cl_2, RT): δ = −75.8 (d, 54 F, $[F(Al(OC(C\mathbf{F}_3)_3)_3)_2]^-$, ^5J(F; F) = 0.5 Hz), −184.9 (br, 1 F, $[\mathbf{F}(Al(OC(CF_3)_3)_3)_2]^-$) ppm. ^{27}Al-NMR (78.2 MHz, CD_2Cl_2, RT): δ = 34.5 (br, 1 Al, $[F(\mathbf{Al}(OC(CF_3)_3)_3)_2]^-$) ppm. ^{125}Te-NMR (94.7 MHz, CD_2Cl_2, RT) δ = 1952.4 (s, $[\mathbf{Te}Cl_3]^+$) ppm. **ATR-IR (Diamond):** $\tilde{\nu}$ [cm^{-1}] = 406 (w), 419 (vw), 449 (m), 536 (m), 569 (w), 642 (w), 725 (vs), 760 (vw), 813 (vw), 866 (w), 965 (vs), 1170 (sh), 1211 (vs), 1239 (s), 1264 (m), 1300 (w), 1355 (vw).**FT-Raman:** $\tilde{\nu}$ [cm^{-1}] = 94 (w), 141 (vs), 158 (w), 168 (m), 236 (w), 290 (w), 327 (m), 334 (s), 343 (s), 363 (w), 375 (vs), 410 (m), 420 (vs), 539 (w), 548 (vw), 568 (w), 573 (w), 753 (s), 817 (w), 886 (vw), 981 (vw), 1140 (vw), 1165 (vw), 1252 (vw), 1264 (vw), 1278 (vw), 1294 (vw), 1311 (vw).

First Preparation of 3 by Decomposition: $Ag[Al(OR^F)_4]$ (250 mg, 0.23 mmol, 1 eq.) and sulfur (8 mg, 0.23 mmol, 1.0 eq.) were weighed into one bulb of a two bulb vessel separated by a glass frit. CH_2Cl_2 (5 ml) was condensed onto the solids and the mixture was stirred for 1 h at room temperature until all the sulfur was dissolved. An atmosphere of chlorine gas (approx. 0.2 g, which corresponds to approx. 25 eq.) was condensed onto the solution. Immediately, a white precipitate of AgCl forms. After stirring for 2 h, the solution was then filtered through the glass frit and the solvent was removed under vacuum until there was only a small fraction of the solvent left. The reaction mixture was kept at room temperature for 5 days until small amounts of **3** suitable for scXRD crystallized. Recorded Raman spectra of the obtained material have only shown fluorescence.

Direct, high-yield Preparation of 3: $Ag[F(Al(OR^F)_3)_2]$ (1000 mg, 0.63 mmol, 1 eq.) and sulfur (20 mg, 0.63 mmol, 1.00 eq.) were weighed into one bulb of a two bulb vessel separated by a glass frit. CH_2Cl_2 (10 ml) was condensed onto the solids and the mixture was stirred for 1 h at room temperature until all the sulfur was dissolved. An atmosphere of chlorine gas (approx. 0.5 g which corresponds to approx. 22 eq.) was condensed onto the solution. Immediately, a green color appears which disappears within

seconds upon stirring and a white precipitate of AgCl forms. After stirring for 2 h, the solution was then filtered through the glass frit and the solvent was removed under vacuum. **3** was obtained as a fine colorless powder (952 mg, 0.59 mmol, 93 %). Crystals suitable for SC-XRD were obtained by dissolving the obtained powder in little CH_2Cl_2, followed by slow cooling to 6 °C until big colorless blocks formed. **NMR**: ^{19}F-NMR (282.5 MHz, CH_2Cl_2, RT): δ = −75.8 (d, 54 F, $[F(Al(OC(C\mathbf{F}_3)_3)_3)_2]^-$, ^5J(F, F) = 0.5 Hz), −184.9 (br, 1 F, $[\mathbf{F}(Al(OC(CF_3)_3)_3)_2]^-$) ppm. ^{27}Al-NMR (78.2 MHz, CH_2Cl_2, RT): δ = 32.8 (br, 1 Al, $[F(\mathbf{Al}(OC(CF_3)_3)_3)_2]^-$) ppm. **ATR-IR (Diamond):** $\tilde{\nu}$ [cm^{-1}] = 449 (m), 523 (vw), 537 (m), 546 (w), 569 (w), 642 (w), 726 (vs), 760 (vw), 812 (vw), 865 (w), 969 (vs), 1070 (vw), 1184 (s), 1210 (vs), 1237 (s), 1273 (m), 1300 (w), 1355 (vw). **FT-Raman:** $\tilde{\nu}$ [cm^{-1}] = 96 (vw), 122 (vw), 206 (vs), 233 (vw), 279 (m), 290 (vw), 326 (m), 368 (vw), 524 (m), 539 (w), 548 (w), 572 (w), 705 (vw), 753 (vs), 818 (w), 974 (vw), 983 (vw), 1136 (vw), 1182 (vw), 1231 (vw), 1261 (vw), 1268 (vw), 1386 (vw), 1312 (vw).

Reactions with Na[Nb(ODipp)$_3$(P$_3$)]*3THF

1a (23 mg, 0.02 mmol, 1.0 eq.) and Na[Nb(P$_3$)(ODipp)$_3$]*3THF (19 mg, 0.02 mmol, 1.0 eq.) were weighed in an NMR tube and a solvent (CD_2Cl_2, 1,2,3,4-tfb, *o*-dfb) (0.7 mL) was condensed onto the solids at −196 °C. The NMR tube was then flame sealed and kept at −40 °C, resulting in a deep red solution over little dark precipitate. The tube was kept at this temperature for 20 h during which the tube was shaken vigorously 5 times. NMR spectra of the sample were measured at −30 °C. **NMR**: ^{31}P-NMR (162.0 MHz, CD_2Cl_2, 243 K): δ = −228.1 (s, 3 P, $[Nb(P_3)(ODipp)_3]^-$), −518.1 (br. 4 P, P$_4$) ppm. ^{31}P-NMR (162.0 MHz, 1,2,3,4-tfb, 243 K): δ = −228.2 (s, 3 P, $[Nb(P_3)(ODipp)_3]^-$), −523.3 (br. 4 P, P$_4$) ppm. ^{31}P-NMR (162.0 MHz, *o*-dfb, 243 K): δ = −227.9 (s, 3 P, $[Nb(P_3)(ODipp)_3]^-$), −523.2 (br. 4 P, P$_4$) ppm.

Reactions with P$_4$

Synthesis of 4: 1a (150 mg, 0.13 mmol, 1.0 eq.) was weighed in a Schlenk tube and a previously prepared solution of P$_4$ (16 mg, 0.13, 1.6 eq.) in CD_2Cl_2 (1.5 mL) was added and the resulting mixture immediately took a reddish brown color. The mixture was stirred for 1 h at room temperature Afterwards, the volume of the solution was reduced to 0.7 mL *in vacuo* and transferred into an NMR tube and flame sealed. **NMR:** ^{19}F-NMR (282.5 MHz, CD_2Cl_2, RT): δ = −69.3 (m, 6 F, $(\mathbf{F}_3C)_2C(O)CF_2$), −74.6 (s, 9 F, $HOC(C\mathbf{F}_3)_3$), −75.7 (s, 36 F, $[Al(OC(C\mathbf{F}_3)_3)_4]^-$), −75.8 (s, 54 F, $[F(Al(OC(C\mathbf{F}_3)_3)_3)_2]^-$), −108.4 (m, 6 F, $(F_3C)_2C(O)C\mathbf{F}_2$), −184.9 (br. 1 F, $[\mathbf{F}(Al(OC(CF_3)_3)_3)_2]^-$) ppm. ^{27}Al-NMR (78.2 MHz, CD_2Cl_2, RT) δ = 34.6 (s, 1 Al, $[\mathbf{Al}(OC(CF_3)_3)_4]^-$) ppm. ^{31}P-NMR (81.0 MHz, CD_2Cl_2, RT): δ = 219.4 (br., 1 P, $\mathbf{P}Cl_3$), 152.2 (dt, 2 P, $[P_2\mathbf{P}_{\mathbf{B2}}PCl_2]^+$, $^1J(^{31}P_B, ^{31}P_C)$ = 341 Hz, $^1J(^{31}P_A, ^{31}P_B)$ = 143 Hz), 104.5 (m, 1 P, $[\mathbf{P}_\mathbf{A}P_2Se_4]^+$), 56.0 (tt, 1 P, $[P_4\mathbf{P}_\mathbf{C}Cl_2]^+$, $^1J(^{31}P_B, ^{31}P_C)$ = 341 Hz, $^2J(^{31}P_A, ^{31}P_C)$ = 27 Hz), 38.2 (m, 2 P, $[P\mathbf{P}_{\mathbf{B}2}Se_4]^+$), −271.1 (td, 2 P,

$[\mathbf{P_{A2}}P_3Cl_2]^+$, $^1J(^{31}P_A, ^{31}P_B)$ = 143 Hz, $^2J(^{31}P_A, ^{31}P_C)$ = 27 Hz), −360.7 (s, 3 P, $[\mathbf{P}_3Se]^+$, $^1J(P, ^{77}Se)$ = 58 Hz), −518.7 (s, 4 P, $\mathbf{P}_4$) ppm. ^{77}Se-NMR (114.5 MHz, CD_2Cl_2, RT): δ = 894 (q, 1 Se, $[P_3\mathbf{Se}]^+$, $^1J(P, ^{77}Se)$ = 58 Hz) ppm.

Synthesis of 5: 2a (100 mg, 0.08 mmol, 1 eq.) was weighed in a Schlenk tube and a previously prepared solution of P_4 (17 mg, 0.13, 1.6 eq.) in CD_2Cl_2 (0.7 mL) was added and the resulting mixture immediately took a dark brownish color. The mixture was stirred for 1 h at room temperature Afterwards, the solution was transferred into an NMR tube and flame sealed. **NMR:** ^{19}F-NMR (356.4 MHz, CD_2Cl_2, RT): δ = −75.6 (s, 36 F, $[Al(OC(C\mathbf{F}_3)_3)_4]^-$) ppm. ^{27}Al-NMR (104.3 MHz, CD_2Cl_2, RT): δ = 34.6 (s, 1 Al, $[\mathbf{Al}(OC(CF_3)_3)_4]^-$) ppm. ^{31}P-NMR (162.0 MHz, CD_2Cl_2, RT): δ = 219.5 (br., 1 P, $\mathbf{P}Cl_3$), 152.3 (dt, 2 P, $[P_2\mathbf{P_{B2}}PCl_2]^+$, $^1J(^{31}P_B, ^{31}P_C)$ = 340 Hz, $^1J(^{31}P_A, ^{31}P_B)$ = 143 Hz), 56.2 (tt, 1 P, $[P_4\mathbf{P_C}Cl_2]^+$, $^1J(^{31}P_B, ^{31}P_C)$ = 340 Hz, $^2J(^{31}P_A, ^{31}P_C)$ = 27 Hz), 9.8 (s, 5 P, unknown P_5Te_3 cluster, $J(^{31}P, ^{125}Te)$ = 62 Hz), −271.4 (td, 2 P, $[\mathbf{P_{A2}}P_3Cl_2]^+$, $^1J(^{31}P_A, ^{31}P_B)$ = 143 Hz, $^2J(^{31}P_A, ^{31}P_C)$ = 27 Hz), −342.9 (s, 3 P, $[\mathbf{P}_3Te]^+$, $^1J(P, ^{125}Te)$ = 145 Hz, $^1J(P, ^{123}Te)$ = 120 Hz), −501.0 (s, 4 P, $\mathbf{P}_4$) ppm. ^{125}Te-NMR (162.0 MHz, CD_2Cl_2, RT): δ = 67.4 (sex., 4 Te, unknown P_5Te_3 cluster, $J(^{31}P, ^{125}Te)$ = 62 Hz), −2212.0 (q, 1 Te, $[P_3Te]^+$, $^1J(P, ^{123}Te)$ = 120 Hz) ppm.

Synthesis of 6: 3 (50 mg, 0.03 mmol, 1 eq.) was weighed in a Schlenk tube and a previously prepared solution of P_4 (6 mg, 0.05, 1.6 eq.) in CD_2Cl_2 (0.7 mL) was added and the resulting mixture was stirred for 1 h at room temperature during which the pale yellow solution turned into a bright yellow. Afterwards, the solution was transferred into an NMR tube and flame sealed. **NMR:** ^{19}F-NMR (282.5 MHz, CD_2Cl_2, RT): δ = −75.8 (s, 54 F, $[F(Al(OC(C\mathbf{F}_3)_3)_3)_2]^-$), −184.9 (br., 1 F, $[\mathbf{F}(Al(OC(CF_3)_3)_3)_2]^-$) ppm. ^{27}Al-NMR (78.2 MHz, CD_2Cl_2, RT): δ = 33.1 (br, 1 Al, $[F(\mathbf{Al}(OC(CF_3)_3)_3)_2]^-$) ppm. ^{31}P-NMR (121.5 MHz, CD_2Cl_2, RT): δ = 219.4 (br., 1 P, $\mathbf{P}Cl_3$), 151.6 (dt, 2 P, $[P_2\mathbf{P_{B2}}PCl_2]^+$, $^1J(^{31}P_B, ^{31}P_C)$ = 341 Hz, $^1J(^{31}P_A, ^{31}P_B)$ = 143 Hz), 110.9 (unknown), 56.2 (tt, 1 P, $[P_4\mathbf{P_C}Cl_2]^+$, $^1J(^{31}P_B, ^{31}P_C)$ = 341 Hz, $^2J(^{31}P_A, ^{31}P_C)$ = 27 Hz), −171.9 (unknown), −247.3 (unknown), −270.5 (td, 2 P, $[\mathbf{P_{A2}}P_3Cl_2]^+$, $^1J(^{31}P_A, ^{31}P_B)$ = 143 Hz, $^2J(^{31}P_A, ^{31}P_C)$ = 27 Hz), −399.2 (s, 3 P, $[\mathbf{P}_3S]^+$), −518.5 (s, 4 P, $\mathbf{P}_4$) ppm.

Reaction on a bigger scale under optimized conditions

$SeCl_3[Al(OR^F)_4]$ (2.0 g, 1.74 mmol, 1.0 eq.) was weighed in a double bulb vessel, dissolved in CH_2Cl_2 (20 mL) and cooled down to −40 °C. A previously prepared solution of P_4 (260 mg, 2.10 mmol, 1.20 eq.) in CH_2Cl_2 (20 mL) was added dropwise over the course of 2 h, during which the clear yellow solution slowly became turbid and orange colored. The resulting mixture was stirred at −40 °C for 20 h. The resulting mixture was then filtered at −40 °C and the resulting filtrate was dried at −40 °C *in vacuo*. The obtained sticky yellow powder (0.9 g) was then finely ground and extracted via a glass frit Soxhlet

extraction with pentane for 16 h, a pale yellow filtrate could be obtained and was discarded. The residue atop of the frit was then collected and all volatiles were removed *in vacuo* until a fine yellow powder (650 mg) could be obtained. It is notable, that a yellow residue was collected in the cold trap of the Schlenk manifold during each removal of volatiles. This residue turns red upon prolonged contact to air, hinting towards the formation of volatile selenium chlorides (e.g. Se_2Cl_2) undergoing slow hydrolysis. **FT-Raman:** $\tilde{\nu}$ [cm^{-1}] = 99 (vw), 125 (vw), 140 (vw), 176 (vw), 184 (vw), 216 (w), 235 (w), 254 (vw), 267 (vw), 280 (w), 322 (m), 331 (m), 361 (vs), 380 (m), 389 (w), 425 (w), 446 (vw), 464 (vw), 474 (vw), 493 (vw), 503 (vw), 537 (w), 562 (vw), 568 (vw), 579 (vw), 608 (vw), 746 (w), 797 (m), 1002 (vw), 1273 (vw), 1294 (vw), 1306 (vw). **ATR-IR (Diamond):** $\tilde{\nu}$ [cm^{-1}] = 440 (m), 535 (m), 560 (w), 571 (vw), 587 (vw), 607 (vw), 665 (vw), 725 (vs), 756 (vw), 831 (vw), 966 (vs), 1160 (m), 1204 (vs), 1238 (m), 1265 (m), 1296 (w), 1351 (vw). ^{19}F-NMR (188.2 MHz, CD_2Cl_2, RT): δ = −75.7 (s, 36 F, $[Al(OC(C\mathbf{F}_3)_3)_4]^-$) ppm. ^{31}P-NMR (81.0 MHz, CD_2Cl_2, RT): δ = 219.4 (br., 1 P, $\mathbf{P}Cl_3$), 152.2 (dt, 2 P, $[P_2\mathbf{P}_{\mathbf{B2}}PCl_2]^+$, $^1J(^{31}P_B, ^{31}P_C)$ = 341 Hz, $^1J(^{31}P_A, ^{31}P_B)$ = 143 Hz), 104.6 (m, 1 P, $[\mathbf{P}_\mathbf{A}P_2Se_4]^+$), 56.0 (tt, 1 P, $[P_4\mathbf{P}_\mathbf{C}Cl_2]^+$, $^1J(^{31}P_B, ^{31}P_C)$ = 341 Hz, $^2J(^{31}P_A, ^{31}P_C)$ = 27 Hz), 38.3 (m, 2 P, $[P\mathbf{P}_{\mathbf{B2}}Se_4]^+$), −271.0 (td, 2 P, $[\mathbf{P}_{\mathbf{A2}}P_3Cl_2]^+$, $^1J(^{31}P_A, ^{31}P_B)$ = 143 Hz, $^2J(^{31}P_A, ^{31}P_C)$ = 27 Hz), −360.4 (s, 3 P, $[\mathbf{P}_3Se]^+$, $^1J(P, ^{77}Se)$ = 58 Hz), −519.0 (s, 4 P, $\mathbf{P}_4$) ppm. MS (ESI, *o*-dfb, m/z^+) m/z = 172.8 ($[P_3{}^{80}Se]^+$, 225.0 ($[P_5{}^{35}Cl_2]^+$)

3.2. Spectral Data of $ECl_3[WCA]$

3.2.1. Spectral Data of $SeCl_3[Al(OR^F)_4]$ 1a

NMR Spectra of 1a

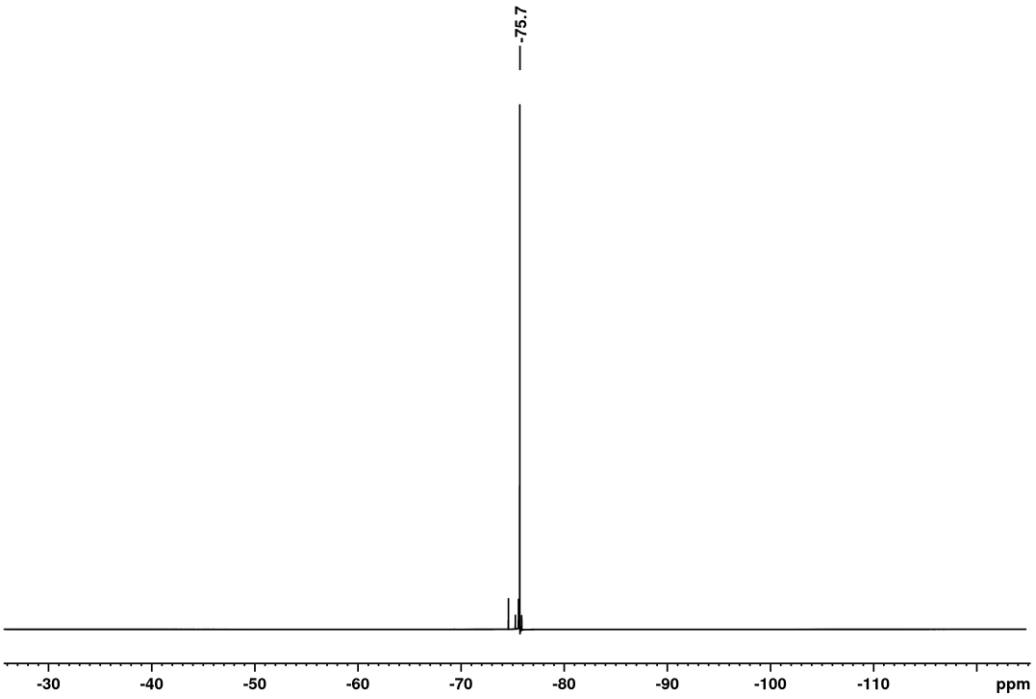

Figure S 2 ^{19}F-NMR spectrum (376.5 MHz, CD_2Cl_2, RT) of **1a**. The small resonance downfield from the anion resonance stems from free alcohol $HOC(CF_3)_3$.

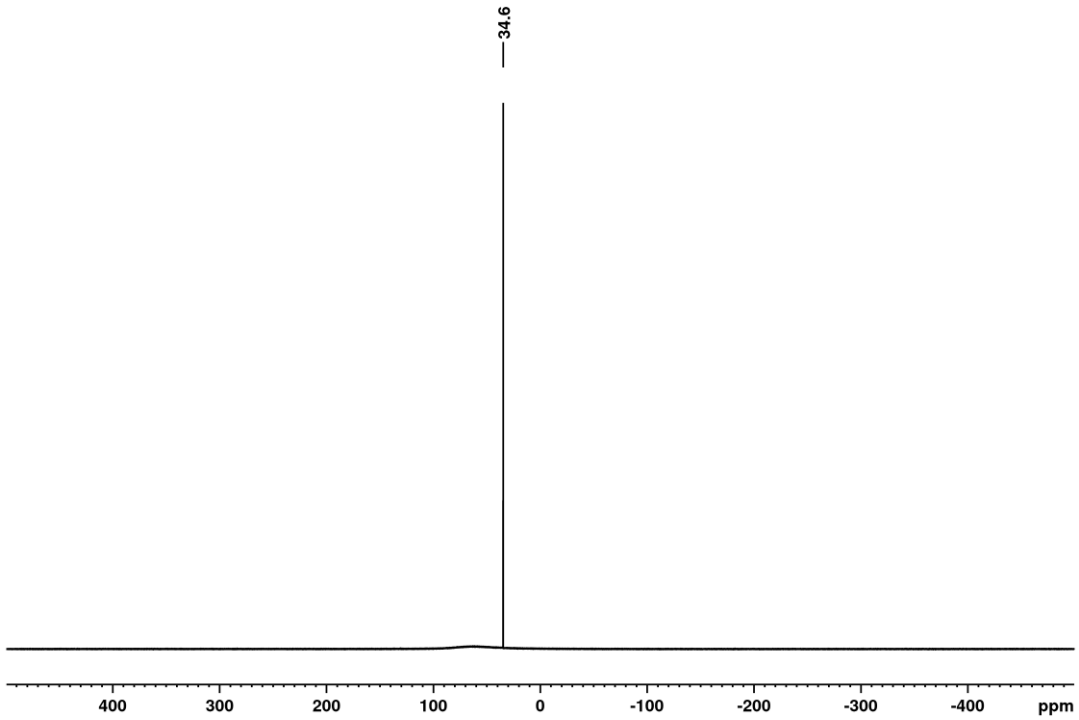

Figure S 3 ^{27}Al-NMR spectrum (104.3 MHz, CD_2Cl_2, RT) of **1a**. The broad resonance at 70 ppm stems from the probe head.

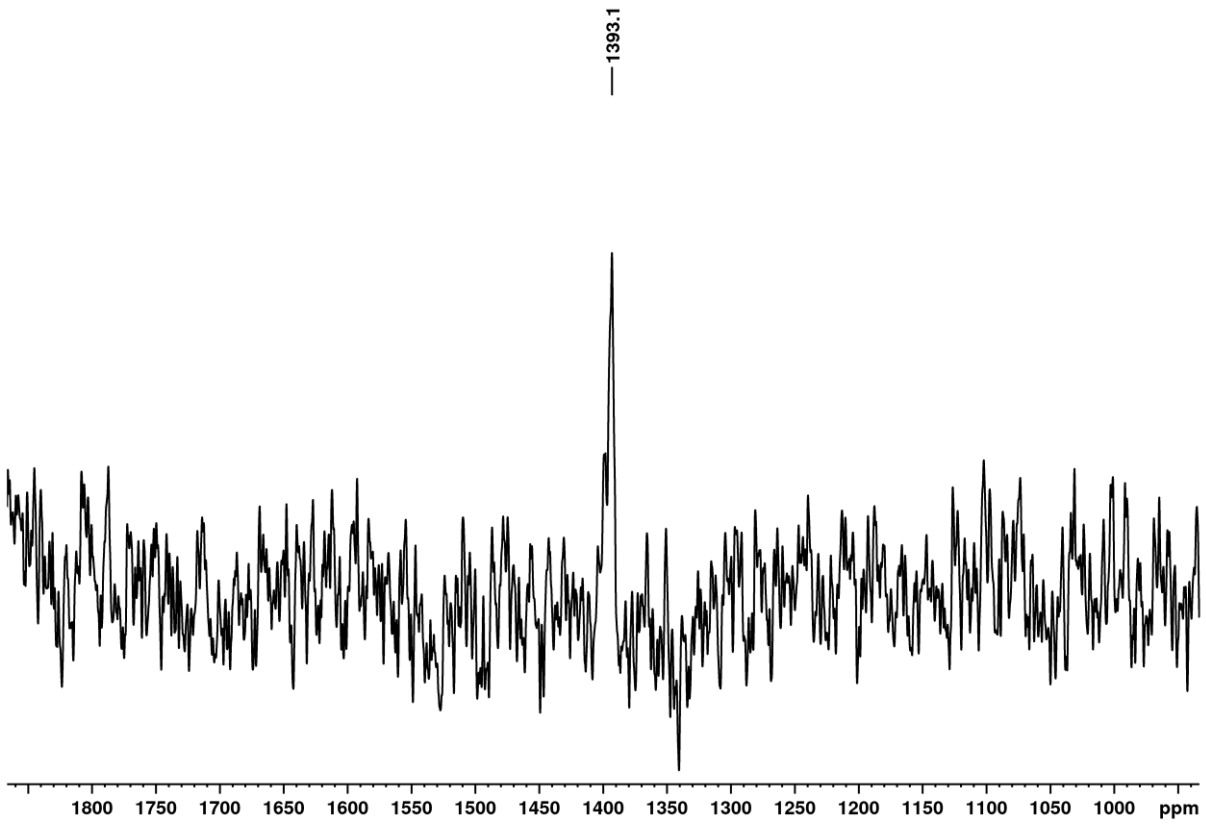

Figure S 4 ^{77}Se-NMR spectrum (76.3 MHz, CD_2Cl_2, RT) of **1a**.

Vibrational Spectra of 1a

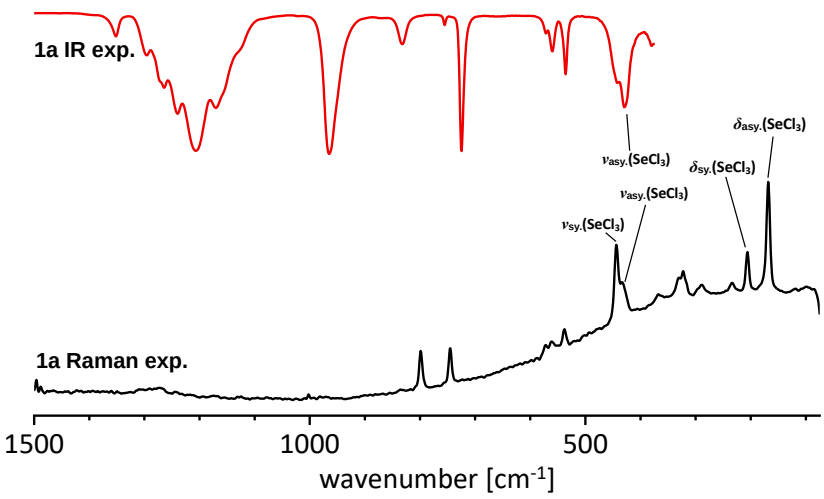

Figure S 5 Raman spectrum (bottom trace) between 65 and 1500 cm^{-1} and IR spectrum (top trace) of **1a** between 380 and 1500 cm^{-1}.

Crystal Structure and Molecular Structure of 1a

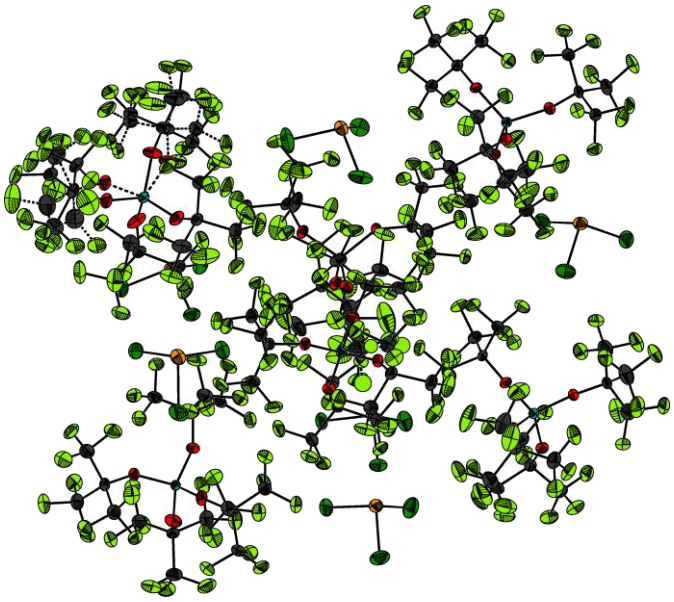

Figure S 6 Close up view of the asymmetric unit of **1a** including the six crystallographically independent $[SeCl_3]^+$ cations and $[Al(OR^F)_4]^-$ anions. The stippled bonds indicate disordered parts.

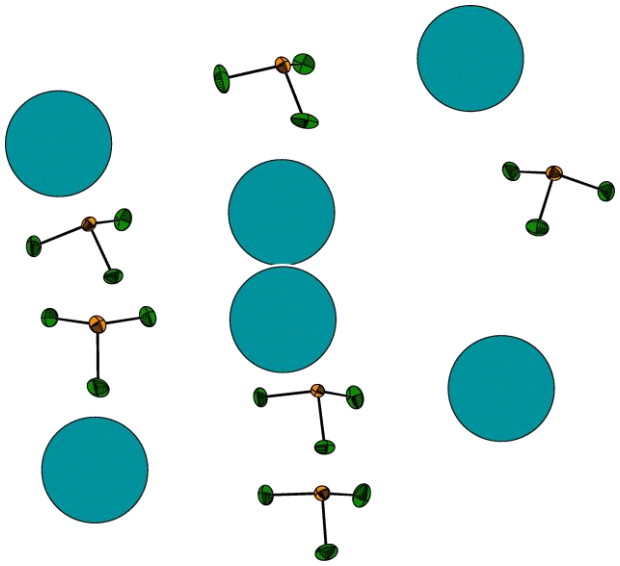

Figure S 7 Close up view of the six crystallogrphically independent $[SeCl_3]^+$ cations in the asymmetric unit of **1a**. For reasons of clarity, the anions have been replaced with blue balls.

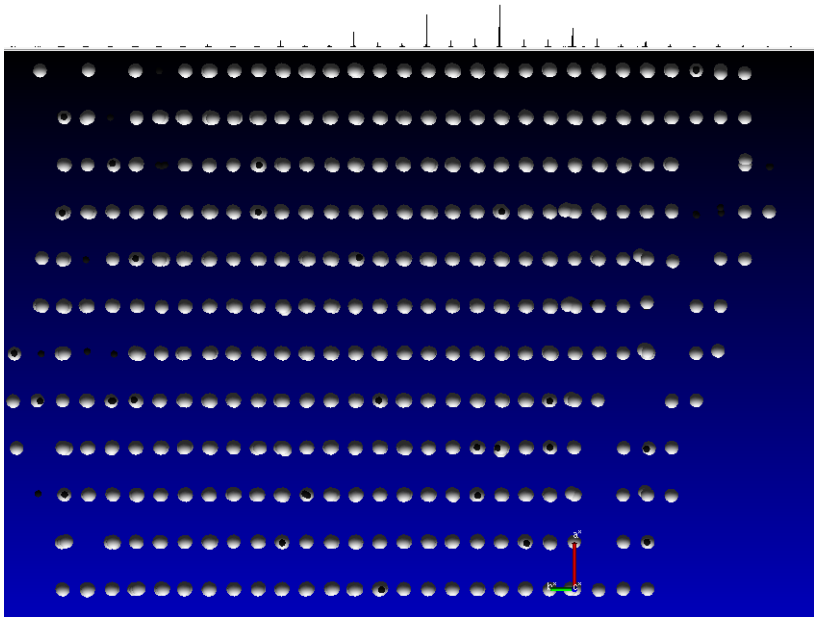

Figure S 8 Close up view of the reciprocal space of the measured data set of **1a** along the b* axis. The top bar shows the summed up intensity and indicates the modulation of the structure.

3.2.2. Spectral Data of $SeCl_3[F(Al(OR^F)_3)_2]$ 1b

NMR Spectra of 1b

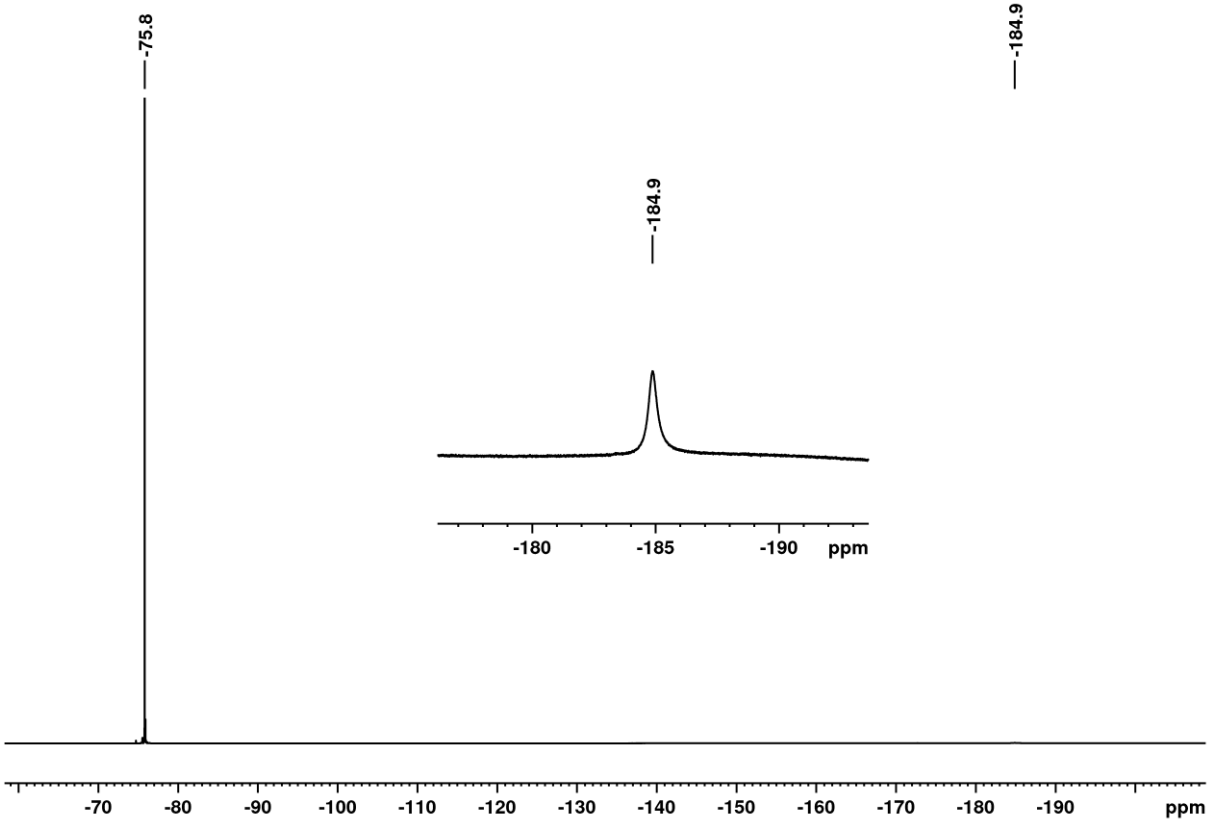

Figure S 9 ^{19}F-NMR spectrum (282.5 MHz, CD_2Cl_2, RT) of **1b**.

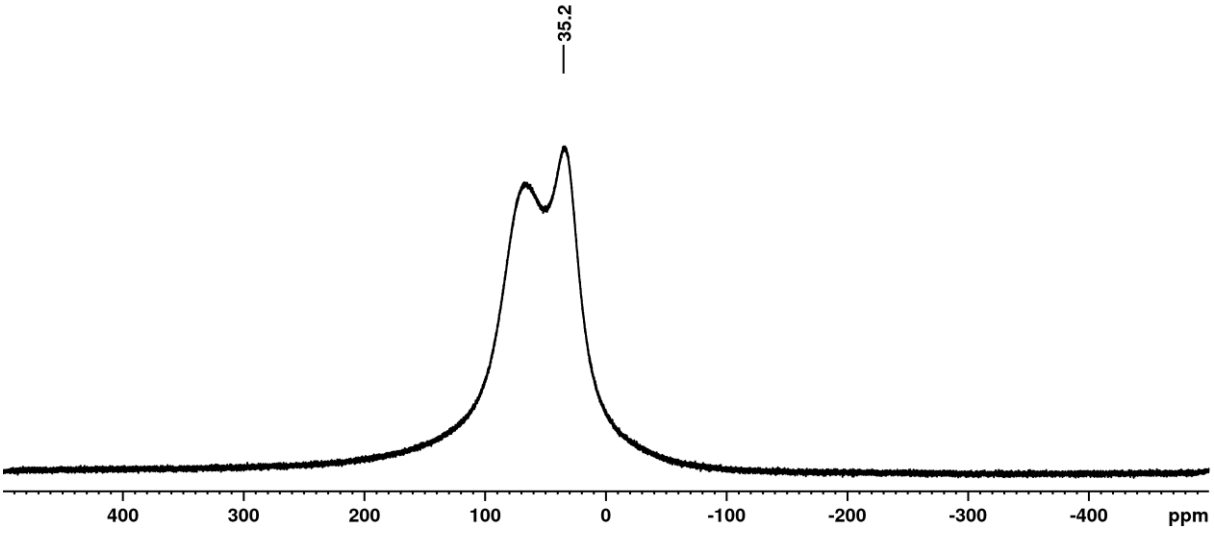

Figure S 10 ^{27}Al-NMR spectrum (78.2 MHz, CD_2Cl_2, RT) of **1b**. The second broad signal ranging from 0 to 100 ppm stems from the probe head.

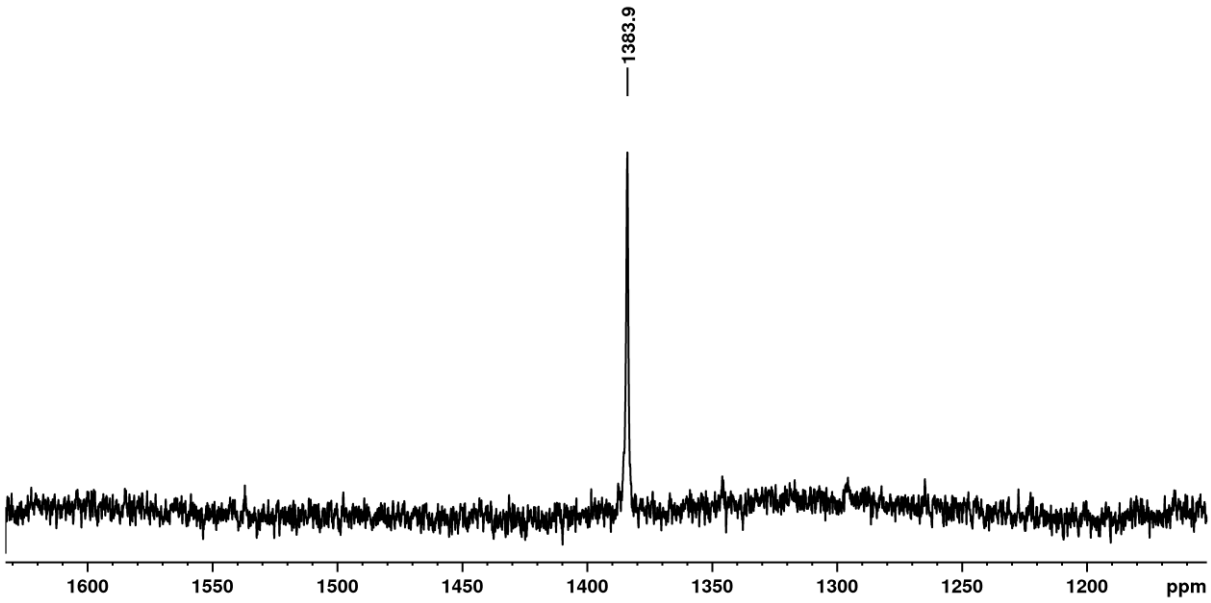

Figure S 11 ^{77}Se-NMR spectrum (57.2 MHz, CD_2Cl_2, RT) of **1b**.

Vibrational Spectra of 1b

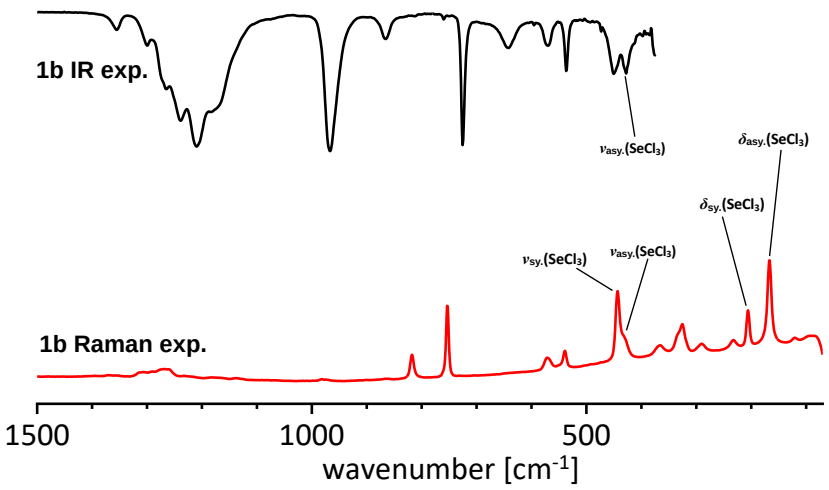

Figure S 12 Raman spectrum (bottom trace) between 65 and 1500 cm^{-1} and IR spectrum (top trace) of **1b** between 380 and 1500 cm^{-1}.

Crystal Structure and Molecular Structure of 1b

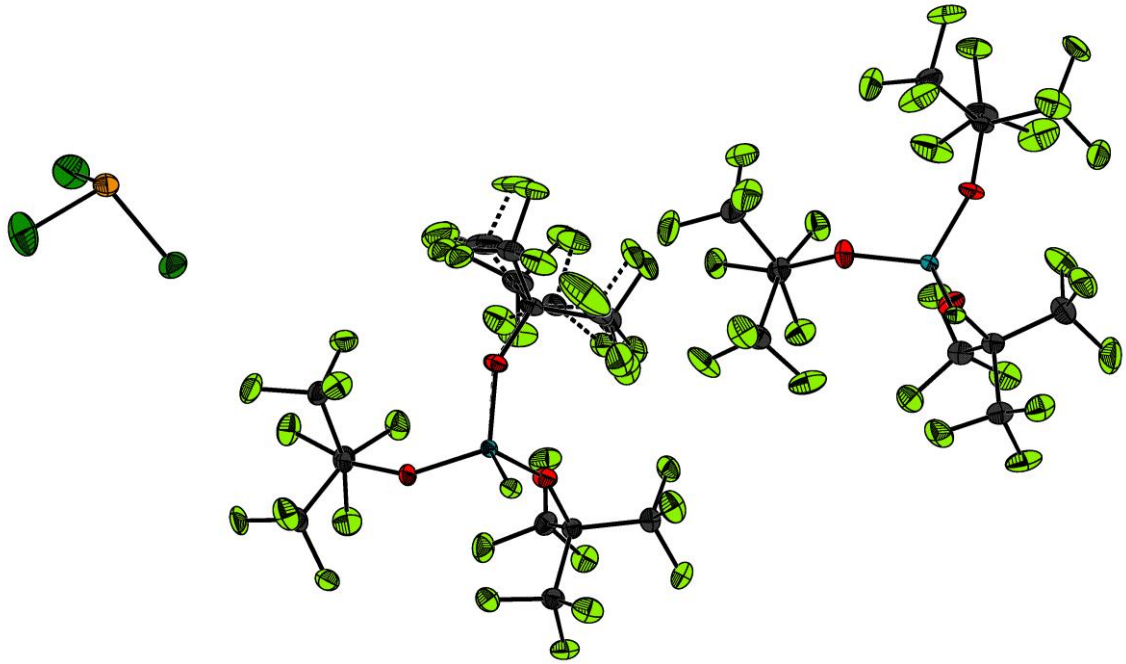

Figure S 13 Asymmetric unit of the crystal structure of **1b** including two halves of the fluoride bridged anion with the (Al-)F atom residing on a special position with occupancy 0.5. The stippled bonds show disordered parts of the structure. All thermal ellipsoids are shown at 50 % probability.

3.2.3. Spectral Data of $SeCl_3[FAl(OR^F)_3]$ 1c

NMR Spectra of 1c

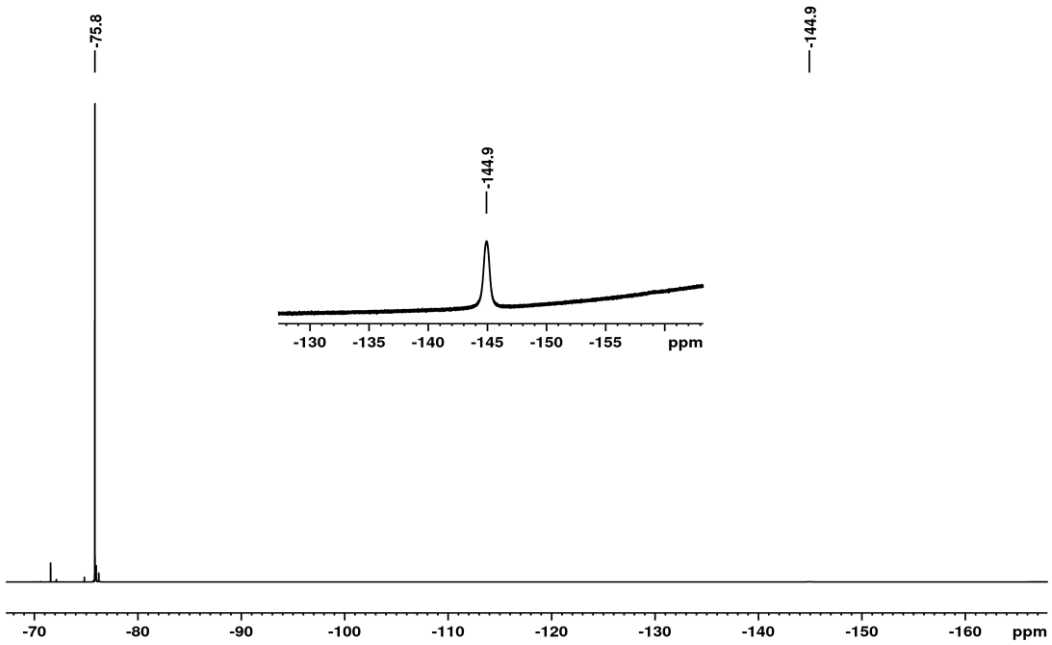

Figure S 14 ^{19}F-NMR spectrum (376.5 MHz, CH_2Cl_2, RT) of **1c**. The small resonance downfield from the anion resonance stems from free alcohol $HOC(CF_3)_3$.

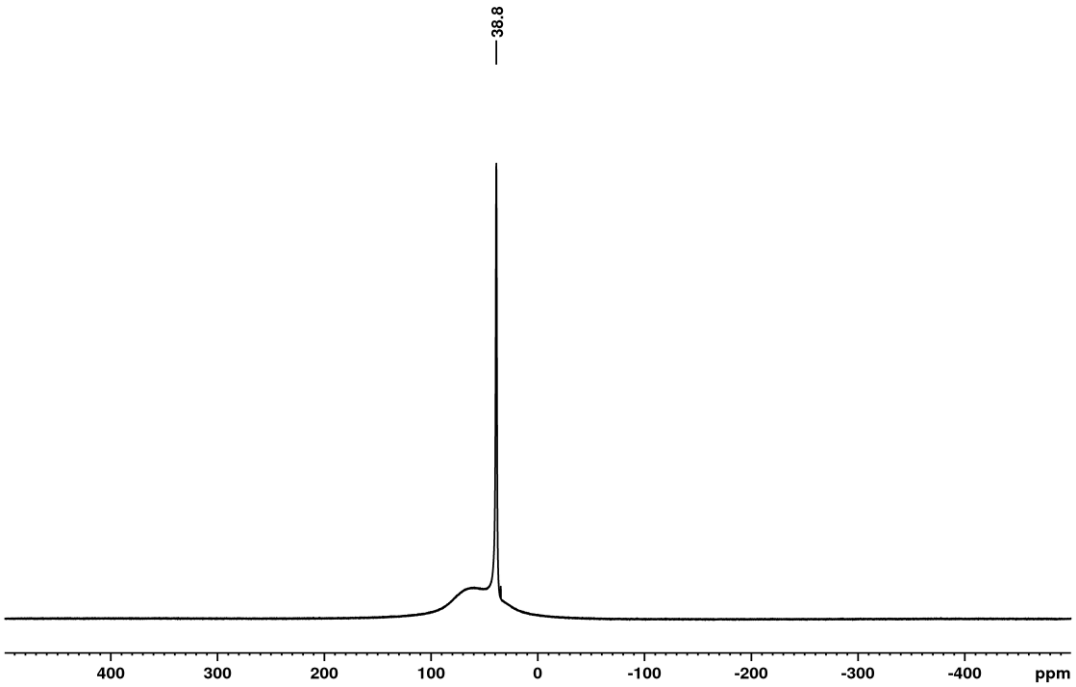

Figure S 15 ^{27}Al-NMR spectrum (104.3 MHz, CH_2Cl_2, RT) of **1c**. The broad signal ranging from 0 to 100 ppm stems from the probe head.

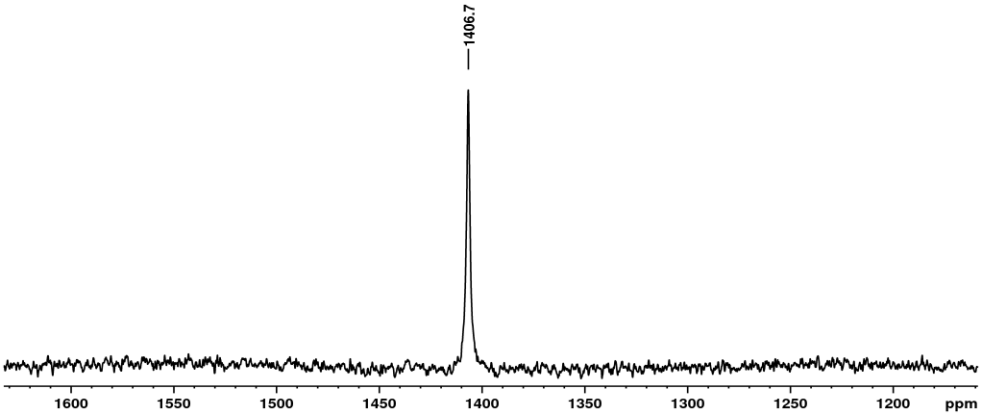

Figure S 16 ^{77}Se-NMR spectrum (76.3 MHz, CH_2Cl_2, RT) of **1c**.

Vibrational Spectra of 1c

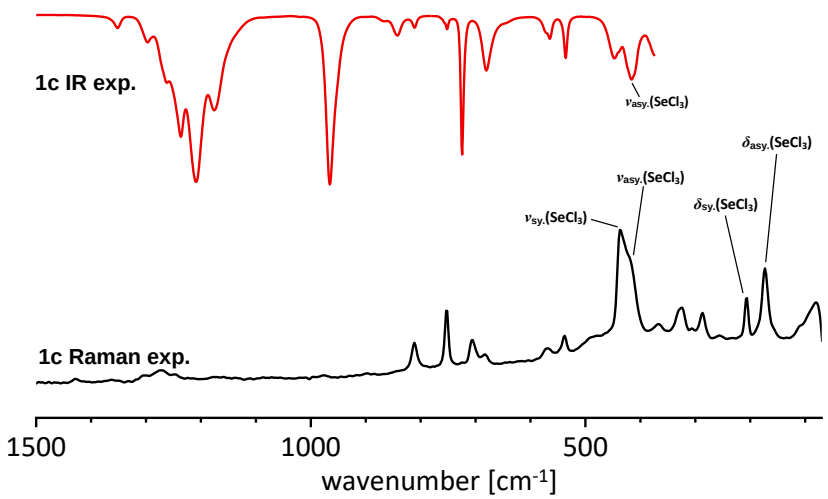

Figure S 17 Raman spectrum (bottom trace) between 65 and 1500 cm^{-1} and IR spectrum (top trace) of **1c** between 380 and 1500 cm^{-1}.

Crystal Structure and Molecular Structure of 1c

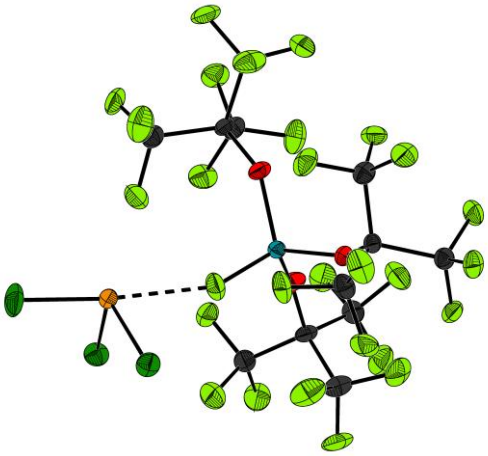

Figure S 18 Close up view of the asymmetric unit of **1c**. All thermal ellipsoids are shown at 50 % probability.

3.2.4. Spectral Data of $TeCl_3[Al(OR^F)_4]$

2a was prepared as previously described in the literature.[2] NMR spectra were recorded in CD_2Cl_2.

NMR Spectra of 2a

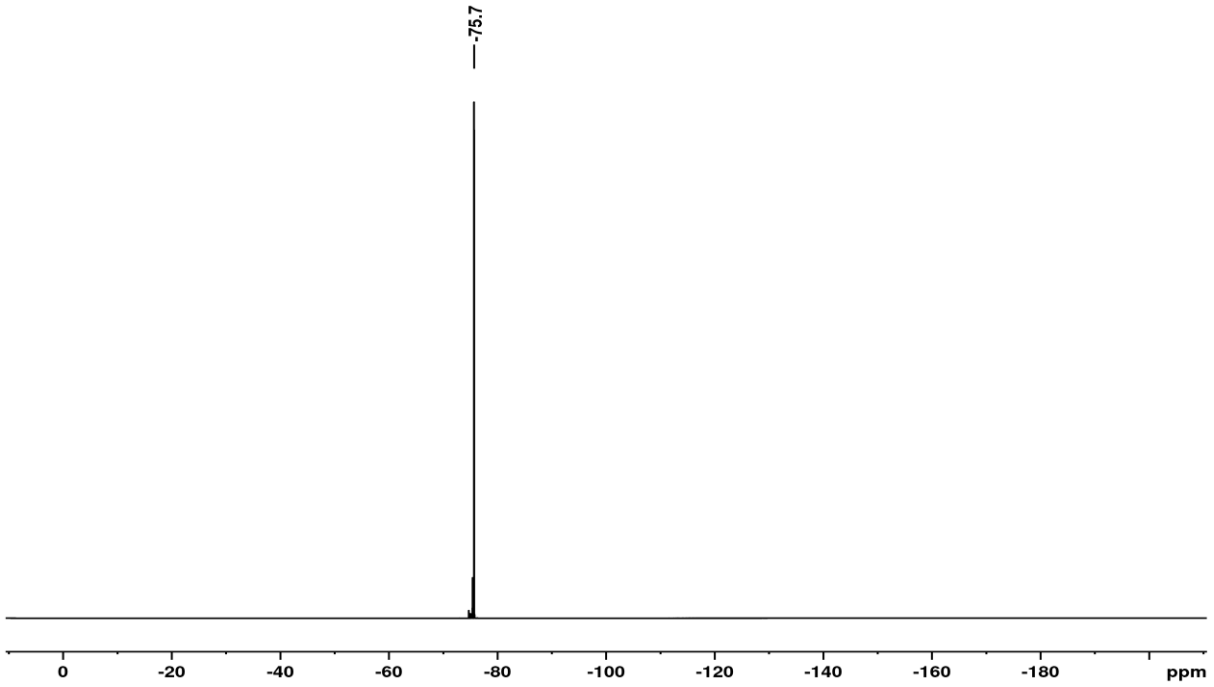

Figure S 19 ^{19}F-NMR spectrum (282.5 MHz, CD_2Cl_2, RT) of **2a**.

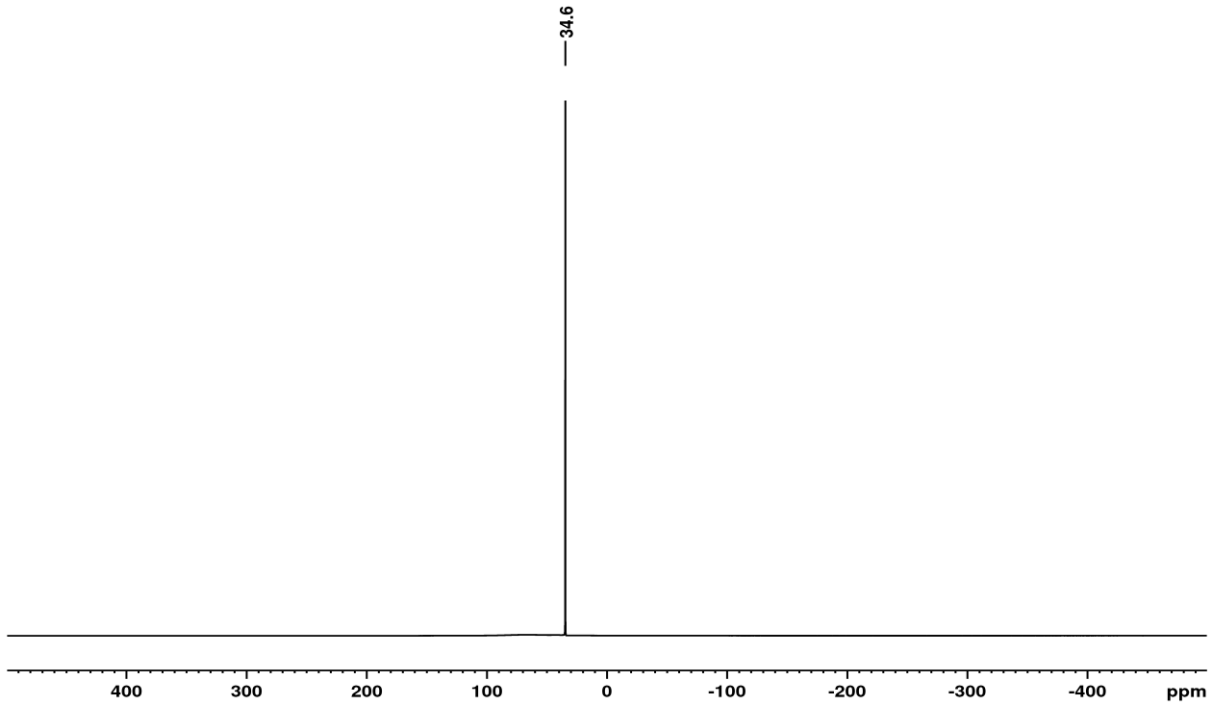

Figure S 20 ^{27}Al-NMR spectrum (78.2 MHz, CD_2Cl_2, RT) of **2a**.

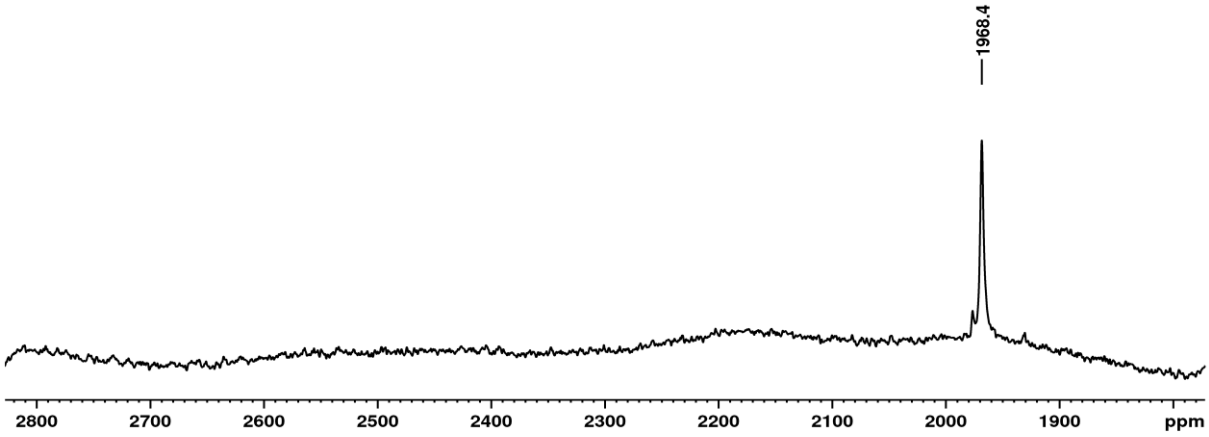

Figure S 21 ^{125}Te-NMR spectrum (94.7 MHz, CD_2Cl_2, RT) of **2a**.

3.2.5. Spectral Data of $TeCl_3[F(Al(OR^F)_3)_2]$ 2b

NMR Spectra

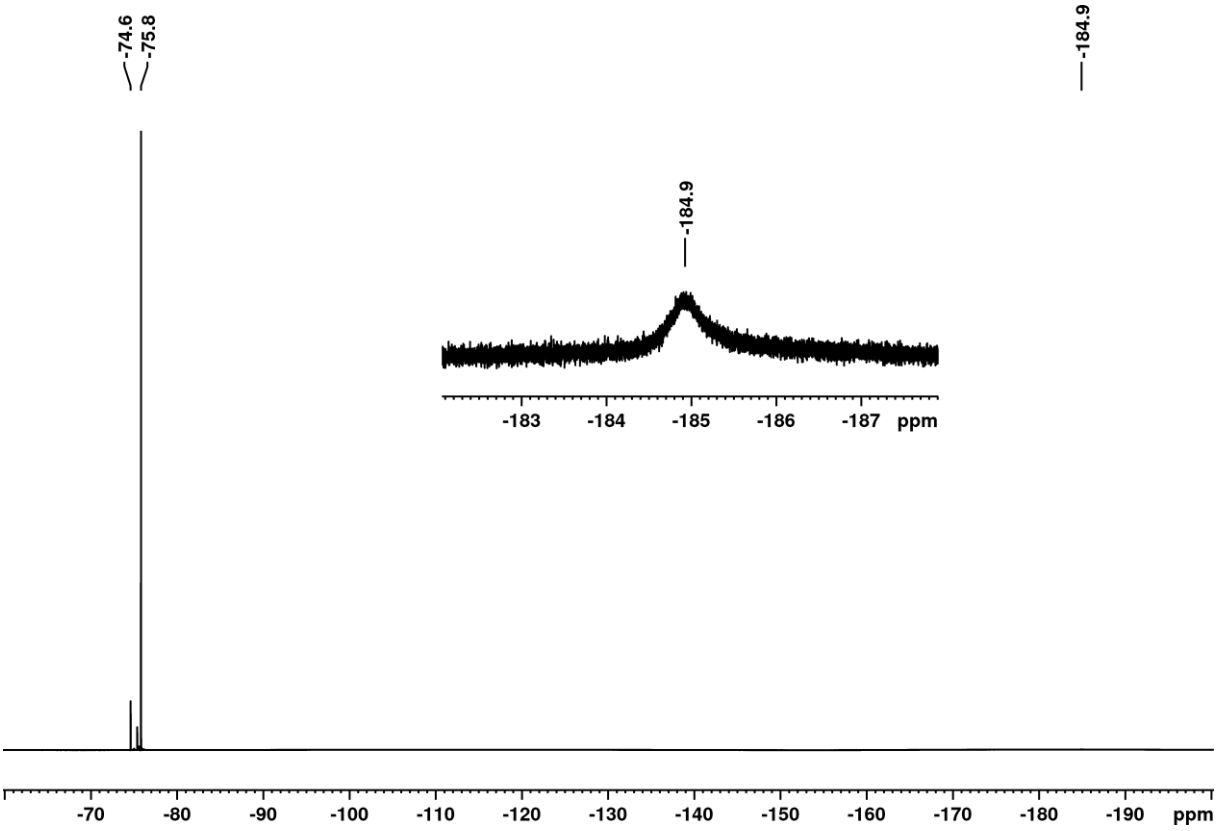

Figure S 22 ^{19}F-NMR spectrum (282.5 MHz, CD_2Cl_2, RT) of **2b**. The small resonance at −74.6 ppm stems from free alcohol $HOC(CF_3)_3$.

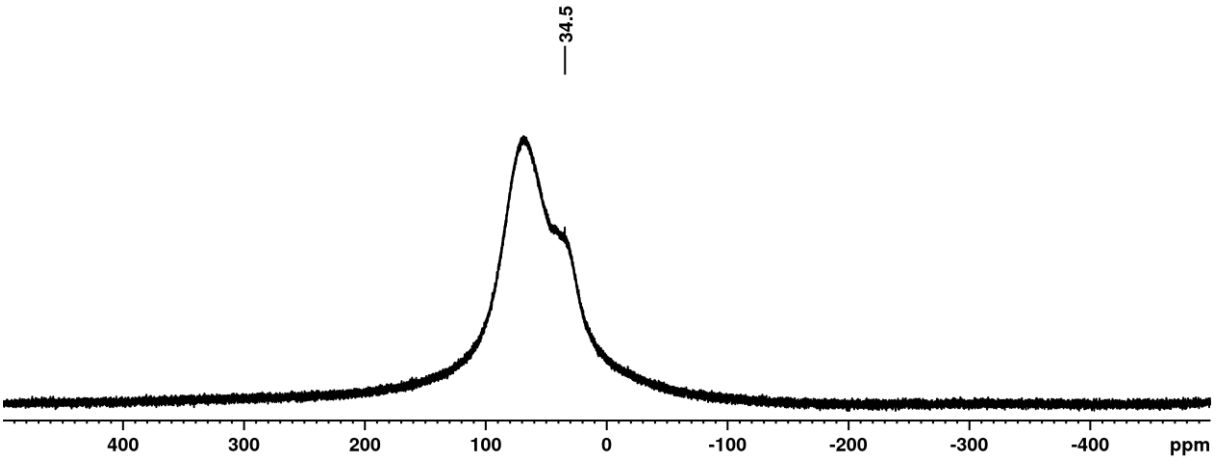

Figure S 23 ^{27}Al-NMR spectrum (78.2 MHz, CD_2Cl_2, RT) of **2b**. The broad resonance from 50 to 100 ppm stems from the probe head.

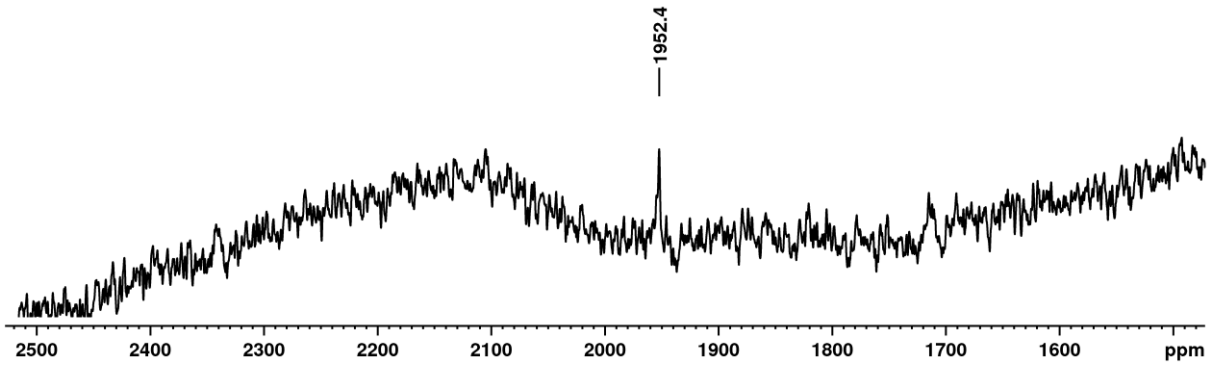

Figure S 24 ^{125}Te-NMR spectrum (94.7 MHz, CD_2Cl_2, RT) of **2b**. The signal to noise ratio is low compared to **2a** because of the limited available amount of substance.

Vibrational Spectra

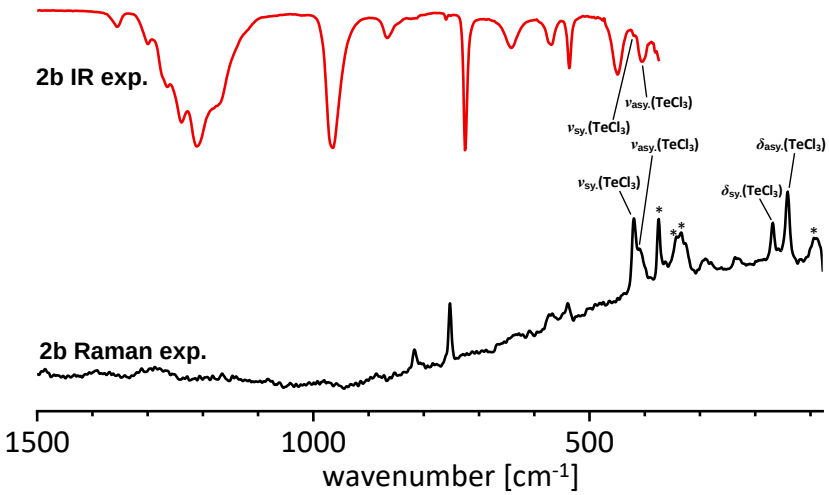

Figure S 25 Raman spectrum (bottom trace) between 75 and 1500 cm^{-1} and IR spectrum (top trace) of **1a** between 380 and 1500 cm^{-1}. The asterisks denote residual amounts of $TeCl_4$.

3.2.6. Spectral Data of $SCl_3[F(Al(OR^F)_3)_2]$ 3

NMR Spectra

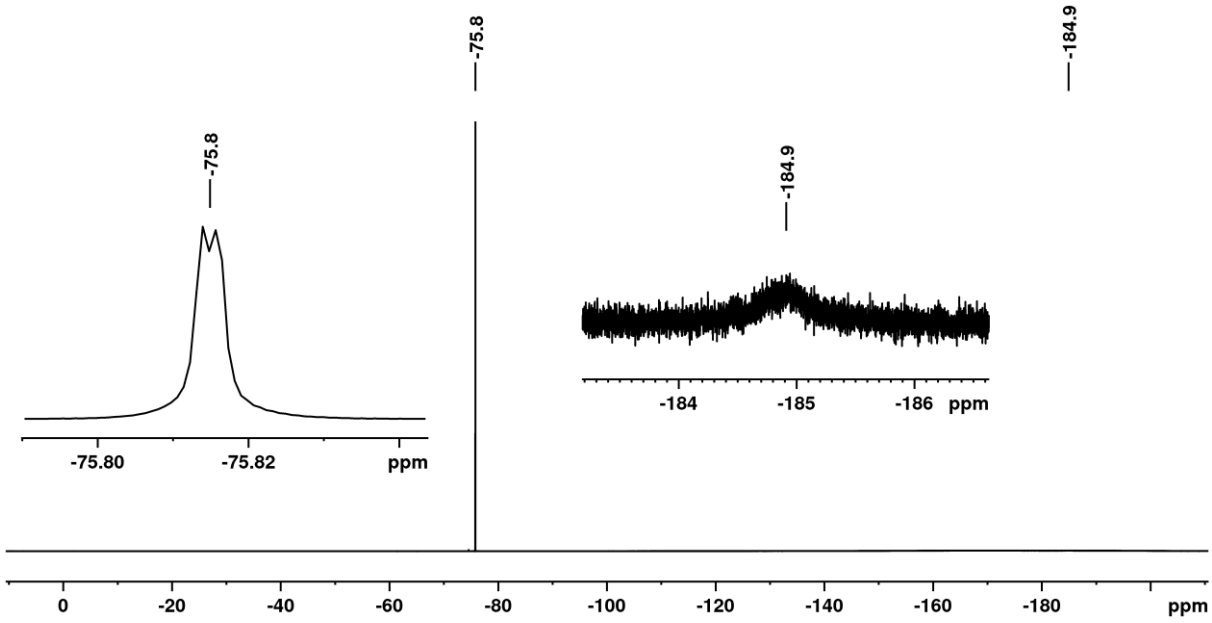

Figure S 26 ^{19}F-NMR spectrum (282.5 MHz, CH_2Cl_2, RT) of **3**.

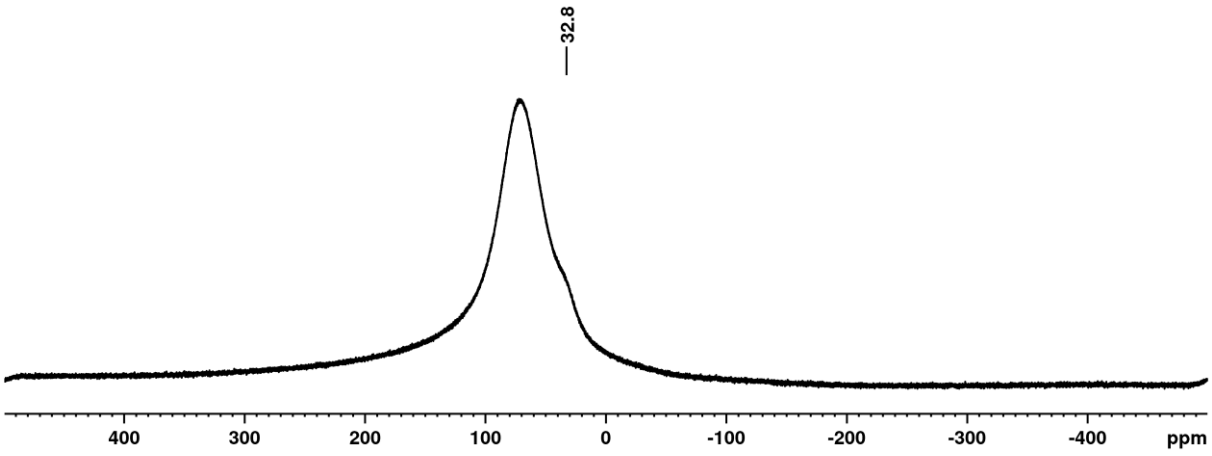

Figure S 27 ^{27}Al-NMR spectrum (78.2 MHz, CD_2Cl_2, RT) of **3**. The broad resonance from 50 to 100 ppm stems from the probe head.

Vibrational Spectra

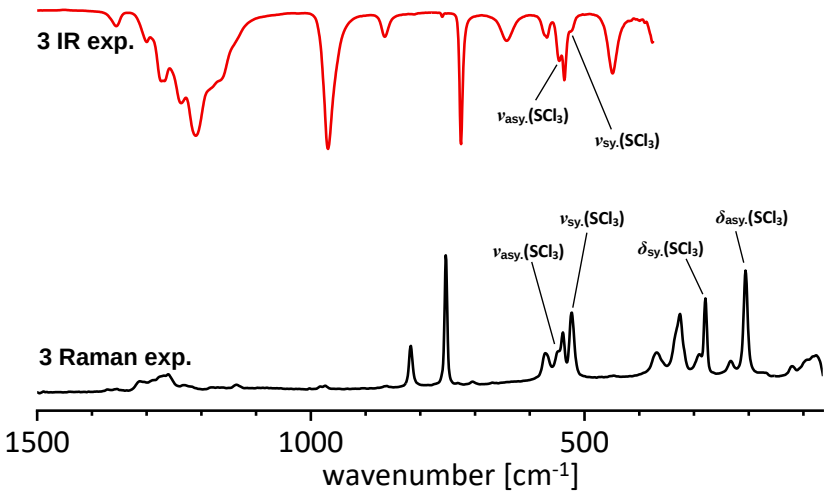

Figure S 28 Raman spectrum (bottom trace) between 65 and 1500 cm^{-1} and IR spectrum (top trace) of **3** between 380 and 1500 cm^{-1}.

Molecular Structure of $SCl_3[F(Al(OR^F)_3)_2]$

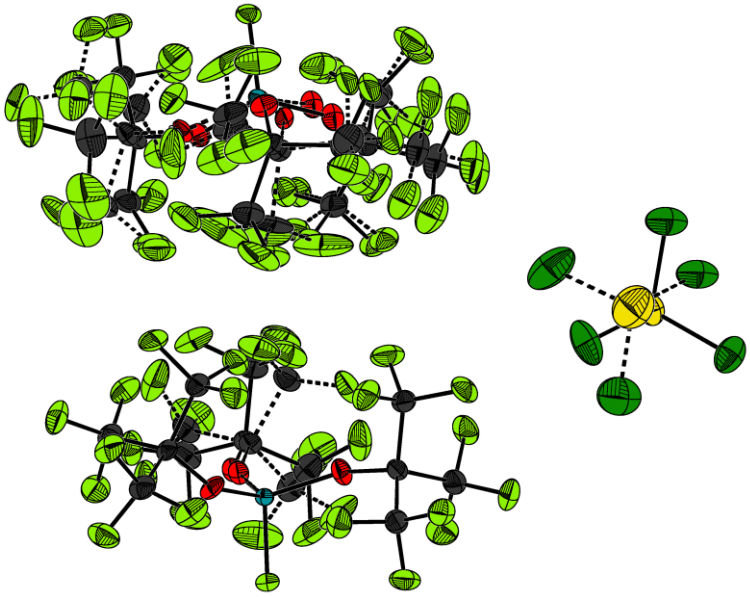

Figure S 29 Asymmetric unit of the crystal structure of **3**. The stippled bonds show disordered parts of the structure. All thermal ellipsoids are shown at 50 % probability. The disordered $[SCl_3]^+$ cation has occupancies of 92 % (non stippled) and 8 % (stippled).

3.2.7. Complete Tables of the Vibrational Spectra of the $ECl_3[WCA]$ salts

Table S 3 Summary of the experimental Raman and IR bands of the $[SeCl_3][WCA]$ salts in powdered samplex of **1a** , **1c** and **1b**. For reference the bands of $SeCl_3[AsF_6]$ are also given.[35] The gray shaded cells indicate vibrational bands of the $[SeCl_3]^+$ cation. All bands are given in [cm^{-1}].

1a Raman	**1a** IR	**1b** Raman	**1b** IR	**1c** Raman	**1c** IR	**$SeCl_3[AsF_6]$** Raman[35]	**Assignment**[a)]
—	—	96 (vw)	—	—	—	—	Anion
—	—	121 (vw)	—	—	—	—	Anion
162 (vs)	—	167 (vs)	—	173 (s)	—	168 (s)	$\delta_{asy.}(SeCl_3)$ (E)
206 (w)	—	206 (m)	—	207 (w)	—	200 (w)	$\delta_{sy.}(SeCl_3)$ (A_1)
234 (vw)	—	233 (vw)	—	256 (vw)	—	—	Anion
289 (vw)	—	290 (vw)	—	287 (w)	—	—	Anion
—	—	—	—	306 (vw)	—	—	Anion
323 (w)	—	325 (w)	—	324 (w)	—	—	Anion
330 (vw)	—	—	—	—	—	—	Anion
354 (vw)	—	—	—	—	—	355 (m)	Anion
368 (vw)	—	366 (vw)	—	367 (vw)	—	—	Anion
407 (vw)	—	—	—	—	—	—	Anion
434 (w)	429 (s)	430 (sh)	428 (m)	418 (sh)	416 (w)	390 (w)	$\nu_{asy.}(SeCl_3)$ (E)
444 (s)	442 (m)	443 (vs)	450 (m)	437 (vs)	447 (w)	437 (vs)	$\nu_{sy.}(SeCl_3)$ (A_1) / Anion
—	—	474 (vw)	473 (vw)	480 (vw)	—	—	Anion
538 (vw)	536 (m)	539 (w)	537 (m)	538 (vw)	536 (w)	—	Anion
562 (vw)	560 (w)	—	—	—	565 (vw)	—	Anion
572 (vw)	571 (vw)	572 (vw)	570 (w)	570 (vw)	—	568 (m)	Anion
—	—	—	642 (w)	—	—	—	Anion
—	—	—	—	683 (vw)	680 (w)	678 (m)	Anion
—	—	—	—	706 (w)	—	—	Anion
—	725 (vs)	—	725 (vs)	725 (vw)	725 (vs)	—	Anion
745 (w)	755 (vw)	753 (vs)	760 (vw)	753 (m)	752 (vw)	—	Anion
799 (w)	—	818 (w)	813 (vw)	811 (w)	811 (vw)	—	Anion
—	832 (w)	—	—		842 (vw)	—	Anion
—	873 (vw)	—	866 (w)		866 (vw)	—	Anion
—	965 (vs)	974 (vw)	967 (vs)	978 (vw)	965 (vs)	—	Anion
—	—	982 (vw)	—	—	—	—	Anion
1002 (vw)	1020 (vw)	—	—	—	—	—	Anion
—	—	—	1076 (vw)	—	—	—	Anion
—	—	1137 (vw)	—	—	—	—	Anion
—	1170 (s)	1182 (vw)	1184 (s)	—	1176 (m)	—	Anion
—	1207 (vs)	—	1210 (vs)	—	1209 (vs)	—	Anion
1246 (vw)	1240 (s)	1232 (vw)	1239 (s)	1247 (vw)	1237 (s)	—	Anion
—	1264 (m)	1261 (vw)	1265 (m)	—	1262 (m)	—	Anion
1282 (vw)	—	1269 (vw)	—	1275 (vw)	—	—	Anion
1291 (vw)	1296 (w)	1290 (vw)	1300 (w)	—	1297 (vw)	—	Anion
—	—	1306 (vw)	—	1305 (vw)	—	—	Anion
1310 (vw)	1352 (vw)	—	1355 (vw)	1362 (vw)	1352 (vw)	—	Anion

w: weak, m: medium, s: strong, sh: shoulder, v: very. a) From a visualization of the calculated spectra.

Table S 4 Summary of the experimental Raman and IR bands of **3**. For reference the bands of $TeCl_3[Al(OR^F)_4]$ including its $TeCl_4$ contaminations and $TeCl_3[AsF_6]$ are also given.[2,35] The gray shaded cells indicate vibrational bands of the $[TeCl_3]^+$ cation. All bands are given in [cm^{-1}].

2b **Raman**	**2b** **IR**	**$TeCl_3[Al(OR^F)_4]$** **Raman[2]**	**$TeCl_3[AsF_6]$** **Raman[35]**	**Assignment[a)]**
94 (w)	—	88 (m)	—	$TeCl_4$ /Anion
141 (vs)	—	144 (m)	150 (m)	$\delta_{asy.}(SeCl_3)$ (E)
158 (w)	—	—	—	Anion
168 (m)		170 (m)	170 (w)	$\delta_{sy.}(SeCl_3)$ (A_1)
236 (w)	—	235 (w)	—	Anion
290 (w)	—	289 (w)	—	Anion
327 (m)	—	321 (w)	—	Anion
334 (s)	—	341 (m)	—	$TeCl_4$
343 (s)	—	347 (m)	—	$TeCl_4$
363 (w)	—	359 sh)	—	Anion
375 (vs)	—	374 (s)	—	$TeCl_4$
410 (m)	406 (w)	408 (m)	385 (s)	$\nu_{asy.}(TeCl_3)$ (E)
420 (vs)	419 (vw)	418 (m)	412 (vs)	$\nu_{sy.}(TeCl_3)$ (A_1)
—	449 (m)	537 (w)	—	Anion
539 (w)	536 (m)	555 (w)	—	Anion
548 (vw)	—	—	538 (vw)	Anion
568 (w)	569 (w)	—	678 (m)	Anion
573 (w)	—	746 (m)	—	Anion
—	642 (w)	798 (m)	—	Anion
—	725 (vs)	—	—	Anion
753 (s)	760 (vw)	—	—	Anion
817 (w)	813 (vw)	—	—	Anion
—	866 (w)	—	—	Anion
886 (vw)	—	—	—	Anion
981 (vw)	965 (vs)	—	—	Anion
1140 (vw)	—	—	—	Anion
1165 (vw)	1170 (sh)	—	—	Anion
—	1211 (vs)	—	—	Anion
—	1239 (s)	—	—	Anion
1252 (vw)	—	—	—	Anion
1264 (vw)	1264 (m)	—	—	Anion
1278 (vw)	—	—	—	Anion
1294 (vw)	1300 (w)	—	—	Anion
1311 (vw)	—	—	—	Anion
—	1355 (vw)	—	—	Anion

Table S 5 Summary of the experimental Raman and IR bands of **3**. For reference the bands of $SCl_3[AsF_6]$ are also given.[35] The gray shaded cells indicate vibrational bands of the $[SCl_3]^+$ cation. All bands are given in [cm^{-1}].

3 **Raman**	**3** **IR**	**$SCl_3[AsF_6]$** **Raman**[35]	**Assignment**[a)]
96 (vw)	—	—	Anion
122 (vw)	—	—	Anion
206 (vs)	—	214 (s)	$\delta_{asy.}(SCl_3)$ (E)
233 (vw)	—	—	Anion
279 (m)	—	284 (m)	$\delta_{sy.}(SCl_3)$ (E)
290 (vw)	—	—	Anion
326 (m)	—	—	Anion
368 (vw)	—	370 (m)	Anion
—	449 (m)	—	Anion
524 (m)	523 (vw)	519 (vs)	$\nu_{sy.}(SCl_3)$ (A_1)
539 (w)	537 (m)	—	Anion
548 (w)	546 (w)	543 (w)	$\nu_{asy.}(SCl_3)$ (E)
572 (w)	569 (w)	574 (w)	Anion
—	642 (w)	—	Anion
705 (vw)	—	683 (m)	Anion
—	726 (vs)	—	Anion
753 (vs)	—	—	Anion
—	760 (vw)	—	Anion
818 (w)	812 (vw)	—	Anion
—	865 (w)	—	Anion
974 (vw)	969 (vs)	—	Anion
983 (vw)	—	—	Anion
—	1070 (vw)	—	Anion
1136 (vw)	—	—	Anion
1182 (vw)	1184 (s)	—	Anion
—	1210 (vs)	—	Anion
1231 (vw)	1237 (s)	—	Anion
1261 (vw)	—	—	Anion
1268 (vw)	1273 (m)	—	Anion
1286 (vw)	—	—	Anion
1312 (vw)	1300 (w)	—	Anion
—	1355 (vw)	—	Anion

w: weak, m: medium, s: strong, sh: shoulder, v: very. a) From a visualization of the calculated spectra.

3.3. Reactions with Na[Nb(P$_3$)(ODipp)$_3$]*3THF

$SeCl_3[Al(OR^F)_4]$ (23 mg 0.02 mmol, 1.0 eq.) and Na[Nb(P$_3$)(ODipp)$_3$]*3THF (19 mg, 0.02 mmol, 1.0 eq.) were weighed in an NMR tube and CD_2Cl_2 (0.7 mL) was condensed onto the solids at −196 °C. The NMR tube was then flame sealed and kept at −40 °C, resulting in a deep red solution over little dark precipitate. The tube was kept at this temperature for 20 h during which the tube was shaken vigorously 5 times. NMR spectra of the sample were measured at −30 °C.

The identical procedure was repeated using the solvents 1,2,3,4-tetrafluorobenzene (1,2,3,4-tfb) and *ortho*-difluorobenzene (*o*-dfb) due to the reported slow decomposition of the $[Nb(P_3)(ODipp)_3]^-$ anion in chlorinated solvents.[36]

NMR: ^{31}P-NMR (162.0 MHz, CD_2Cl_2, 243 K): δ = −228.1 (s, 3 P, $[Nb(P_3)(ODipp)_3]^-$), −518.1 (br. 4 P, P_4) ppm. ^{31}P-NMR (162.0 MHz, 1,2,3,4-tfb, 243 K): δ = −228.2 (s, 3 P, $[Nb(P_3)(ODipp)_3]^-$), −523.3 (br. 4 P, P_4) ppm. ^{31}P-NMR (162.0 MHz, *o*-dfb, 243 K): δ = −227.9 (s, 3 P, $[Nb(P_3)(ODipp)_3]^-$), −523.2 (br. 4 P, P_4) ppm.

The ^{1}H-NMR spectra show partial decomposition of the $[Nb(P_3)(ODipp)_3]^-$ anion, whereas the ^{19}F and the ^{27}Al-NMR spectra indicate that the $[Al(OR^F)_4]^-$ is stable under the chosen reaction conditions. The ^{31}P-spectra of all three reactions show the emergence of a broad signal around −520 ppm that can be assigned to P_4, next to the signal of residual P_3-synthon at −228 ppm. No residual $[SeCl_3]^+$ cation could be detected in the ^{77}Se spectrum.

It can be assumed that all available $[SeCl_3]^+$ cations acted as a chlorinating agent towards the P_3^{3-} synthon and generated PCl_3 *in situ*. The PCl_3 then immediately reacted with residual $[Nb(P_3)(ODipp)_3]^-$ anion to form P_4 until all PCl_3 has vanished leaving only the residual $[Nb(P_3)(ODipp)_3]^-$ and the generated P_4. This generation of P_4 from $[Nb(P_3)(ODipp)_3]^-$ is similar to the synthesis of AsP_3[37] which itself is gained from the reaction of $AsCl_3$ with the P_3^{3-} synthon.

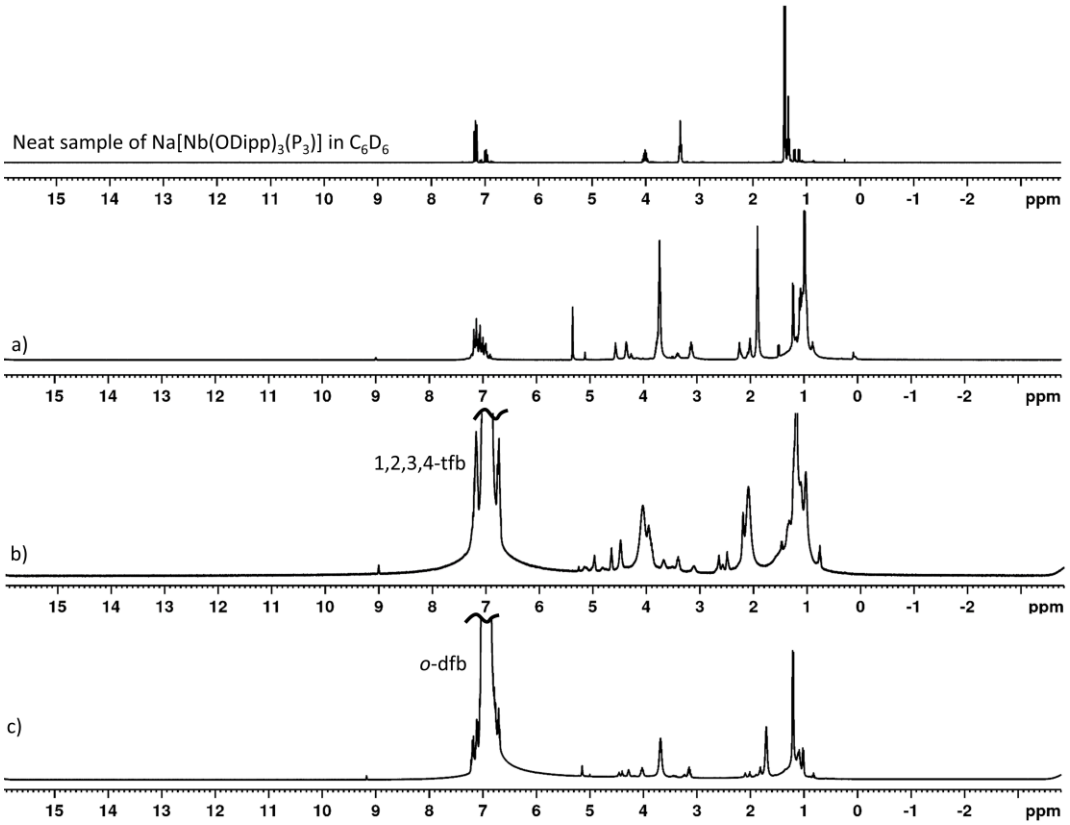

Figure S 30 ^{1}H-NMR spectra (400.2 MHz, in CD_2Cl_2 (a), 1,2,3,4-tfb (b) *o*-dfb (c), 243 K) of the product obtained by the reaction of **1a** with Na[Nb(P$_3$)(ODipp)$_3$]*3THF. For comparison the ^{31}P spectrum of a neat sample of the used Na[Nb(P$_3$)(ODipp)$_3$]*3THF in C_6D_6 is shown (top trace).

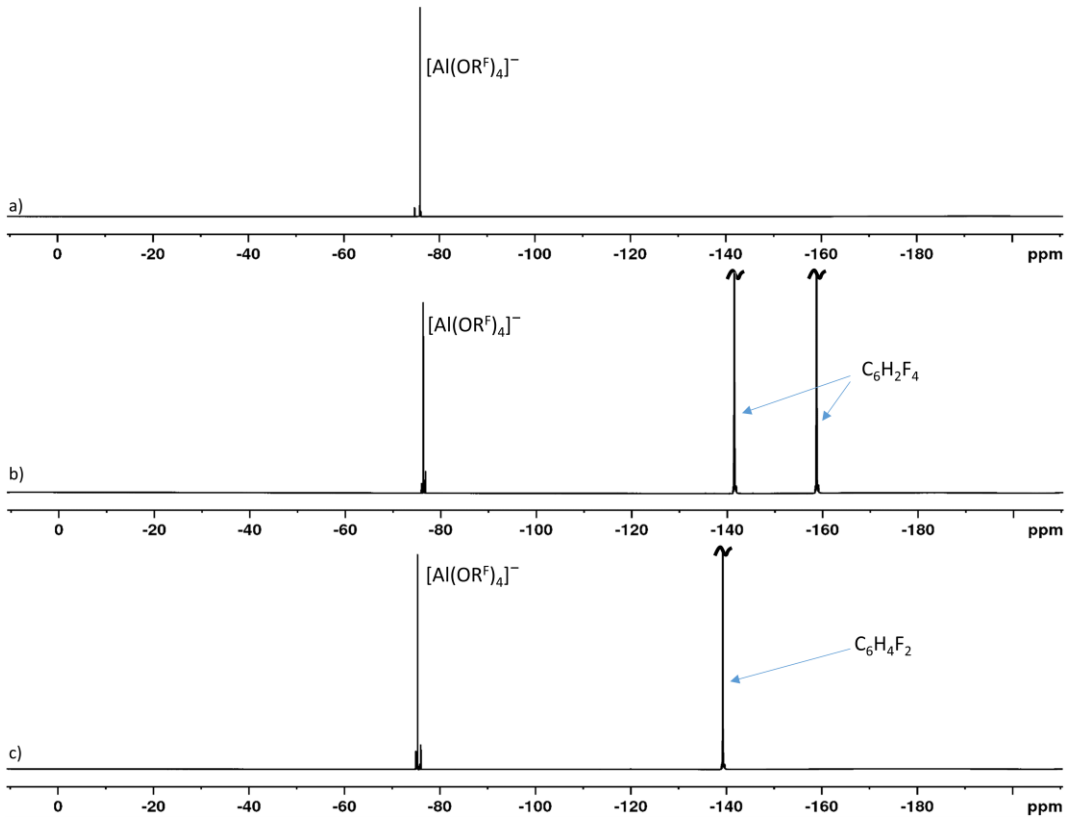

Figure S 31 ^{19}F-NMR spectra (356.4 MHz, in CD_2Cl_2 (a), 1,2,3,4-tfb (b) *o*-dfb (c), 243 K) of the product obtained by the reaction of **1a** with Na[Nb(P$_3$)(ODipp)$_3$]*3THF.

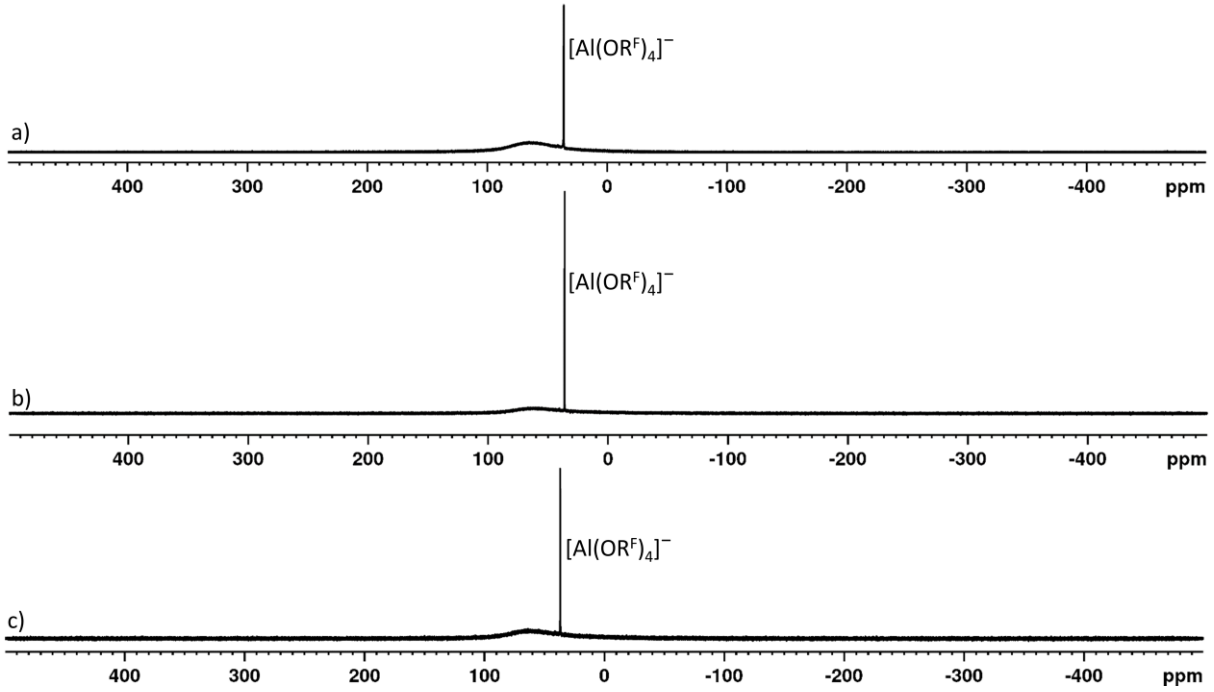

Figure S 32 ^{27}Al-NMR spectra (104.3 MHz, in CD_2Cl_2 (a), 1,2,3,4-tfb (b) *o*-dfb (c), 243 K) of the product obtained by the reaction of **1a** with Na[Nb(P$_3$)(ODipp)$_3$]*3THF.

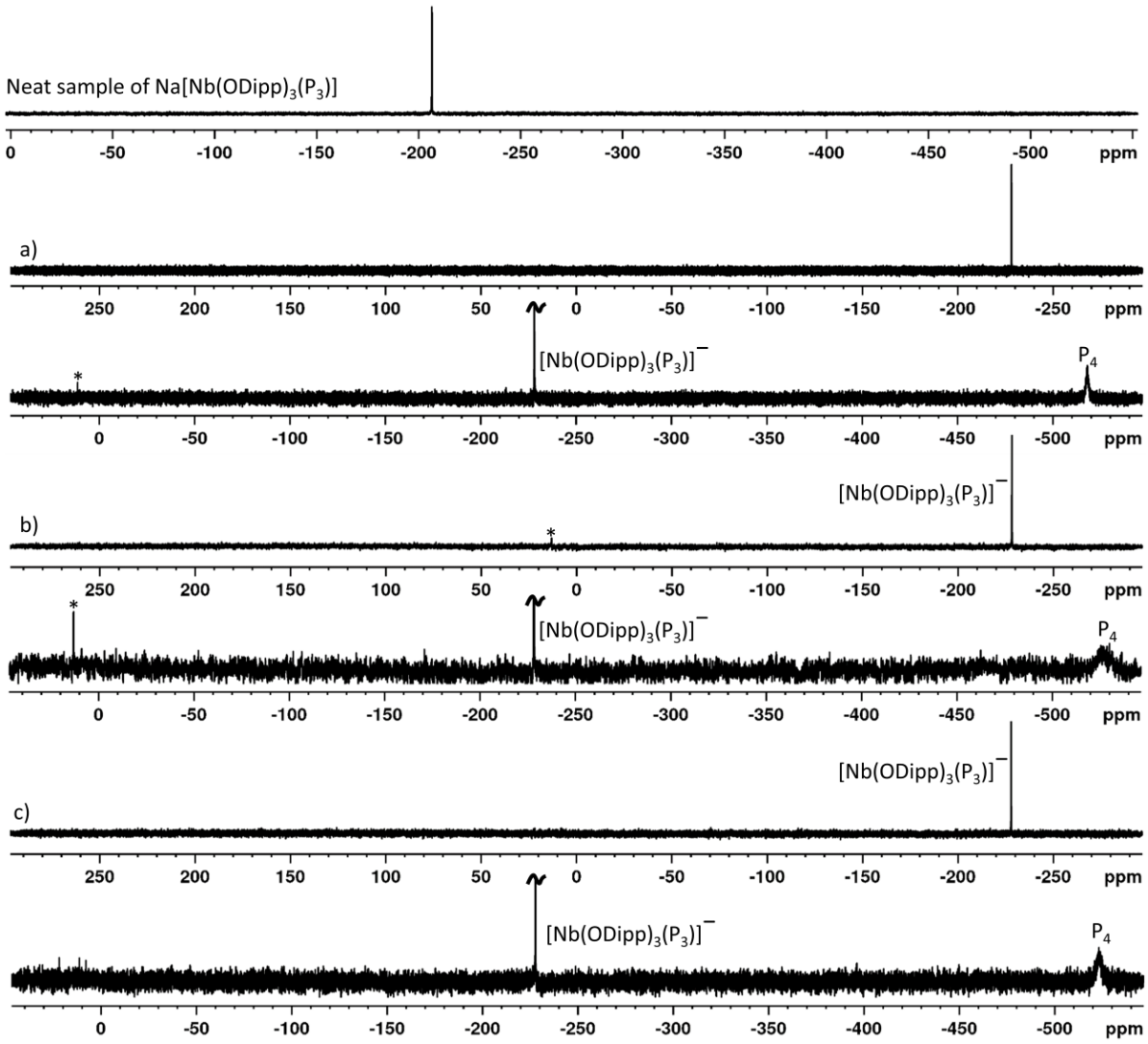

Figure S 33[31]P-NMR spectra (162.0 MHz, in CD_2Cl_2 (a), 1,2,3,4-tfb (b) and *o*-dfb (c), at 243 K) of the product obtained by the reaction of **1a** with Na[Nb(P_3)(ODipp)$_3$]*3THF. The asterisk denotes minor amounts of an unknown substance. For comparison the [31]P spectrum of a neat sample of the used Na[Nb(P_3)(ODipp)$_3$]*3THF in C_6D_6 is shown (top trace).

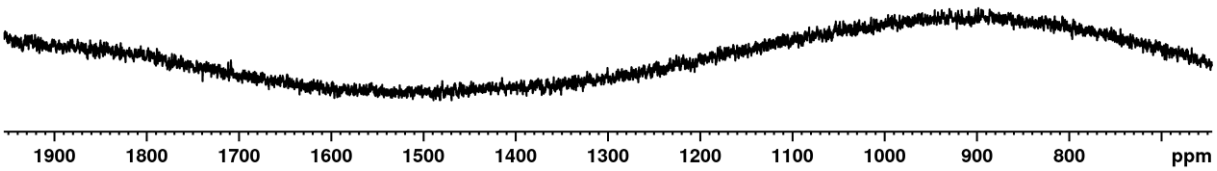

Figure S 34 [77]Se-NMR spectrum (76.4 MHz, 1,2,3,4-tfb, 243 K) of the product obtained by the reaction of **1a** with Na[Nb(P_3)(ODipp)$_3$]*3THF.

3.4. Reactions with White Phosphorus

3.4.1. Solvent Screening

To test if the selectivity of the formation of $[P_3Se]^+$ can be enhanced by choosing a solvent different than CH_2Cl_2, several common solvents (fluorobenzene (= PhF), ortho-difluorobenzene (= *o*-dfb), C_6F_{14}, SO_2, mixture of CH_2Cl_2/CS_2 (9 : 1 / v : v)) were tested for their performance with reactions on an NMR-tube scale. No noteworthy solvent dependency in favor of the formation of $P_3Se[Al(OR^F)_4]$ could be discovered. In the case of fluoroarenes, unselective reactions as well as solvent degradation was observed, several other fluorinated arenes could be detected such as 1-chloro-4-fluorobenzene due to the strongly chlorinating properties of **1a**. The reaction in SO_2 or in C_6F_{14} also led to $[PCl_4]^+$, whereas the reaction in a mixture of CH_2Cl_2 and CS_2 led to no formation of $[P_3Se]^+$ and $[P_5Cl_2]^+$ at all and only other unknown products could be observed. Significant anion decomposition was observed in PhF, *o*-dfb and in the mixture of CH_2Cl_2/CS_2.

Table S 6 Typical product distributions and ratios obtained from the reaction of **1a** with P_4 in different solvents. The ratios are calculated considering all listed products and omitting residual P_4.

Product	*o*-dfb[c]		PhF[c]		SO_2		C_6F_{14}		CH_2Cl_2 / CS_2 (9 : 1)[d]	
	Integral	Ratio	Integral	Ratio	Integral	Ratio	Integral	Ratio	Integral	Ratio
$[P_3Se]^+$	3.1	20 %	2.1	20 %	0.6	5 %	0.3	4 %	—	—
$[P_5Cl_2]^+$[a]	1.0	10 %	—	—	1.0	12 %	1.0	19 %	—	—
$[P_3Se_4]^+$[b]	4.8	47 %	1.6	23 %	1.5	18 %	0.2	4 %	—	—
$[PCl_4]^+$	—	—	1.0	29 %	2.2	53 %	1.7	65 %	—	—
PCl_3	1.2	23 %	1.0	29 %	0.5	12 %	0.2	8 %	Main product	—

[a] The signal of both P_A was integrated, except for the reaction in *o*-dfb, where the signal of P_B was used due to overlaps of other sipdeproducts with the signal of P_A. [b] The signal of both P_B was integrated. [c] When PhF is used, no $[P_5Cl_2]^+$ forms but several other signals belonging to undiscernible side products occur, hence no ratio of $[P_5Cl_2]^+$ to $[P_3Se]^+$ can be given. When *o*-dfb is used, $[P_5Cl_2]^+$ is stable but other undiscernible side products occur.[d] When CS_2 is added, no formation of $[P_5Cl_2]^+$ and $[P_3Se]^+$ occurs, of the usual product, only PCl_3 is observed

Reaction in PhF: 1a (100 mg, 0.09 mmol, 1.0 eq.) and P_4 (11 mg, 0.09 mmol, 1.0 eq.) were weighed in a Schlenk flask and *o*-dfb (1 mL) was condensed onto the solids at −196 °C. The resulting reddish brown mixture was stirred for 10 minutes to allow the P_4 to dissolve. The mixture was transferred into an NMR tube that was flame sealed at −196 °C and subsequently analyzed via NMR-spectroscopy. **NMR:** ^{1}H-NMR (300.2 MHz, PhF, RT): δ = 3.5 (br., 1 H, **H**OC$(CF_3)_3$), 6.67(m, fluorobenzene derivatives), 6.97 (m, fluorobenzene derivatives) ppm. ^{19}F-NMR (282.5 MHz, PhF, RT): δ = −69.7 (m, 6 F, $(\mathbf{F}_3C)_2C(O)CF_2$), −74.8 (s, 36 F, $[Al(O(C(C\mathbf{F}_3)_3)_4]^-$), −75.0 (br., unknown $F_mAl(OC(C\mathbf{F}_3)_3)_n$ moiety), −75.2 (d, 54 F, $[F(Al(OC(C\mathbf{F}_3)_3)_3)_2]^-$, ^5J(F, F) = 0.5 Hz), −75.3 (br., unknown $F_mAl(OC(C\mathbf{F}_3)_3)_n$ moiety), −75.4 (br., 27 F, $[FAl(OC(C\mathbf{F}_3)_3)_3]^-$), −108.9 (m, 2 F, $(F_3C)_2C(O)C\mathbf{F}_2$), −116.3 (tt, 1 F, 1-fluoro-4-chlorobenzene, ^3J(H, F) = 8 Hz, ^4J(H, F) = 5 Hz), −144.0 (br., unknown $\mathbf{F}_mAl(OC(CF_3)_3)_n$ moiety), −152.5 (br., 1 F, $[\mathbf{F}Al(OC(CF_3)_3)_3]^-$), −161.4 (br., unknown $\mathbf{F}_mAl(OC(CF_3)_3)_n$ moiety), −163.1 (br., unknown $\mathbf{F}_mAl(OC(CF_3)_3)_n$ moiety), −172.1 (br., 1 F, $[\mathbf{F}(Al(OC(CF_3)_3)_3)_2]^-$) ppm. ^{27}Al-NMR (78.2 MHz, PhF, RT) δ = 35.2 (s, 1 Al, $[\mathbf{Al}(OC(CF_3)_3)_4]^-$) ppm.

^{31}P-NMR (121.5 MHz, PhF, RT): δ = 219.5 (br., 1 P, **P**Cl_3), 101.6 (m, 1 P, [$\mathbf{P_A}P_2Se_4$]$^+$), 81.7 (br., 1 P, [PCl_4]$^+$), 57.8 (unknown side product), 35.4 (m, 2 P, [P$\mathbf{P_{B2}}Se_4$]$^+$), −60.1 (unknown side product), −284.9 (unknown side product), −293.3 (unknown side product), −301.8 (unknown side product), −373.9 (s, 3 P, [$\mathbf{P}_3$Se]$^+$, ^1J(P, ^{77}Se) = 58 Hz), −524.7 (s, 4 P, $\mathbf{P}_4$) ppm.

Reaction in *o*-dfb: 1a (150 mg, 0.13 mmol, 1.0 eq.) and P_4 (16 mg, 0.13, 1.0 eq.) were weighed in a Schlenk flask and *o*-dfb (1 mL) was condensed onto the solids at −196 °C. The resulting reddish brown mixture was stirred for 5 minutes to allow the P_4 to dissolve. The mixture was transferred into an NMR tube that was flame sealed at −196 °C and subsequently analyzed via NMR-spectroscopy. **NMR:** ^{1}H-NMR (300.2 MHz, *o*-dfb, RT): δ = 3.70 (br., 1 H, **H**$OC(CF_3)_3$), 6.85 (m, difluorobenzene derivatives) ppm. ^{19}F-NMR (376.5 MHz, *o*-dfb, RT): δ = −70.0 (m, 6 F, $(\mathbf{F}_3C)_2C(O)CF_2$), −75.1 (s, 36 F, [$Al(O(C(C\mathbf{F}_3)_3)_4]^-$), −75.3 (br., unknown $F_mAl(OC(C\mathbf{F}_3)_3)_n$ moiety), −75.4 (d, 54 F, [$F(Al(OC(C\mathbf{F}_3)_3)_3)_2]^-$, ^5J(F, F) = 0.6 Hz), −75.5 (br., unknown $F_mAl(OC(C\mathbf{F}_3)_3)_n$ moiety), −75.6 (br., 27 F, [$FAl(OC(C\mathbf{F}_3)_3)_3]^-$), −113.7 (m, 2 F, $(F_3C)_2C(O)C\mathbf{F}_2$), −135.7 3 (m, difluorobenzene derivative), −140.9 (m, difluorobenzene derivative), −152.8 (br., 1 F, [**F**$Al(OC(CF_3)_3)_3]^-$), −161.7 (br., unknown $\mathbf{F}_mAl(OC(CF_3)_3)_n$ moiety), −163.0 (br., unknown $\mathbf{F}_mAl(OC(CF_3)_3)_n$ moiety), −172.2 (br., 1 F, [**F**$(Al(OC(CF_3)_3)_3)_2]^-$) ppm. ^{27}Al-NMR (78.2 MHz, *o*-dfb, RT) δ = 35.0 (s, 1 Al, [**Al**$(OC(CF_3)_3)_4]^-$), −12.3 (br. unknown aluminate) ppm. ^{31}P-NMR (121.5 MHz, *o*-dfb, RT): δ = 219.9 (br., 1 P, **P**Cl_3), 176.7 (unknown), 158.9 (dt, 2 P, [$P_2\mathbf{P_{B2}}PCl_2$]$^+$, $^1J(^{31}P_B, ^{31}P_C)$ = 340 Hz, $^1J(^{31}P_A, ^{31}P_B)$ = 143 Hz), 124.2 (unknown), 96.8 (m, 1 P, [$\mathbf{P_A}P_2Se_4$]$^+$), 53.3 (tt, 1 P, [$P_4\mathbf{P_C}Cl_2$]$^+$, $^1J(^{31}P_B, ^{31}P_C)$ = 340 Hz, $^2J(^{31}P_A, ^{31}P_C)$ = 27 Hz), 38.2 (unknown), 29.2 (m, 2 P, [P$\mathbf{P_{B2}}Se_4$]$^+$), 8.2 (unknown), −64.4 (unknown), −256.9 (unknown), −282.9 (td, 2 P, [$\mathbf{P_{A2}}P_3Cl_2$]$^+$, $^1J(^{31}P_A, ^{31}P_B)$ = 143 Hz, $^2J(^{31}P_A, ^{31}P_C)$ = 27 Hz), −285.3 (unknown), −381.7 (s, 3 P, [$\mathbf{P}_3$Se]$^+$, ^1J(P, ^{77}Se) = 58 Hz), −527.1 (s, 4 P, $\mathbf{P}_4$) ppm.

Reaction in SO_2: 1a (150 mg, 0.13 mmol, 1.0 eq.) and P_4 (16 mg, 0.13, 1.0 eq.) were weighed in a sealable J. Young NMR tube and SO_2 (0.7 mL) was condensed onto the solids at −196 °C. The resulting mixture immediately took a reddish brown color and analyzed via NMR-spectroscopy. **NMR:** ^{19}F-NMR (376.5 MHz, SO_2, RT): δ = −75.7 (s, 36 F, [$Al(OC(C\mathbf{F}_3)_3)_4]^-$) ppm. ^{27}Al-NMR (104.3 MHz, SO_2, RT) δ = 34.1 (s, 1 Al, [**Al**$(OC(CF_3)_3)_4]^-$) ppm. ^{31}P-NMR (162.0 MHz, SO_2, RT): δ = 221.2 (br., 1 P, **P**Cl_3), 156.8 (dt, 2 P, [$P_2\mathbf{P_{B2}}PCl_2$]$^+$, $^1J(^{31}P_B, ^{31}P_C)$ = 340 Hz, $^1J(^{31}P_A, ^{31}P_B)$ = 144 Hz), 96.3 (m, 1 P, [$\mathbf{P_A}P_2Se_4$]$^+$), 87.9 (br., 1 P, [PCl_4]$^+$), 56.3 (tt, 1 P, [$P_4\mathbf{P_C}Cl_2$]$^+$, $^1J(^{31}P_B, ^{31}P_C)$ = 340 Hz, $^2J(^{31}P_A, ^{31}P_C)$ = 27 Hz), 29.9 (m, 2 P, [P$\mathbf{P_{B2}}Se_4$]$^+$), −276.7 (td, 2 P, [$\mathbf{P_{A2}}P_3Cl_2$]$^+$, $^1J(^{31}P_A, ^{31}P_B)$ = 144 Hz, $^2J(^{31}P_A, ^{31}P_C)$ = 27 Hz), −376.0 (s, 3 P, [$\mathbf{P}_3$Se]$^+$, ^1J(P, ^{77}Se) = 58 Hz), −516.5 (s, 4 P, $\mathbf{P}_4$) ppm.

Reaction in C_6F_{14}: $Ag[Al(OR^F)_4]$ (100 mg, 0.09 mmol, 1.0 eq.) and P_4 (12 mg, 0.09 mmol, 1.0 eq.) were weighed on one side of a double bulb Schlenk vessel without a glass frit separating both glass tubes. $SeCl_4$ (21 mg, 0.09 mmol, 1.0 eq.) was weighed into the other side of the reaction vessel. Thoroughly degassed C_6F_{14} (10 mL, 6 freeze/pump/thaw cycles) was condensed into the side containing the silver salt and the white phosphorus and stirred vigorously for 10 min. The obtained suspension was then poured onto the $SeCl_4$ and stirred for 2 d. After this time, an orange precipitate formed above a colorless solution. All volatiles were removed *in vacuo* and SO_2 was condensed onto the obtained solids and the obtained mixture was stirred vigorously for 5 min. Afterwards, the small amount of orange red precipitate was allowed to settle and the obtained orange solution was decanted to the other side of the reaction vessel. After removing all the volatiles *in vacuo* an orange solid was obtained that was dissolved in SO_2 and analyzed via NMR spectroscopy. **NMR:** ^{19}F-NMR (188.3 MHz, SO_2, RT): δ = −74.9 (s, 9 F, $HOC(C\mathbf{F}_3)_3$), −75.7 (s, 36 F, $[Al(OC(C\mathbf{F}_3)_3)_4]^-$) ppm. ^{31}P-NMR (81.0 MHz, SO_2, RT): δ = 221.2 (br., 1 P, $\mathbf{P}Cl_3$), 156.8 (dt, 2 P, $[P_2\mathbf{P_{B2}}PCl_2]^+$, $^1J(^{31}P_B, ^{31}P_C)$ = 340 Hz, $^1J(^{31}P_A, ^{31}P_B)$ = 144 Hz), 96.6 (m, 1 P, $[\mathbf{P_A}P_2Se_4]^+$), 87.9 (br., 1 P, $[PCl_4]^+$), 56.4 (tt, 1 P, $[P_4\mathbf{P_C}Cl_2]^+$, $^1J(^{31}P_B, ^{31}P_C)$ = 340 Hz, $^2J(^{31}P_A, ^{31}P_C)$ = 27 Hz), 30.3 (m, 2 P, $[P\mathbf{P_{B2}}Se_4]^+$), −276.2 (td, 2 P, $[\mathbf{P_{A2}}P_3Cl_2]^+$, $^1J(^{31}P_A, ^{31}P_B)$ = 144 Hz, $^2J(^{31}P_A, ^{31}P_C)$ = 27 Hz), −375.4 (s, 3 P, $[\mathbf{P}_3Se]^+$, ^1J(P, ^{77}Se) = 58 Hz), −508.6 (s, 4 P, $\mathbf{P}_4$) ppm.

Reaction in a CH_2Cl_2 / CS_2 mixture: 1a (240 mg, 0.21 mmol, 1.0 eq.) was weighed in Schlenk flask ans dissolved in CH_2Cl_2 (4 mL), P_4 (35 mg, 0.28, 1.3 eq.) was dissolved in a mixture of CH_2Cl_2 and CS_2 (6 mL, 5/1 (v/v)) and was added dropwise using a glass funnel to the solution of **1a**. The resulting mixture immediately took a yellow color and. After stirring for 17 h, the volume of the solution was reduced *in vacuo* 1 mL and transferred into a sealable J. Young NMR tube and analyzed via NMR-spectroscopy. **NMR:** ^{19}F-NMR (282.5 MHz, CH_2Cl_2/CS_2 (9:1 (v/v)), RT): δ = −74.5 (s, 9 F, $HOC(C\mathbf{F}_3)_3$), −75.6 (s, 36 F, $[Al(OC(C\mathbf{F}_3)_3)_4]^-$), −75.6 (s, unknown), −75.7 (d, 54 F, $[F(Al(OC(C\mathbf{F}_3)_3)_3)_2]^-$, ^5J(F, F) = 0.6 Hz), −75.8 (d, $[FAl(OC(C\mathbf{F}_3)_3)_3]^-$, ^5J(F, F) = 2 Hz) ppm. ^{27}Al-NMR (78.2 MHz, CH_2Cl_2/CS_2 (9:1 (v/v)), RT) δ = 34.6 (s, 1 Al, $[\mathbf{Al}(OC(CF_3)_3)_4]^-$) ppm. ^{31}P-NMR (121.5 MHz, CH_2Cl_2/CS_2 (9:1 (v/v)), RT): δ = 219.0 (br., 1 P, $\mathbf{P}Cl_3$), 106.2 (m, 1 P, $[\mathbf{P_A}P_2Se_4]^+$), 40.4 (m, 2 P, $[P\mathbf{P_{B2}}Se_4]^+$), 39.6 (br. 1 P, possibly $PSCl_3$, *fwhm* (full width at half maximum) = 30 Hz), 31.4 (q., 1 P, unknown, J(P, P) = 72 Hz), −112.6 (d., 3 P, unknown, J(P, P) = 72 Hz), −119.0 (d, unknown, J(P, X) = 27 Hz), −520.4 (s, 4 P, $\mathbf{P}_4$) ppm.

NMR spectra of the Reactions in different solvents

in PhF

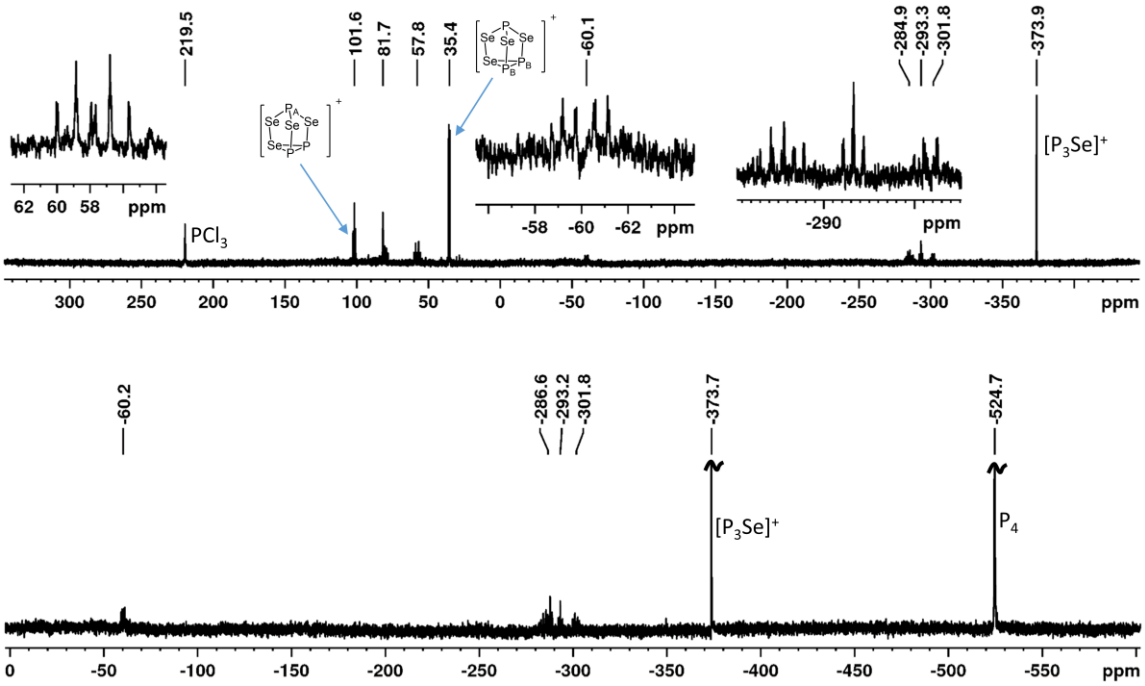

Figure S 35 ^{31}P-NMR spectra (121.5 MHz, PhF, RT) of the product obtained by the reaction of **1a** with P_4 in PhF from 350 to −400 ppm (top trace) and from 0 to –600 ppm (bottom trace). The non-labeled peaks correspond to unknown side products.

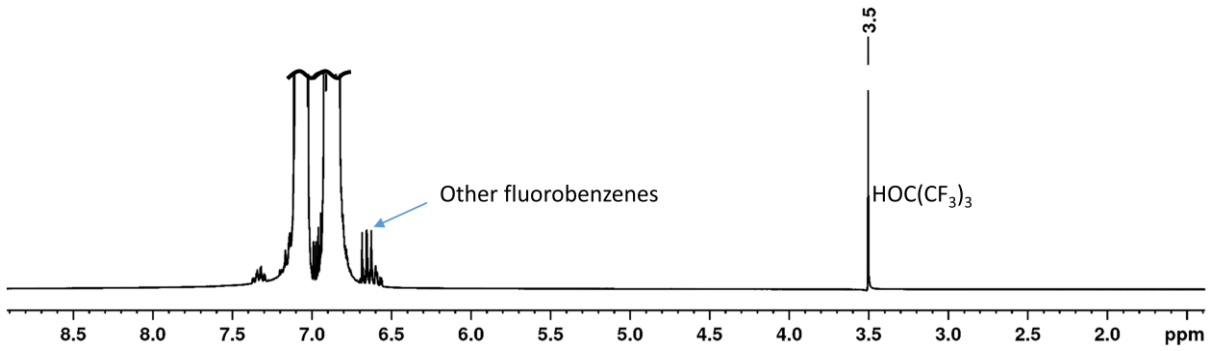

Figure S 36 ^{1}H-NMR spectrum (300.2 MHz, PhF, RT) of the product obtained by the reaction of **1a** with P_4 in PhF. The blue arrow marks fluorobenzene derivatives generated during the course of this reaction not present in the crude spectra of the used solvent. Between both signals of PhF are also signals of flurobenzene derivatives generated during the course of the reaction.

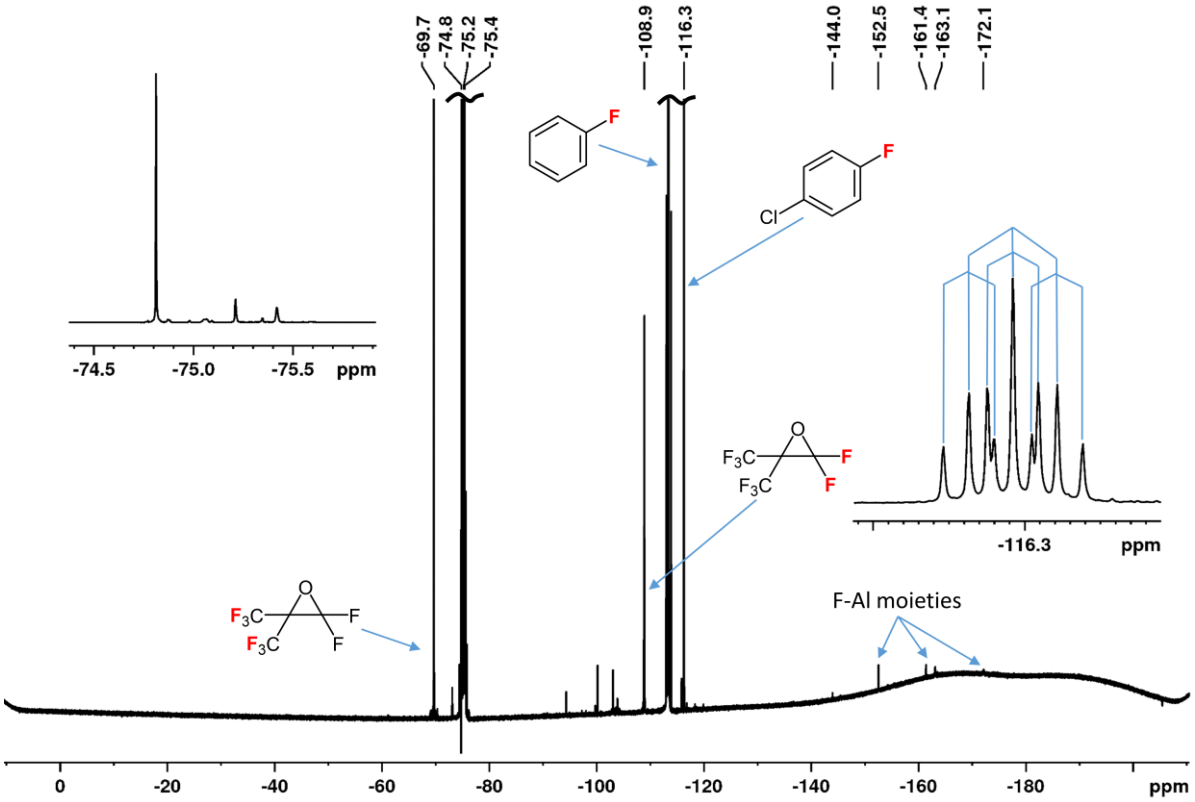

Figure S 37 ^{19}F-NMR spectrum (282.5 MHz, PhF, RT) of the product obtained by the reaction of **1a** with P_4 in PhF. The zoomed in part on the right shows the splitting pattern of 1-chloro-4-fluorobenzene.

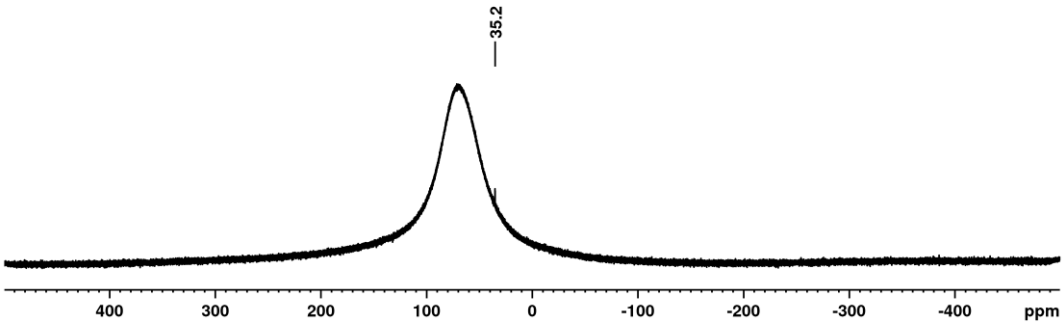

Figure S 38 ^{27}Al-NMR spectrum (78.2 MHz, PhF, RT) of the product obtained by the reaction of **1a** with P_4 in PhF. The broad resonance at 70 ppm stems from the probe head.

in *o*-dfb

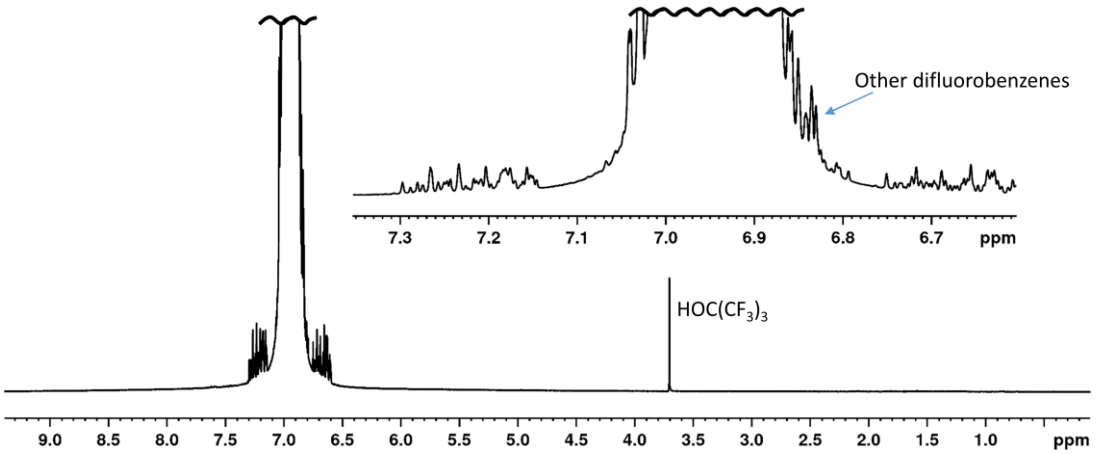

Figure S 39 ^{1}H-NMR spectrum (300.2 MHz, *o*-dfb, RT) of the product obtained by the reaction of **1a** with P_4 in PhF. The blue arrow marks difluorobenzene derivatives generated during the course of the reaction not present in the crude spectra of the used solvent.

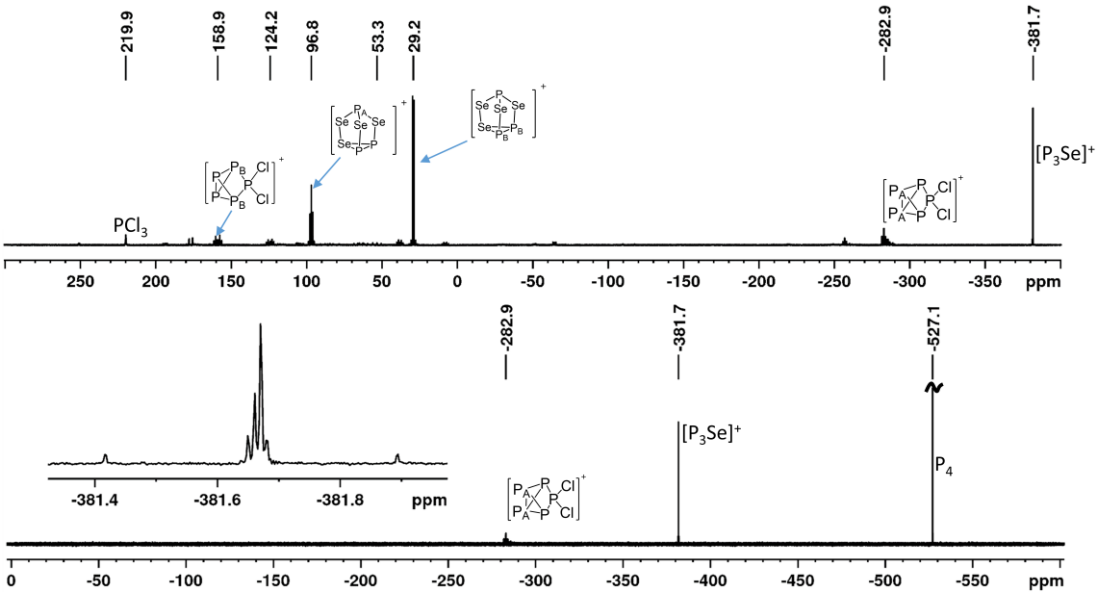

Figure S 40 ^{31}P-NMR spectra (121.5 MHz, *o*-dfb, RT) of the product obtained by the reaction of **1a** with P_4 in *o*-dfb from 300 to 400 ppm (top trace) and from 0 to –600 ppm (bottom trace).

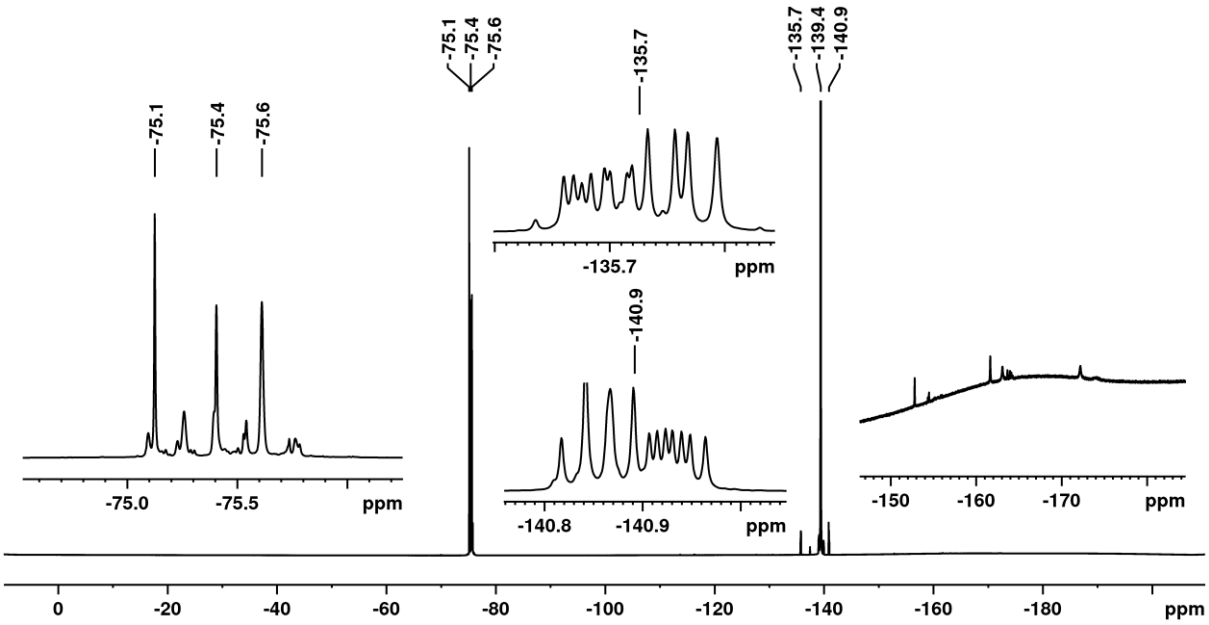

Figure S 41 ^{19}F-NMR spectrum (282.5 MHz, *o*-dfb, RT) of the product obtained by the reaction of **1a** with P_4 in *o*-dfb. Very weak peaks of the epoxide and unknown $F_mAl(OR^F)_n$ moieties are not separately shown here but listed in the table of the experimental part.

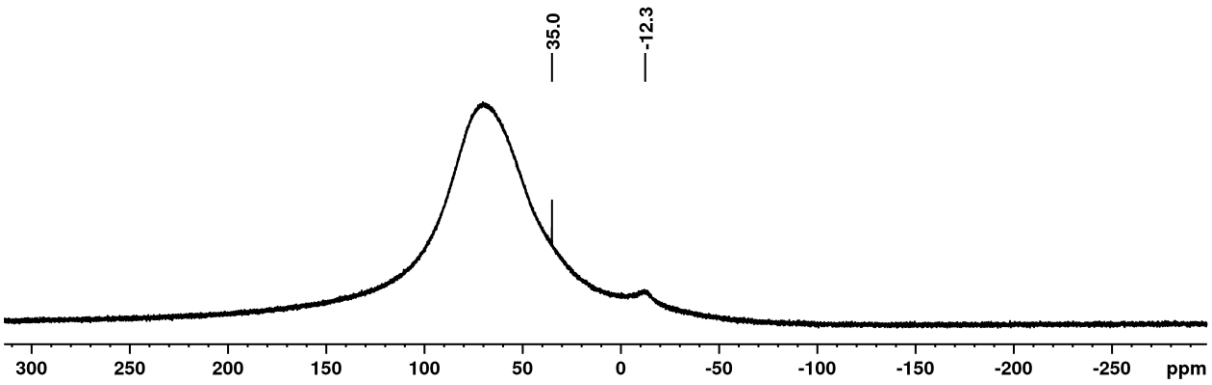

Figure S 42 ^{27}Al-NMR spectrum (78.2 MHz, *o*-dfb, RT) of the product obtained by the reaction of **1a** with P_4 in *o*-dfb. The broad resonance at 70 ppm stems from the probe head.

in SO_2

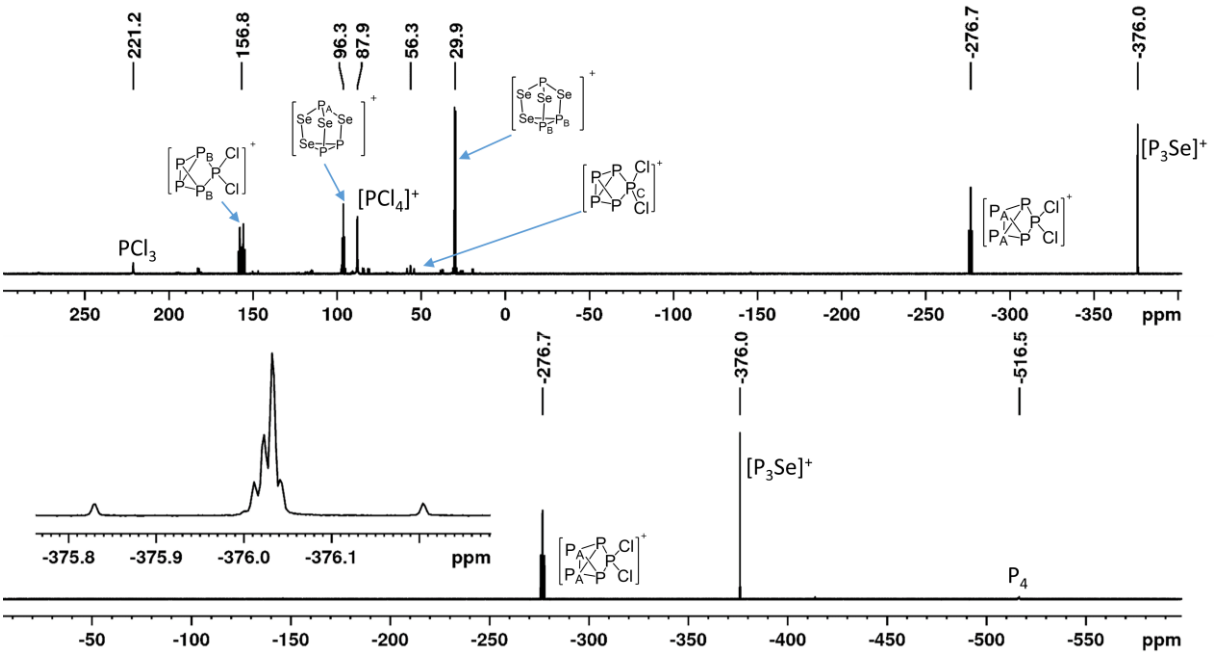

Figure S 43 ^{31}P-NMR spectra (162.0 MHz, SO_2, RT) of the product obtained by the reaction of **1a** with P_4 in SO_2 from 300 to 400 ppm (top trace) and from 0 to –600 ppm (bottom trace).

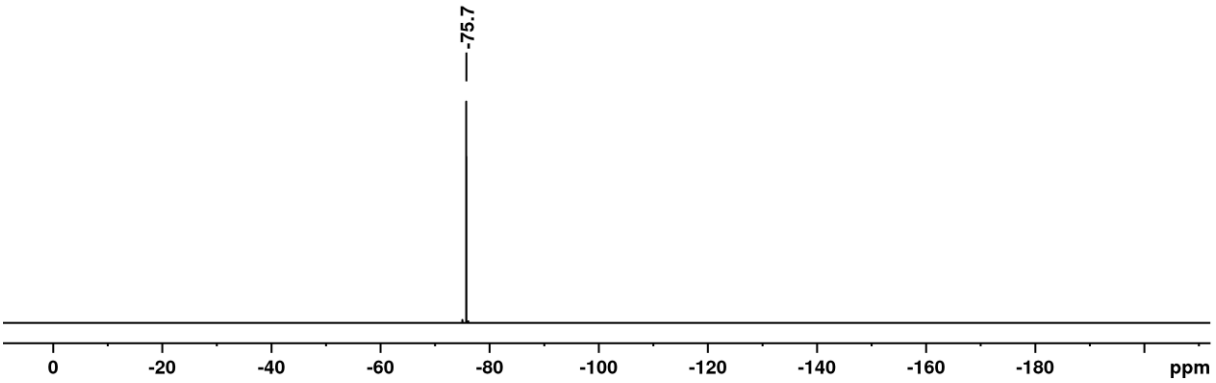

Figure S 44 ^{19}F-NMR spectrum (376.5 MHz, SO_2, RT) of the product obtained by the reaction of **1a** with P_4 in SO_2.

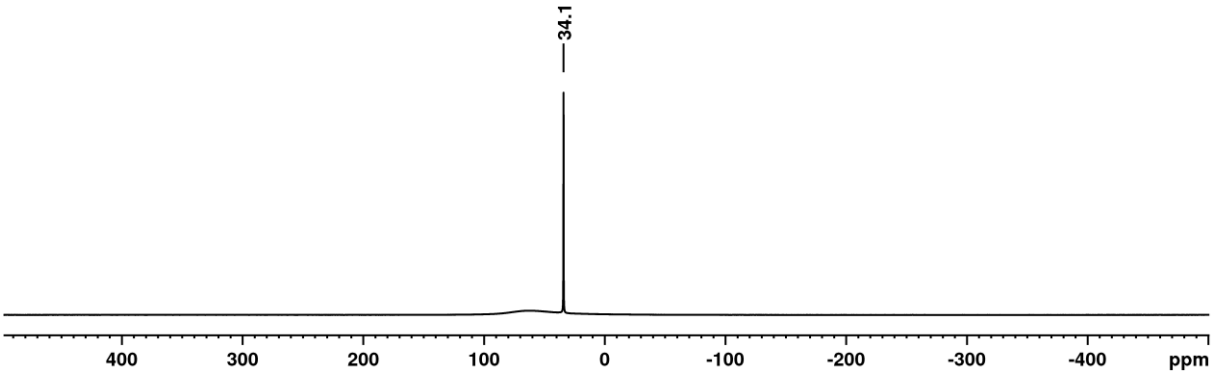

Figure S 45 ^{27}Al-NMR spectrum (104.3 MHz, SO_2, RT) of the product obtained by the reaction of **1a** with P_4 in SO_2. The broad resonance at 70 ppm stems from the probe head.

in C_6F_{14}

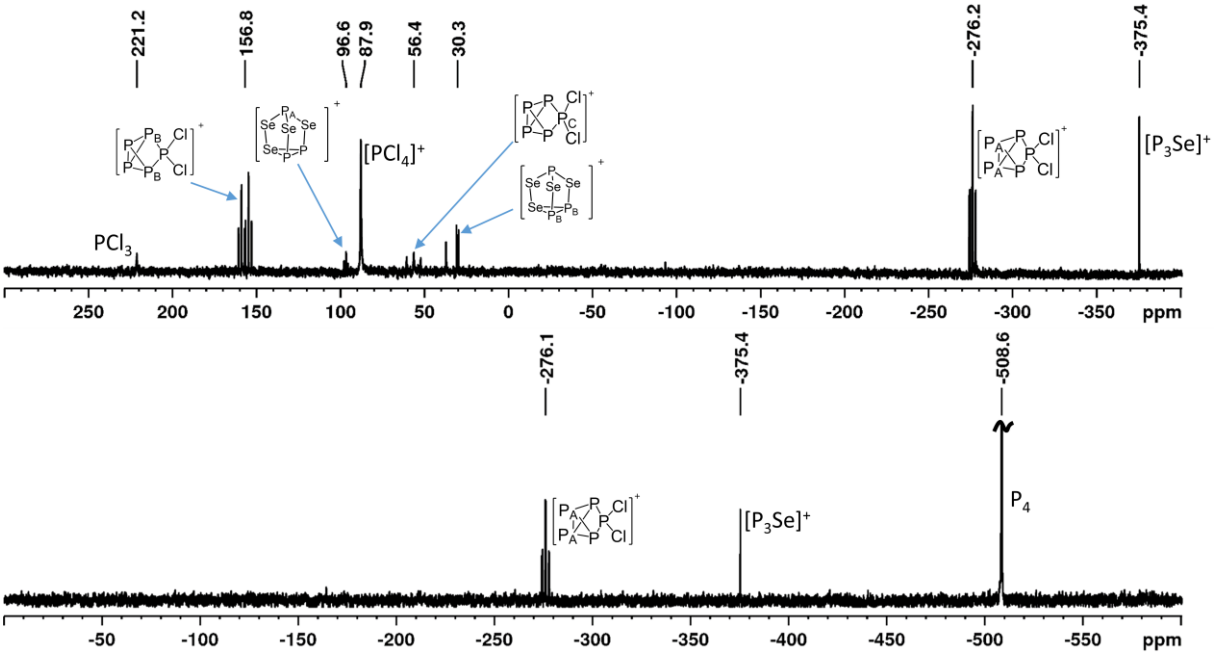

Figure S 46 ^{31}P-NMR spectra (81.0 MHz, SO_2, RT) of the product obtained by the reaction of **1a** with P_4 in C_6F_{14} after extraction with SO_2 from 300 to 400 ppm (top trace) and from 0 to –600 ppm (bottom trace).

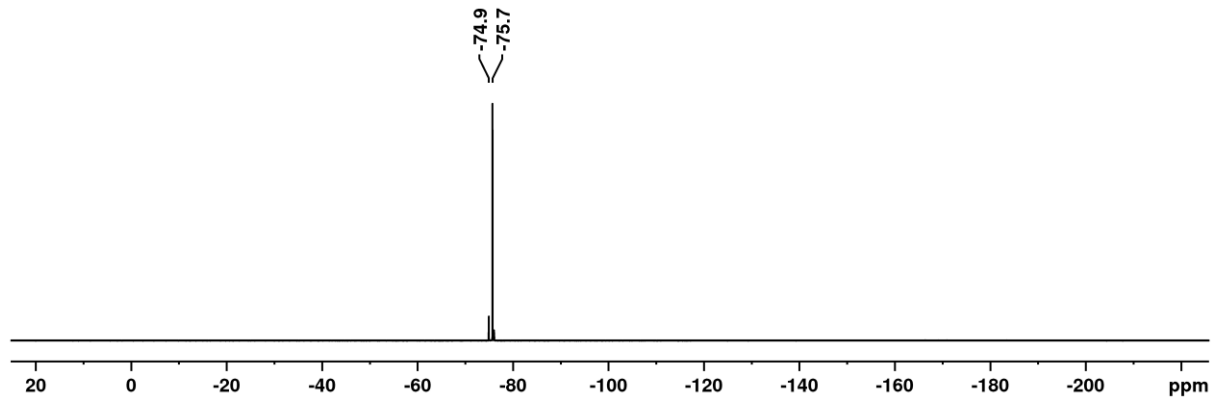

Figure S 47 ^{19}F-NMR spectrum (188.3 MHz, SO_2, RT) of the product obtained by the reaction of **1a** with P_4 in C_6F_{14} after extraction with SO_2.

in a CH_2Cl_2 / CS_2 mixture (9 : 1)

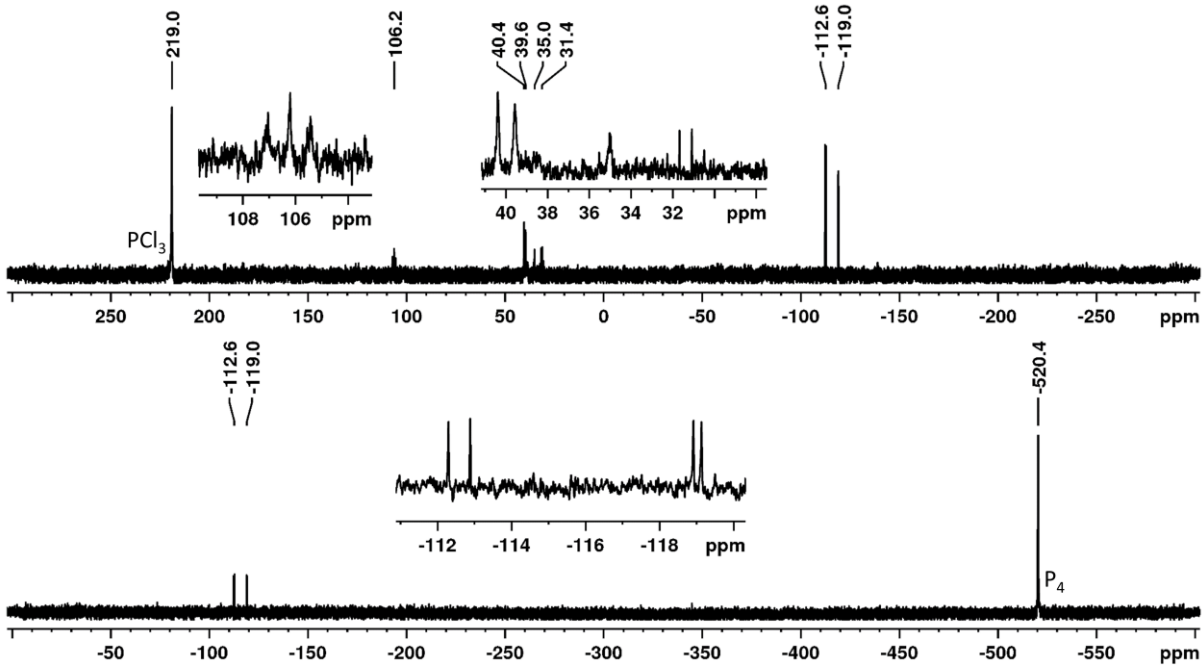

Figure S 48 ^{31}P-NMR spectra (121.5 MHz, CH_2Cl_2/CS_2 (9:1), RT) of the product obtained by the reaction of **1a** with P_4 in a mixture of CS_2/CH_2Cl_2 (1 : 9) from 300 to −300 ppm (top trace) and from 0 to –600 ppm (bottom trace).

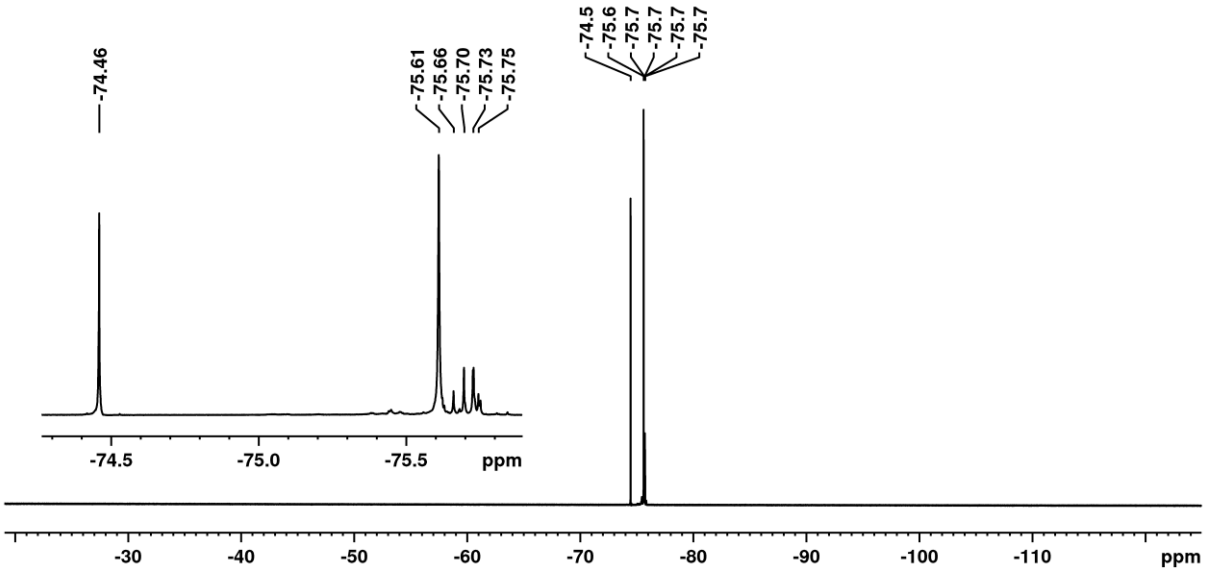

Figure S 49 ^{19}F-NMR spectrum (282.5 MHz, CH_2Cl_2/CS_2 (9:1), RT) of the product obtained by the reaction of **1a** with P_4 in a mixture of CS_2/CH_2Cl_2 (1 : 9). The broad signal of $[F(Al(ORF)_3)_2]^-$ at −185 ppm could not be detected due to the low amount of this substance in the sample.

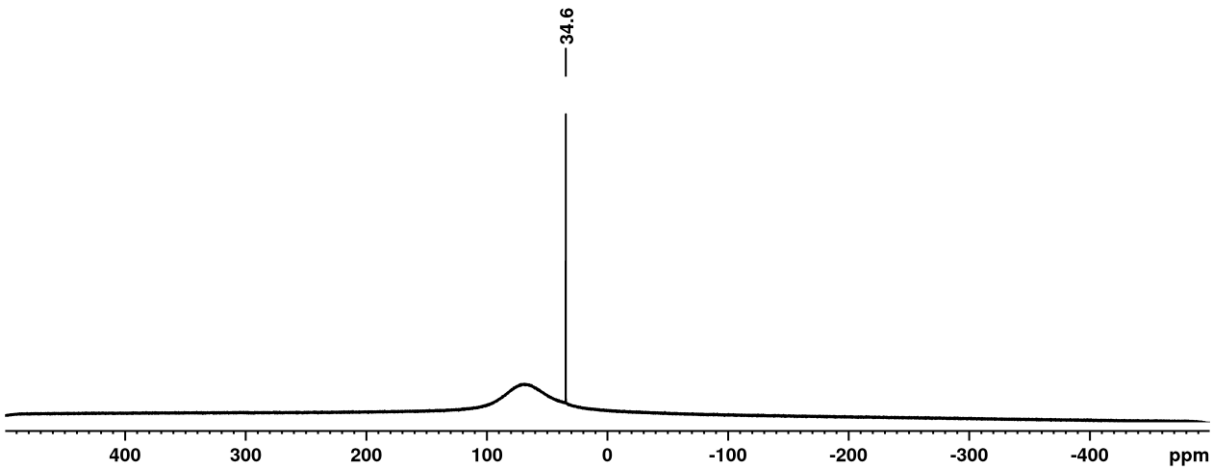

Figure S 50 ^{27}Al-NMR spectrum (78.2 MHz, CH_2Cl_2/CS_2 (9:1), RT) of the product obtained by the reaction of **1a** with P_4 in a mixture of CS_2/CH_2Cl_2 (1 : 9). The broad resonance at 70 ppm stems from the probe head.

3.4.2. Anion screening

To test the necessity of well performing WCAs and test performance of different anions for the generation of $[P_3Se]^+$ salts and to possibly improve the selectivity of the target reaction $SeCl_3[AlCl_4]$ as well as $SeCl_3[F(Al(OR^F)_3)_2]$ (**1b**) and $SeCl_3[FAl(OR^F)_3)]$ (**1c**) were tested next to $SeCl_3[Al(OR^F)_4]$. **1c** uses the basic anion $[FAl(OR^F)_3]^-$ that has shown its advantages compared to $[Al(OR^F)_4]^-$ and $[F(Al(OR^F)_3)_2]^-$ in terms of single crystal structures, yielding excellent structural data without superstructure or disorder.

Reaction of $SeCl_3[AlCl_4]$ with P_4

$SeCl_3[AlCl_4]$ (35 mg, 0.10 mmol, 1 eq.) and a piece of P_4 (12 mg, 0.10 mmol, 1 eq.) were weighed together into a J. Young sealable NMR tube so that both reactands are not in immediate contact. The NMR tube was then cooled down to −196 °C before letting the P_4 slide down onto the $SeCl_3[AlCl_4]$ to avoid both reactands from already reacting upon contact of the powders as it was observed in a previous reaction. CD_2Cl_2 (0.7 ml) was condensed onto the solids and the reaction mixture was vigorously shaken. **NMR:** ^{31}P-NMR (81.0 MHz, CD_2Cl_2, RT): δ = −523.4 (s, $P_{4/dissolved}$), −459.7 (br. $P_{4/solid}$), 84.5(s, $[PCl_4]^+$), 219.3 (br., PCl_3) ppm.

The pale yellow solution turned red, presumably of precipitated Se_{red} generated through reduction of $[SeCl_3]^+$ with P_4 and was analyzed via NMR spectroscopy. The main products were PCl_3 as well as $PCl_4[AlCl_4]$ along with trace amounts of $[P_3Se]^+$ (<1 %) (Figure S 51).

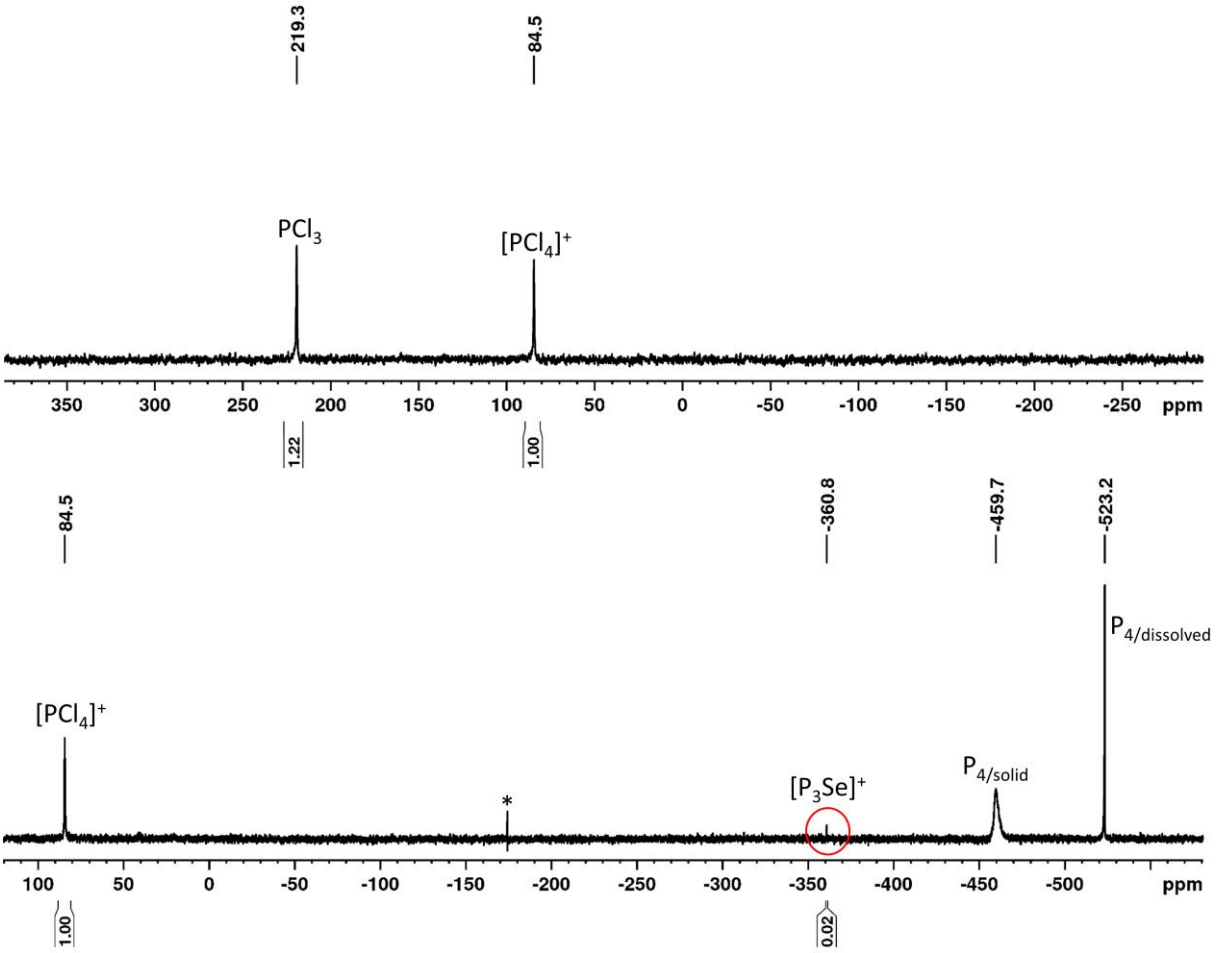

Figure S 51 ^{31}P-NMR spectra (81.0 MHz, CD_2Cl_2, RT) of the product obtained by the reaction of $SeCl_3[AlCl_4]$ with P_4 from 400 to −300 ppm (top trace) and from 120 to –580 ppm (bottom trace). The asterisk denotes an artifact.

Reaction of $SeCl_3[FAl(OR^F)_3]$ (1c) with P_4

P_4 (25 mg, 0.2 mmol, 0.9 eq.) was added to a solution of **1c** (200 mg, 0.21 mmol, 1.0 eq.) in CH_2Cl_2 (1 mL) in a sealable NMR-tube with a J. Young valve and vigorously shaken. The initially yellow solution quickly turned orange and was analyzed via NMR-spectroscopy. **NMR:** ^{19}F-NMR (282.5 MHz, CH_2Cl_2, RT): δ = −58.4 (ddec., 4 F, P**F**$_4$OC(CF$_3$)$_3$,), ^1J(P, F) = 926 Hz, ^5J(F, F) = 5 Hz), −66.5 (d, 3 F, P**F**$_3$X$_2$, ^1J(P, F) = 947 Hz), −71.7 (quintd., 9 F, PF$_4$OC(C**F**$_3$)$_3$, ^5J(F, F) = 5 Hz, ^4J(P, F) = 1.5 Hz), −74.7 (s, 9 F, HOC(C**F**$_3$)$_3$), −75.7 (s, 36 F, [Al(OC(C**F**$_3$)$_3$)$_4$]$^-$), −75.8 (s, 54 F, [F(Al(OC(C**F**$_3$)$_3$)$_3$)$_2$]$^-$), −75.9 (s, 27 F, [FAl(OC(C**F**$_3$)$_3$]$^-$), −80.2 (d, 2 F, P**F**$_2$X, ^1J(P, F) = 1060 Hz), −86.1 (d, 2 F, P**F**$_2$X, ^1J(P, F) = 973 Hz), −89.5 (d, 1 F, P**F**X$_2$, ^1J(P, F) = 1074 Hz), −168.6 (br, 1F, [**F**Al(OC(CF$_3$)$_3$]$^-$), −184.9 (br, 1F, [**F**(Al(OC(CF$_3$)$_3$)$_2$]$^-$) ppm. ^{27}Al-NMR (78.2 MHz, CH_2Cl_2, RT): δ = 38.8 (br., 1 Al, [F(**Al**(OR^F)$_3$]$^-$), 34.7 (s., 1 Al, [**Al**(OR^F)$_4$]$^-$), 32.1 (s., 2 Al, [F(**Al**(OR^F)$_3$)$_2$]$^-$) ppm. ^{31}P-NMR (121.5 MHz, CH_2Cl_2, RT): δ = 87.1(br., 1 P, **P**F$_3$ complexes), −37.5 (t, 1 P, **P**F$_2$X, ^1J(P, F) = 973 Hz), −39.1 (d, 1 P, **P**FX$_2$, ^1J(P, F) = 1074 Hz), −39.3 (t, 1P **P**F$_2$X, ^1J(P, F) = 1060 Hz), −79.1 (q, 1 P, **P**F$_3$X$_2$, ^1J(P, F) = 947 Hz), −80.4 (quintdec, 1 P, **P**F$_4$OC(CF$_3$)$_3$, ^1J(P, F) = 926 Hz, ^4J(P, F) = 1.5 Hz), −82.4 (d, 1 P, **P**FX$_4$, ^1J(P,

F) = 895 Hz) ppm. ^{77}Se-NMR (57.2 MHz, CH_2Cl_2, RT): no signal detected.

No $[P_3Se]^+$ was detected. Several decomposition products containing PF, PF_2, PF_3 and PF_4 groups form such as $PF_4OC(CF_3)_3$, which can be deduced from the characteristic splittings of the resonances in the ^{31}P spectra showing ^1J(P, F) couplings. The broad resonance at −87.1 ppm in the ^{31}P-NMR spectrum most likely stems from PF_3 that undergoes quick exchange reactions. The broad resonance from −50 to −90 ppm in the ^{19}F-spectrum can also most likely be assigned to these substances. The other decomposition products are also visible in the ^{19}F-NMR spectra. The ^{27}Al-spectra indicate nearly complete decomposition of the $[FAl(OR^F)_3]^-$ anion, resulting in the formation of $[F(Al(OR^F)_3)_2]^-$ and a small amount of $[Al(OR^F)_4]^-$ anion. The ^{77}Se-NMR spectrum did not show any resonances of the $[SeCl_3]^+$ cation, indicating that all $[SeCl_3]^+$ was consumed. The $[F\text{-}Al(OR^F)_3]^-$ anion is labile towards fluoride abstraction by the generated cations.

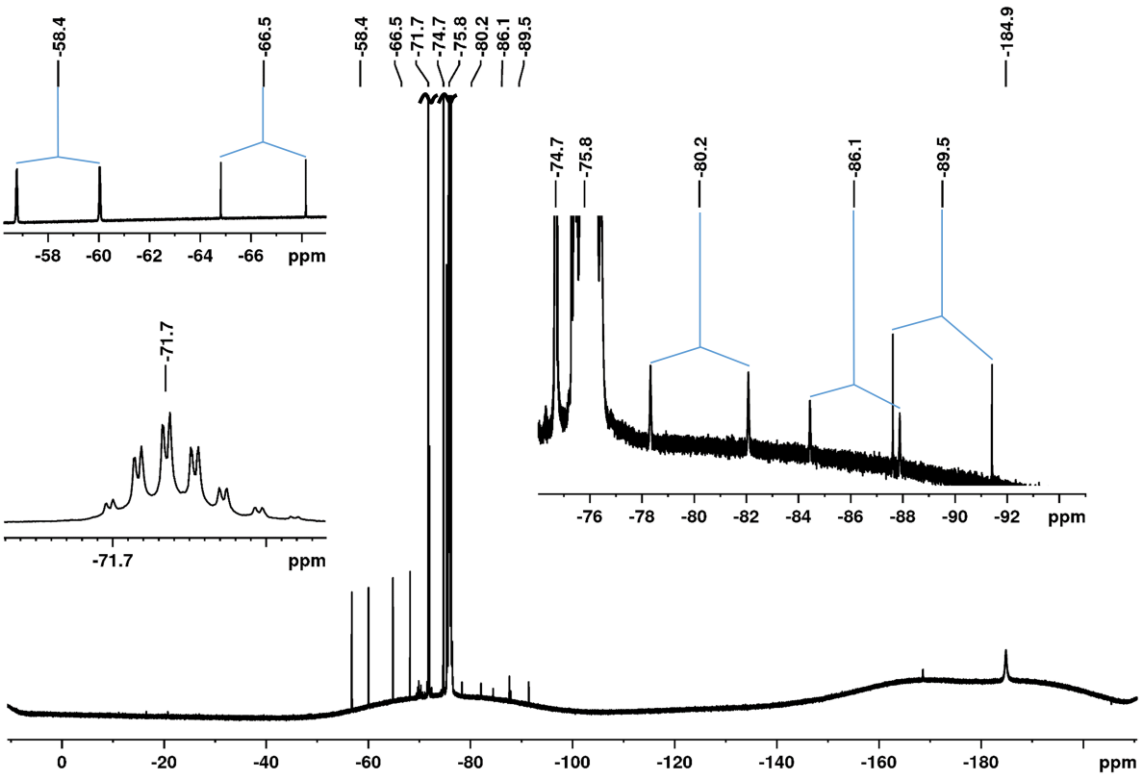

Figure S 52 ^{19}F-NMR spectrum (282.5 MHz, CH_2Cl_2, RT) of the product obtained by the reaction of **1c** with P_4.

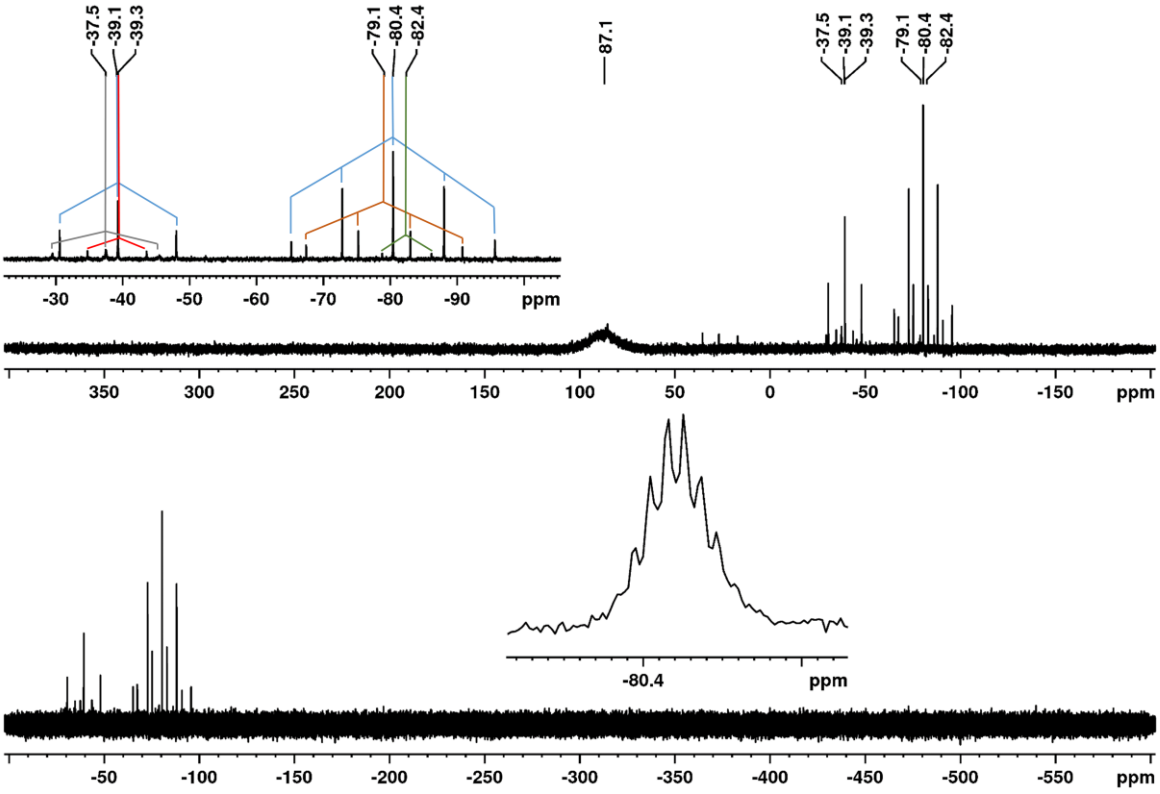

Figure S 53 ^{31}P-NMR spectra (121.5 MHz, CH_2Cl_2, RT) of the product obtained by the reaction of $SeCl_3[AlCl_4]$ with P_4 from 400 to −200 ppm (top trace) and from 0 to –600 ppm (bottom trace). The inset in the bottom trace shows the decett splitting of PF_4OR^F.

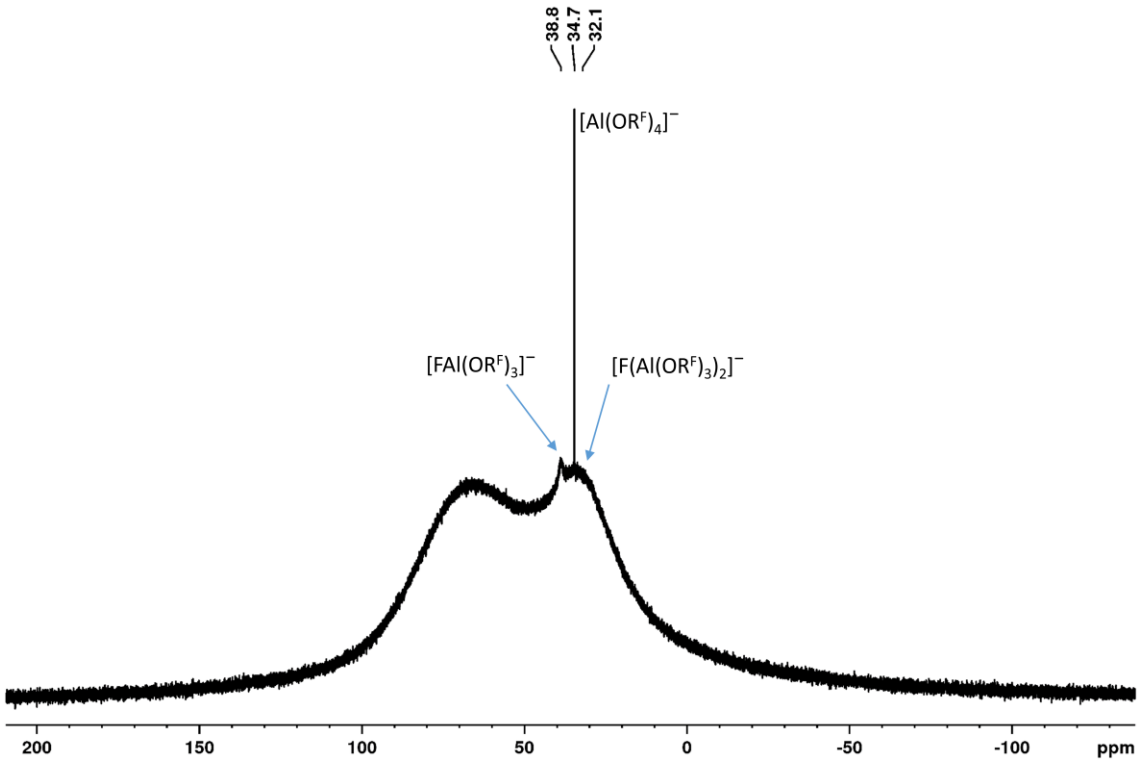

Figure S 54 ^{27}Al-NMR spectrum (78.2 MHz, CH_2Cl_2, RT) of the product obtained by the reaction of **1c** with P_4. The broad resonance at 70 ppm stems from the probe head.

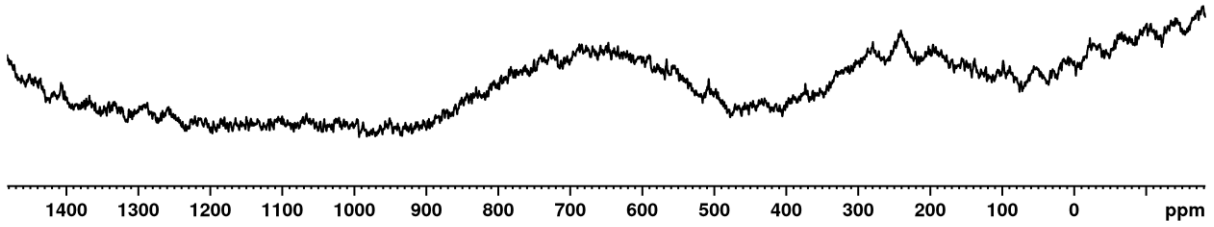

Figure S 55 ^{77}Se-NMR spectrum (57.2 MHz, CH_2Cl_2, RT) of the product obtained by the reaction of **1c** with P_4.

Reaction of $SeCl_3[F(Al(OR^F)_3)_2]$ with P_4

To test the crystallization behavior of product mixtures obtained from reactions of P_4 with **1b** was tested. A reaction according to the optimized reaction conditions was tested with **1b** (250 mg **1b**, 23 mg P_4, Reaction at −40 °C, Extraction with Pentane). The obtained yellow powder was analyzed via NMR spectroscopy and has shown no better selectivities than reactions with **1a**. Crystallization attempts (slow cooling / vapor diffusion) from the obtained material has only yielded minor amounts of crystals of $Ag(P_4)_2[F(Al(OR^F)_3)_2]$. **NMR:** ^{19}F-NMR (376.5 MHz, CH_2Cl_2, RT): δ = −74.6 (s, 9 F, $HOC(C\mathbf{F}_3)_3$), −75.8 (s, 54 F, $[F(Al(OC(C\mathbf{F}_3)_3)_3)_2]^-$), −184.9 (br, 1F, $[\mathbf{F}(Al(OC(CF_3)_3)_2]^-$) ppm. ^{31}P-NMR (162.0 MHz, CD_2Cl_2, RT): δ = 219.4 (br., 1 P, $\mathbf{P}Cl_3$), 152.0 (dt, 2 P, $[P_2\mathbf{P_{B2}}PCl_2]^+$, $^1J(^{31}P_B, ^{31}P_C)$ = 340 Hz, $^1J(^{31}P_A, ^{31}P_B)$ = 144 Hz), 104.8 (m, 1 P, $[\mathbf{P_A}P_2Se_4]^+$), the signal at 56 ppm of $[P_5Cl_2]^+$ could not be detected due to the low concentration of the sample, 38.5 (m, 2 P, $[P\mathbf{P_{B2}}Se_4]^+$), −270.6 (td, 2 P, $[\mathbf{P_{A2}}P_3Cl_2]^+$, $^1J(^{31}P_A, ^{31}P_B)$ = 144 Hz, $^2J(^{31}P_A, ^{31}P_C)$ = 27 Hz), −359.8 (s, 3 P, $[\mathbf{P}_3Se]^+$, ^1J(P, ^{77}Se) = 58 Hz), −523.2 (s, 4 P, $\mathbf{P}_4$) ppm.

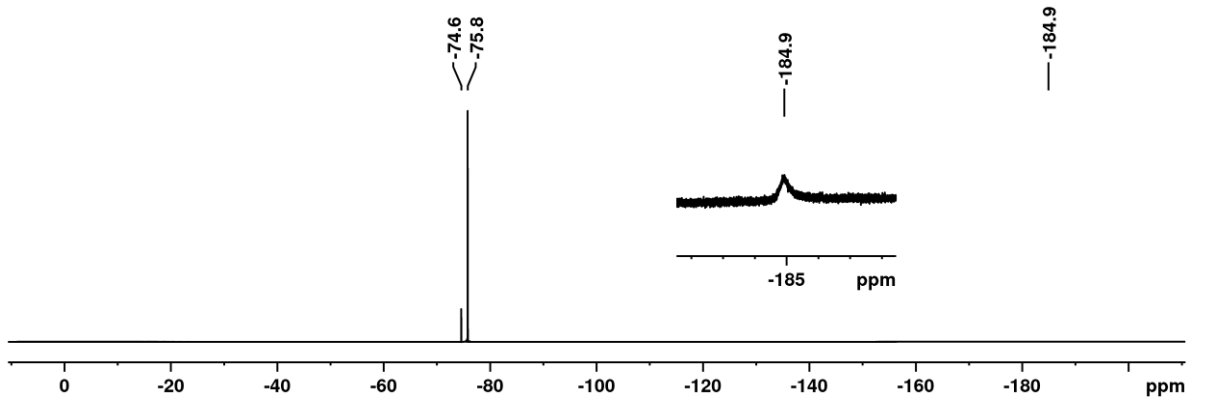

Figure S 56 ^{19}F-NMR spectrum (376.5 MHz, CD_2Cl_2, RT) of the product obtained by the reaction of **1b** with P_4. The small signal at −74.6 stems from free alcohol $HOC(CF_3)_3$.

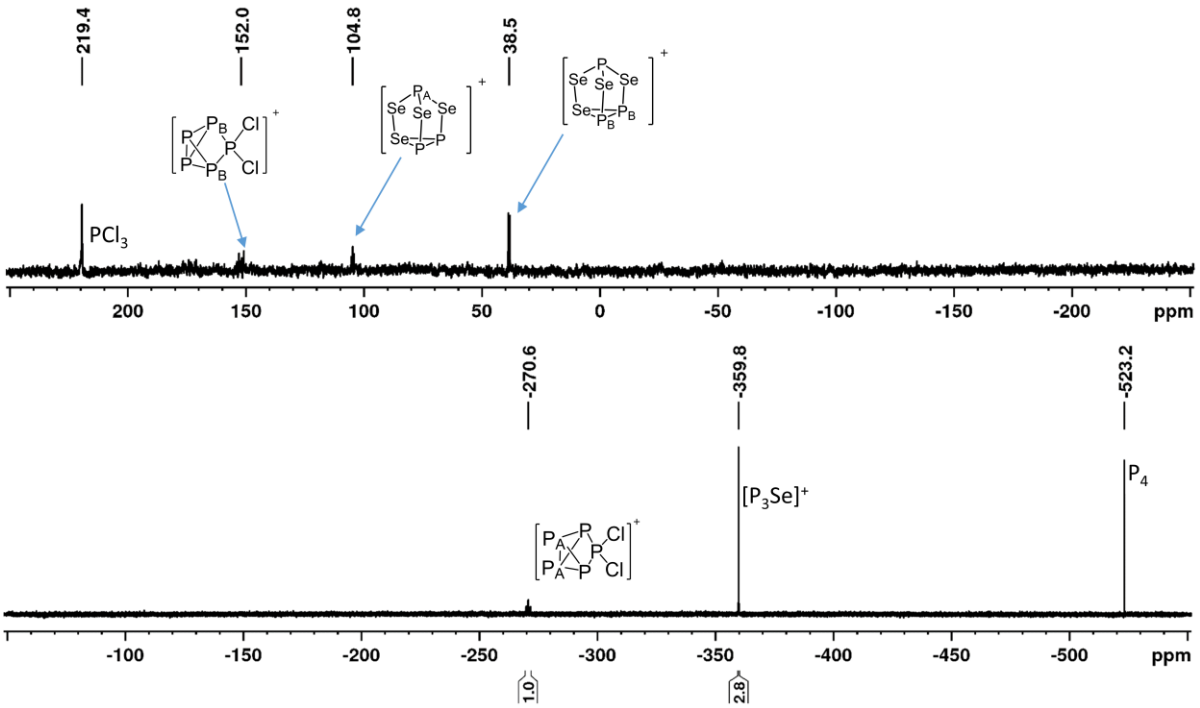

Figure S 57 ^{31}P-NMR spectra (162.0 MHz, CD_2Cl_2, RT) of the product obtained by the reaction of **1b** with P_4 from 250 to −250 ppm (top trace) and from −150 to –600 ppm (bottom trace).

Typical Reactions of ECl_3[WCA] with P_4

3.4.3.1 Typical reaction with $SeCl_3$[WCA] ([WCA]$^-$ = [Al(OR^F)$_4$]$^-$ and [F(Al(OR^F)$_3$)$_2$]$^-$)

The experimental procedure on the scale of an NMR-tube reaction and on a bigger scale is already given in chapter 3.1. To record a well-resolved ^{31}P spectrum properly showing the isotopic pattern generated by the different isotopomers, a ^{31}P spectrum at higher fields (600 MHz spectrometer) was recorded (Figure S 63). A ^{77}Se spectrum was also obtained at higher fields, clearly showing the quartet of the ^{77}Se nucleus of $[P_3Se]^+$.

Table S 7 Typical product distribution obtained from the reaction of $SeCl_3$[A] with P_4.

Product	**Starting conditions**				**Optimized conditions**			
	Integral	**Product Ratio**[c]	**Ratio of Cations**[d]	**Ratio $[P_3Se]^+$: $[P_5Cl_2]^+$**	**Integral**	**Product Ratio**[c]	**Ratio of Cations**[d]	**Ratio $[P_3Se]^+$: $[P_5Cl_2]^+$**
$[P_3Se]^+$	1.7	13 %	28 %	1.1	2.8	23 %	48 %	1.9
$[P_5Cl_2]^+$[a]	1.0	11 %	25 %		1.0	12 %	26 %	
$[P_3Se_4]^+$[b]	1.9	22 %	47 %		1.0	12 %	26 %	
PCl_3	2.4	54 %	—		2.2	53 %	—	

[a] The signal of both P_A atoms was integrated. [b] The signal of both P_B was integrated. [c] Calculated with respect to all products. [d] Calculated with respect to all cations, omitting the neutral product PCl_3.

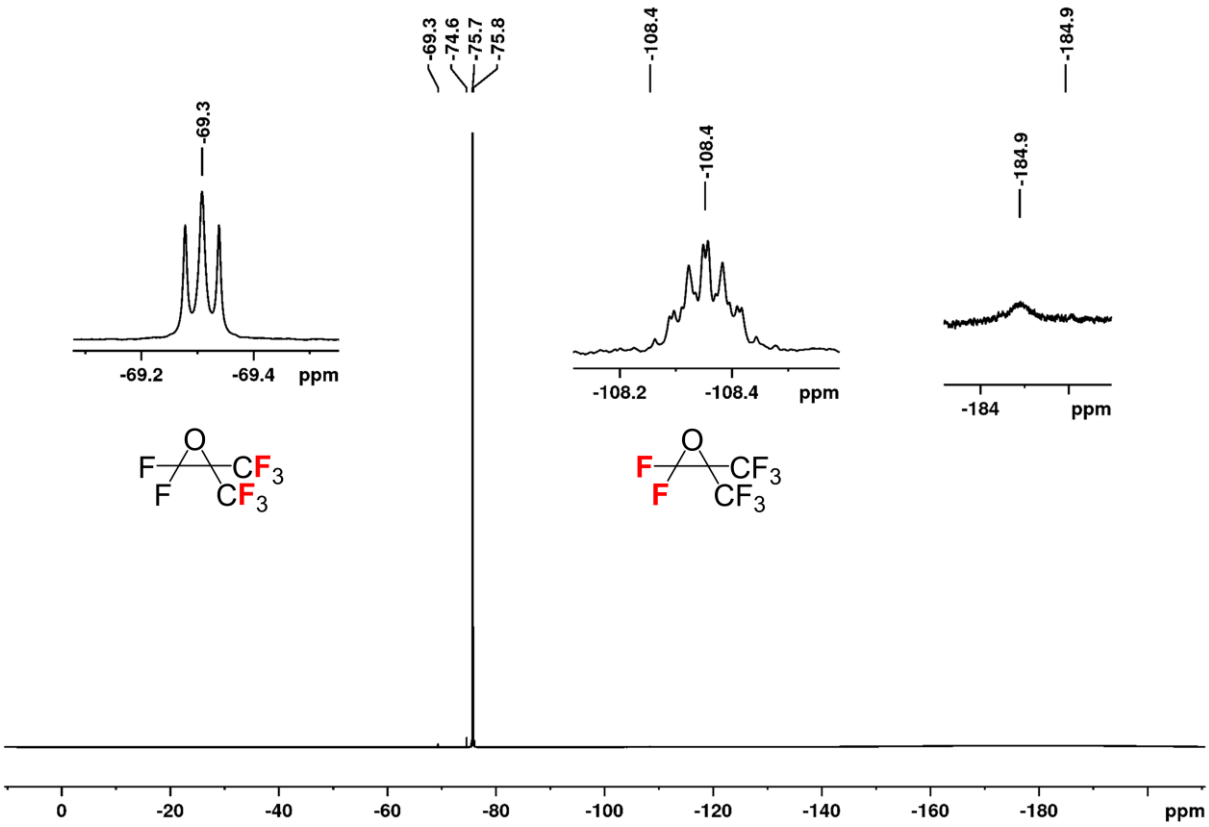

Figure S 58 ^{19}F-NMR spectrum (282.5 MHz, CD_2Cl_2, RT) of the product obtained by the reaction of **1a** with P_4.

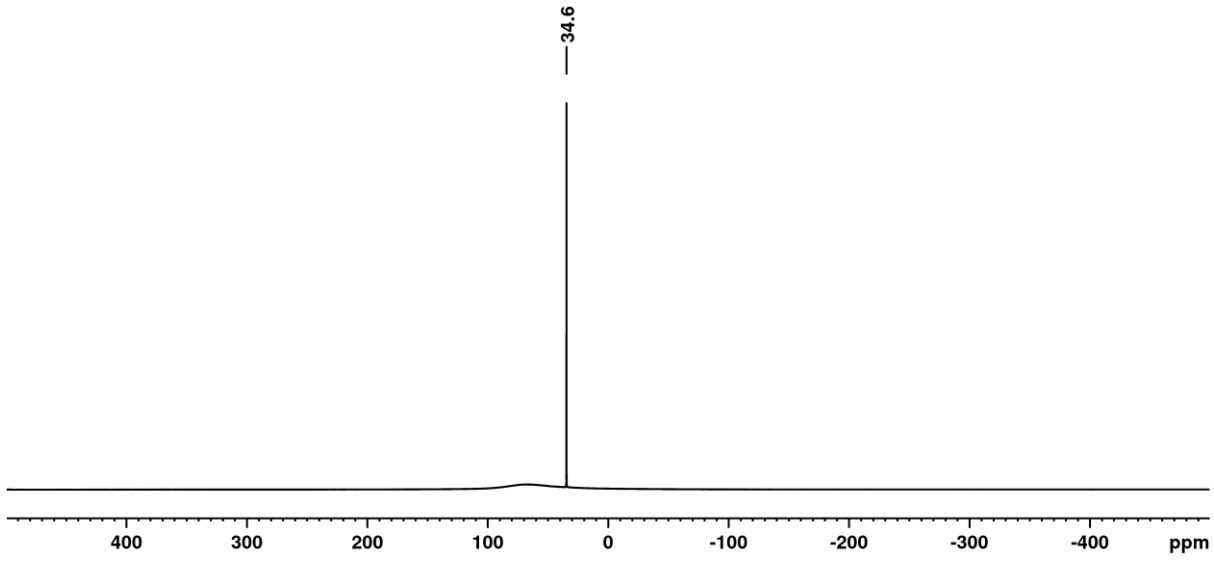

Figure S 59 ^{27}Al-NMR spectrum (78.2 MHz, CD_2Cl_2, RT) of the product obtained by the reaction of **1a** with P_4. The broad resonance at 70 ppm stems from the probe head.

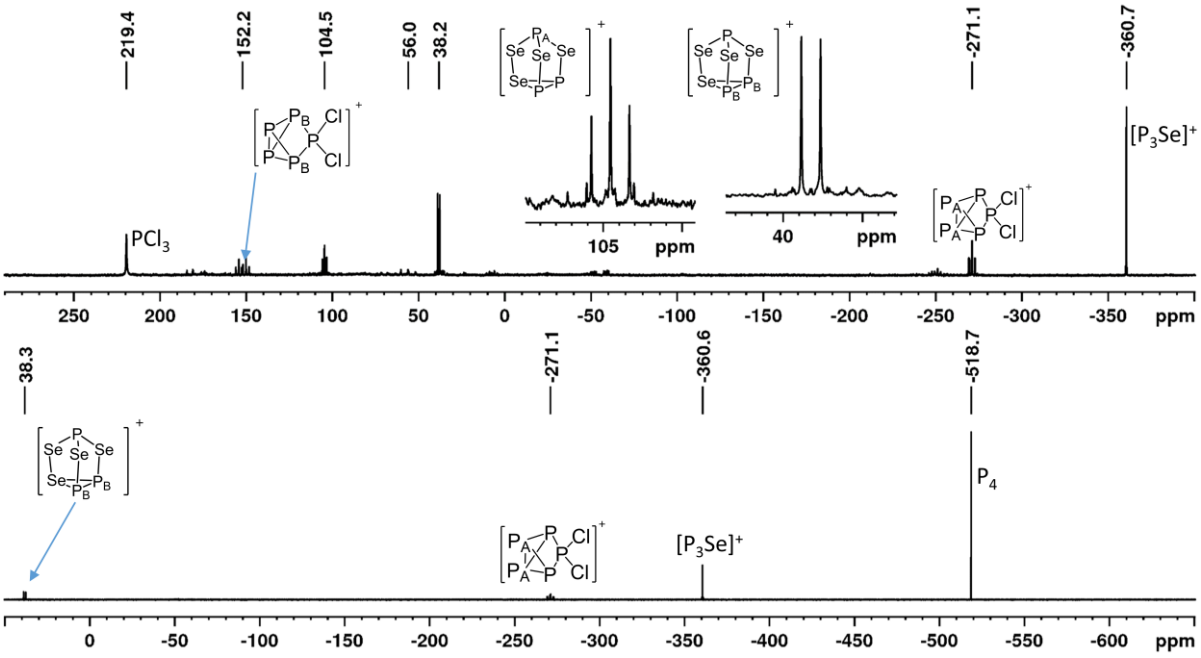

Figure S 60 Combined view of the ^{31}P-NMR spectra (81.0 MHz, CD_2Cl_2, RT) of the product obtained by the reaction of **1a** with P_4. From 300 to −400 ppm (top) and from 0 to −600 ppm (bottom).

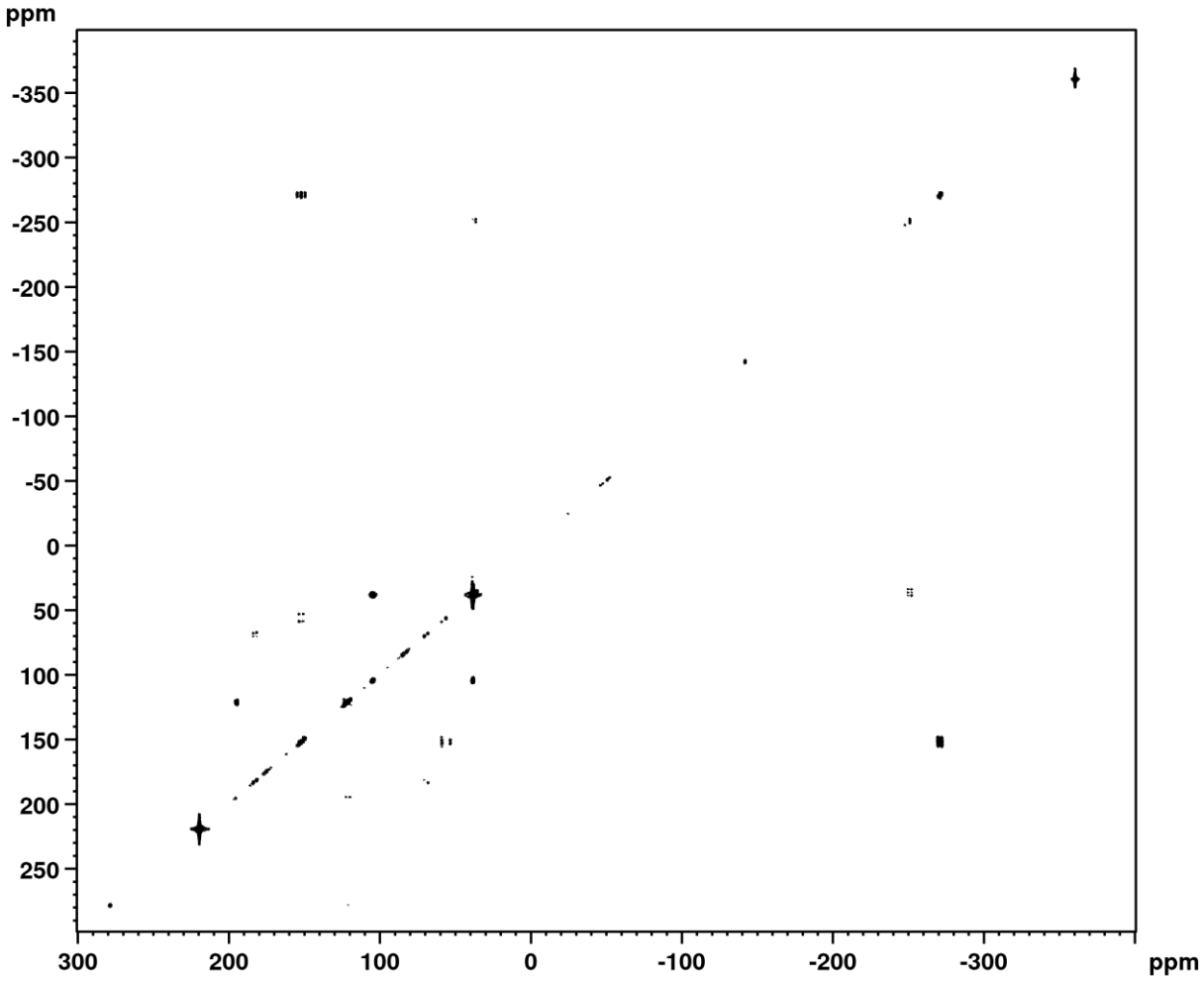

Figure S 61 ^{31}P, ^{31}P COSY (121.5 MHz, CD_2Cl_2, RT) of the product obtained by the reaction of **1a** with P_4.

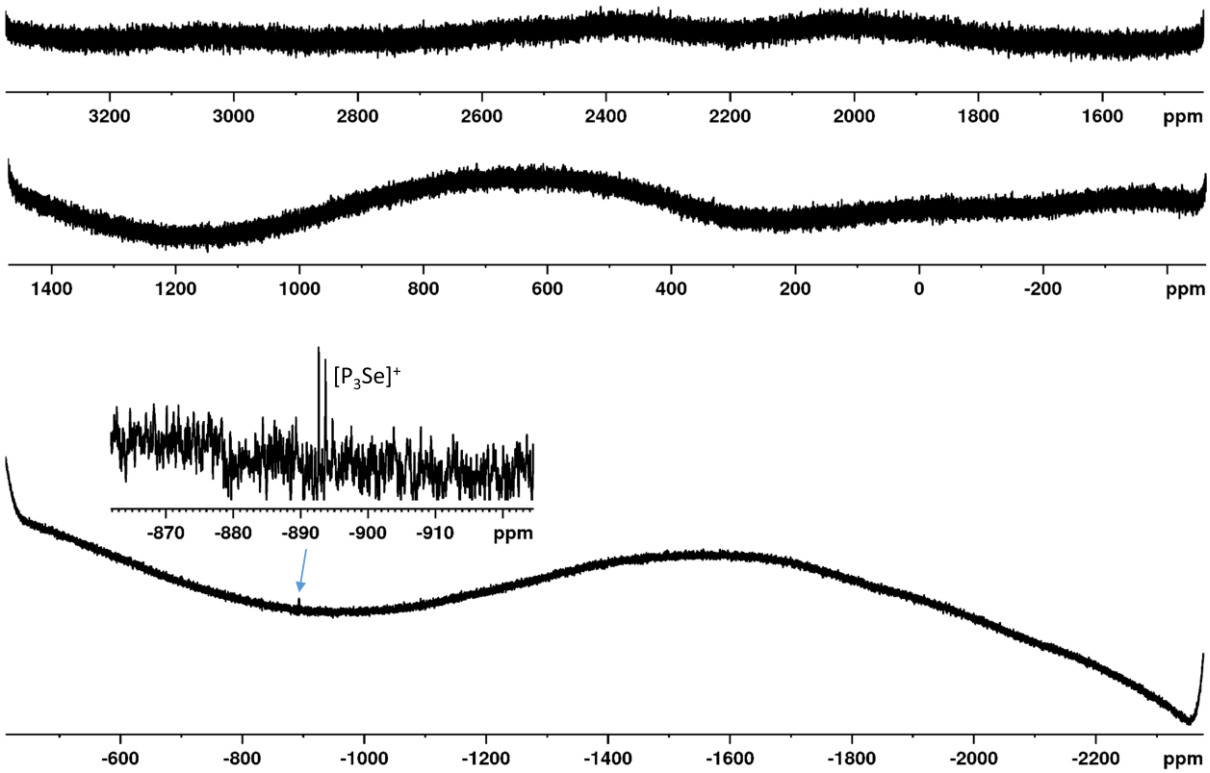

Figure S 62 Combined view of the ^{77}Se-NMR spectra (57.2 MHz, CD_2Cl_2, RT) of the product obtained by the reaction of **1a** with P_4 over the whole spectral range. From 3400 to 1400 ppm (top), 1500 to −500 ppm (middle) and −400 to −2400 ppm (bottom).

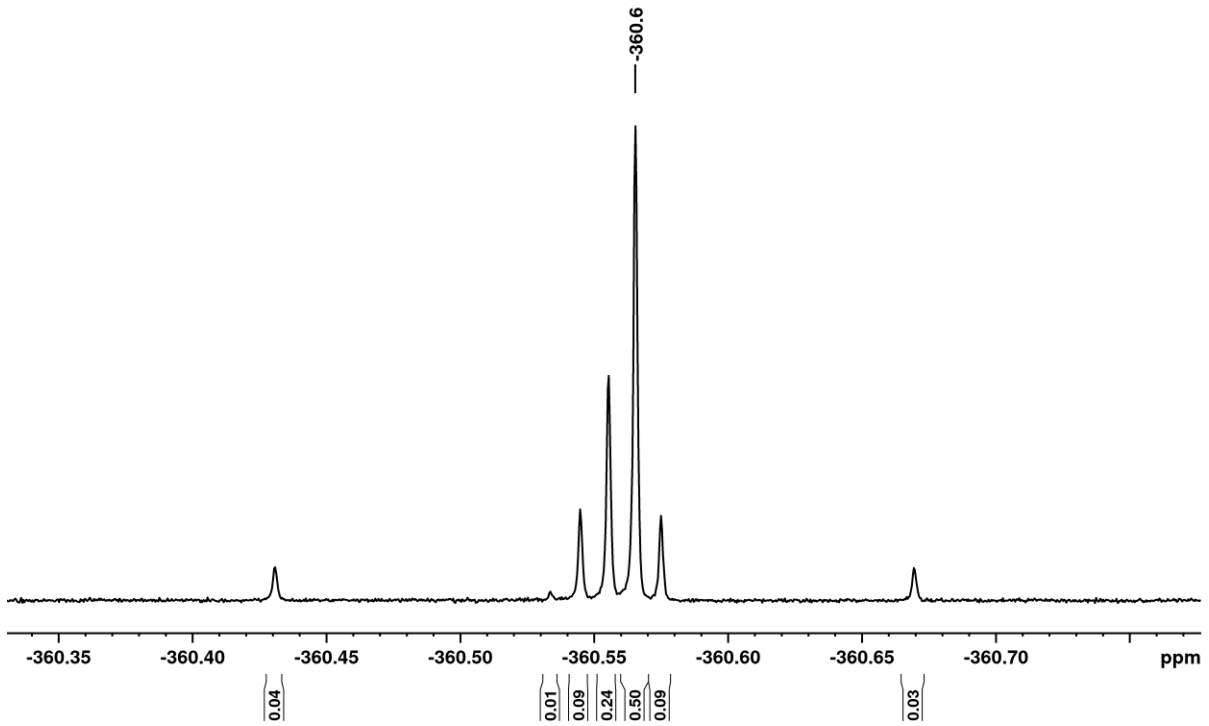

Figure S 63 Close up view of the isotope pattern generated by the different isotopomers of selenium in $[P_3Se]^+$ in the ^{31}P-NMR spectrum (243.0 MHz, CD_2Cl_2, RT)

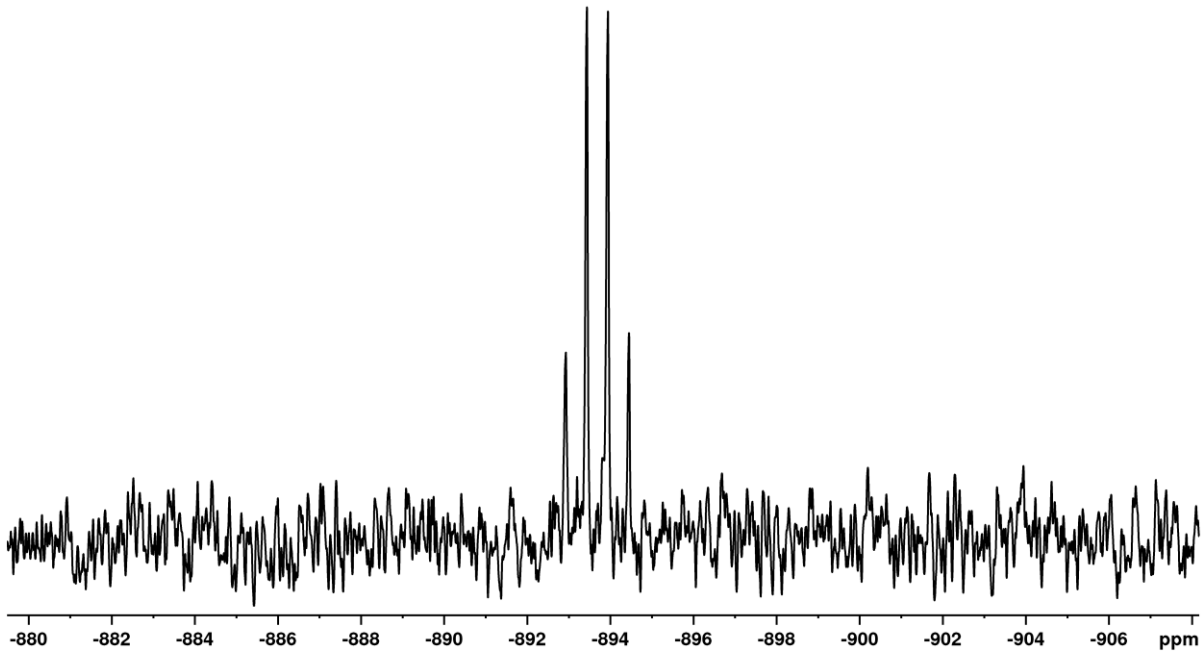

Figure S 64 Close up view of the quartet splitting of $[P_3Se]^+$ in the ^{77}Se-NMR spectrum (114.5 MHz, CD_2Cl_2, RT).

3.4.3.2. Reaction on a bigger scale under optimized reaction conditions

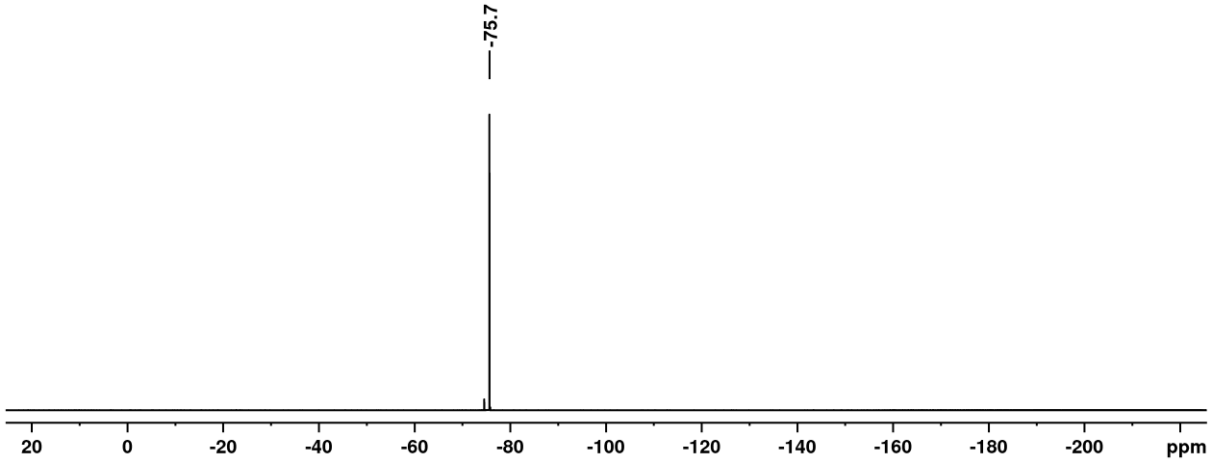

Figure S 65 ^{19}F-NMR spectrum (188.2 MHz, CD_2Cl_2, RT) of the product obtained by the reaction of **1a** with P_4 on a bigger scale under optimized reaction conditions. The small resonance downfield from the anion resonance stems from small amounts of free alcohol $HOC(CF_3)_3$.

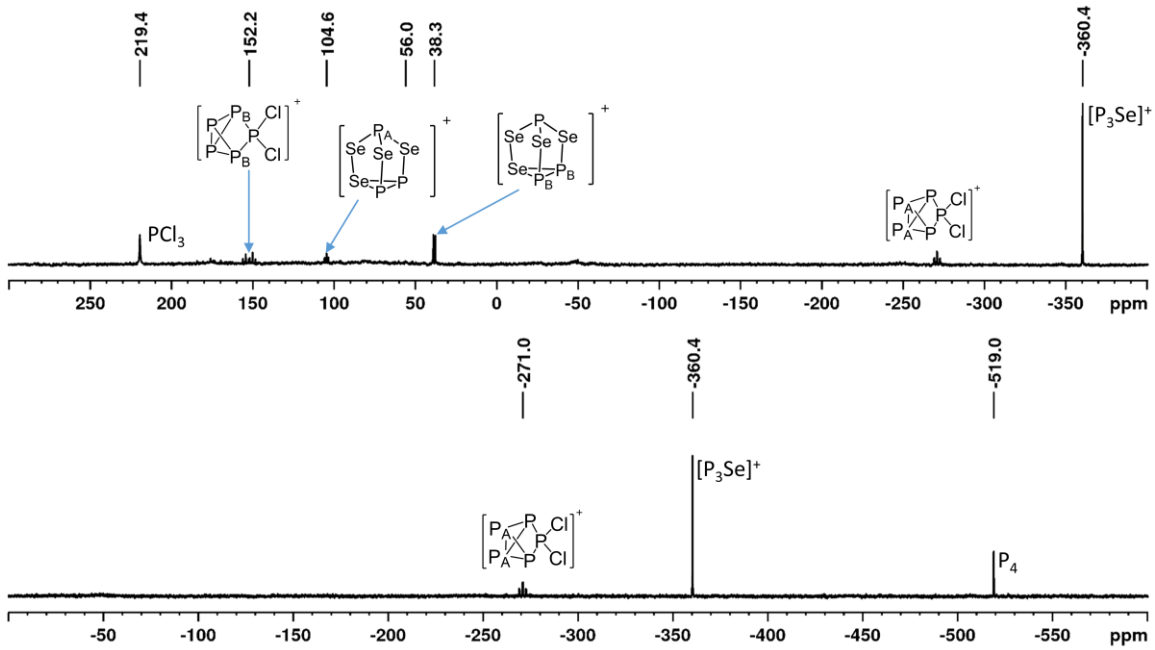

Figure S 66 Combined view of the ^{31}P-NMR spectra (81.0 MHz, CD_2Cl_2, RT) of the product obtained by the reaction of **1a** with P_4 on a bigger scale over the whole spectral range. From 300 to −400 ppm (top) and from 0 to −600 ppm (bottom).

IR and Raman Spectrum of 4 obtained from the optimized reaction conditions

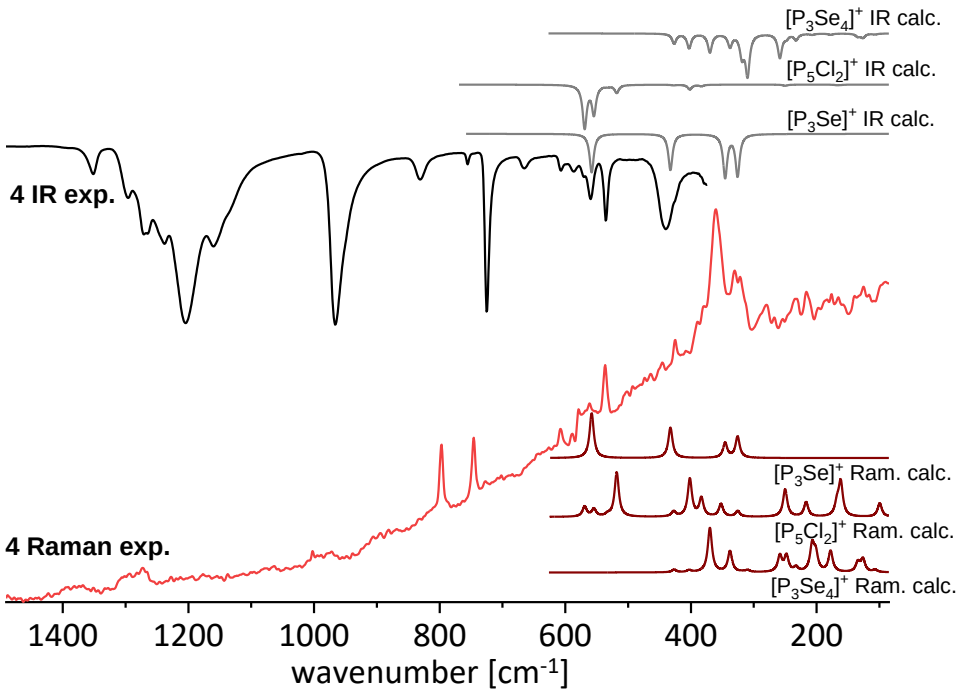

Figure S 67 Experimental IR (1500 to 440 cm^{-1}) and Raman (1500 to 85 cm^{-1}) spectra of the product mixture obtained in the optimized synthesis of **4**, together with the calculated IR and Raman spectra of $[P_3Se]^+$, $[P_5Cl_2]^+$ and $[P_3Se_4]^+$ at the (RIJ)BP86/def2−TZVPP level.

Table S 8 Summary of the experimental Raman and IR bands of samples obtained from the synthesis of **4** as well as that of the known $NMe_4[Al(OR^F)_4]$ for comparison (*Chem. Eur. J.* **2009**, *15*, 1966 – 1976). The calculated bands of $[P_5Cl_2]^+$ and $[P_3Se]^+$ (RIJ)BP86/def2−TZVPP) are also given. All bands are given in [cm^{-1}].

$NMe_4[Al(OR^F)_4]$		**4**	**4**	$[P_5Cl_2]^+$	$[P_3Se]^+$	$[P_3Se_4]^+$	Se_2Cl_2	Se_2Cl_2[a)]	**Assignment**[b)]
Raman	**IR**	**Raman**	**IR**	**Raman**	**Raman**	**Raman**	**Raman**[38]	**IR**[38]	
		99 (vw)	—	99 a_2	—	107 a''	91 (10)	—	$[P_5Cl_2]^+$ / $[P_3Se_4]^+$
		125 (vw)	—	—	—	126 a'	133 (36)	—	$[P_3Se_4]^+$ /Se_2Cl_2
		140 (vw)	—	162 a_1	—	134 a''	148 (14)	—	$[P_5Cl_2]^+$ / $[P_3Se_4]^+$ /Se_2Cl_2
		176 (vw)	—	167 b_2	—	178 a'	—	—	$[P_5Cl_2]^+$ / $[P_3Se_4]^+$
		184 (vw)	—	—	—	201 a''	—	—	$[P_3Se_4]^+$
		216 (w)	—	217 b_1	—	207 a'	—	—	$[P_5Cl_2]^+$ / $[P_3Se_4]^+$
235 (w)		235 (w)	—	—	—	233 a'	—	—	Anion and/or $[P_3Se_4]^+$
		254 (vw)	—	250 a_1	—	248 a''	—	—	$[P_5Cl_2]^+$ / $[P_3Se_4]^+$
		267 (vw)	—	—	—	258 a'	—	—	$[P_3Se_4]^+$
289 (w)	289 (w)	280 (w)	—	—	—	310 a'	289 (12)	—	Anion and/or $[P_3Se_4]^+$ /Se_2Cl_2
322 (s)	316 (w)				326 *e*	319 a''	—	—	Anion and/or $\nu_{asy.}$(P–Se) / $[P_5Cl_2]^+$ /
		322 (m)	—	326 a_1					$[P_3Se_4]^+$
		331 (m)	—	352 a_2	346 a_1	338 a'	—	—	$\nu_{sy.}$(P–Se) / $[P_5Cl_2]^+$ / $[P_3Se_4]^+$
368 (m)		361 (vs)	—	—	—	370 a'	357 (100)	—	$[P_3Se_4]^+$ /P_4 / Se_2Cl_2
		380 (m)	—	383 b_1	—	—	—	—	$[P_5Cl_2]^+$
		389 (w)	—	402 a_1	—	403 a''	—	—	$[P_5Cl_2]^+$ / $[P_3Se_4]^+$
		425 (w)	—	428 b2	433 *e*	427 a'	420 (1)	—	$\nu_{asy.}$(P_3) / $[P_5Cl_2]^+$ / $[P_3Se_4]^+$
453 (ms)	449 (m)	446 (vw)	440 (m)	—	—	—	—	436 (w)	Se_2Cl_2 / Anion
		464 (vw)	—	—	—	—	—	—	P_4
		474 (vw)	—	—	—	—	—	—	—
		493 (vw)	—	—	—	—	—	—	—
		503 (vw)	—	518 a_1	—	—	—	—	$[P_5Cl_2]^+$
538 (mw)	536 (m)	537 (w)	535 (m)	533 b_2	—	—	—	—	Anion and/or $[P_5Cl_2]^+$
562 (mw)	560 (mw)	562 (vw)	560 (w)	554 b_1	—	—	—	—	Anion and/or $[P_5Cl_2]^+$
572 (mw)	571 (w)	568 (vw)	571 (vw)	569 a_1	—	—	—	—	Anion and/or $[P_5Cl_2]^+$
		579 (vw)	—	—	570 a_1	—	—	—	$\nu_{sy.}$(P_3) $[SeP_3]^+$
		—	587 (vw)	—	—	—	—	581 (vw)	Se_2Cl_2
		608 (vw)	607 (vw)	—	—	—	—	—	P_4
		—	665 (vw)	—	—	—	—	—	Anion
	725 (s)	—	725 (vs)	—	—	—	—	—	Anion
747 (s)	756 (w)	746 (w)	756 (vw)	—	—	—	—	—	Anion
794 (s)		797 (m)	—	—	—	—	—	—	Anion
832 (w)	831 (m)	—	831 (vw)	—	—	—	—	—	Anion
976 (mw)	967 (sh)	—	966 (vs)	—	—	—	—	—	Anion
		1002 (vw)	—	—	—	—	—	—	Anion
1135 (mw)	1163 (s)	—	1160 (m)	—	—	—	—	—	Anion
		—	1204 (vs)	—	—	—	—	—	Anion
1239 (mw)	1237 (vs)	—	1238 (m)	—	—	—	—	—	Anion
1272 (mw)	1271 (vs)	1273 (vw)	1265 (m)	—	—	—	—	—	Anion
	1296 (s)	1294 (vw)	1296 (w)	—	—	—	—	—	Anion
1307 (w)		1306 (vw)	—	—	—	—	—	—	Anion
1352 (w)	1351 (ms)	—	1351 (vw)	—	—	—	—	—	Anion

w: weak, m: medium, s: strong, sh: shoulder, v: very. [b)] The bands from the FIR spectrum of Se_2Cl_2 were not included, as no FIR spectra of **4** could be recorded. [a)] From a visualization of the calculated spectra. Exact assignments of the vibrations of $[P_3Se_4]^+$ and $[P_5Cl_2]^+$ are not given.

Mass spectrum of 4

In order to obtain a mass spectrum of **4**, the reaction conditions were first optimized, and the crude reaction mixture (in CH_2Cl_2) was diluted to a micromolar solution by the addition of *o*-dfb. In contrast to CH_2Cl_2, *o*-dfb is well-suited for ESI experiments. While the resulting mass spectrum (Figure S 68) contains signals for $[P_3Se]^+$ (*m*/*z* 172.8) and $[P_5Cl_2]^+$ (*m*/*z* 225.0) as the main species, the isotope pattern around the peak at *m*/*z* 172.8 (blue inset) does not exactly match that expected for $[P_3Se]^+$. However, CID experiments (CID = collision-induced dissociation) on the signals between *m*/*z* 165 and *m*/*z* 176 at

different collision energies (Figure S 69) cause the fragmentation of an isobaric impurity prior to the fragmentation of $[P_3Se]^+$. Thus, the isotopic pattern of selenium becomes obvious and proves the presence of $[P_3Se]^+$. The latter cation, however, is very stable and does not produce fragment ions, which might serve as an independent means of identification. Also the identity of the isobaric impurity remains unknown.

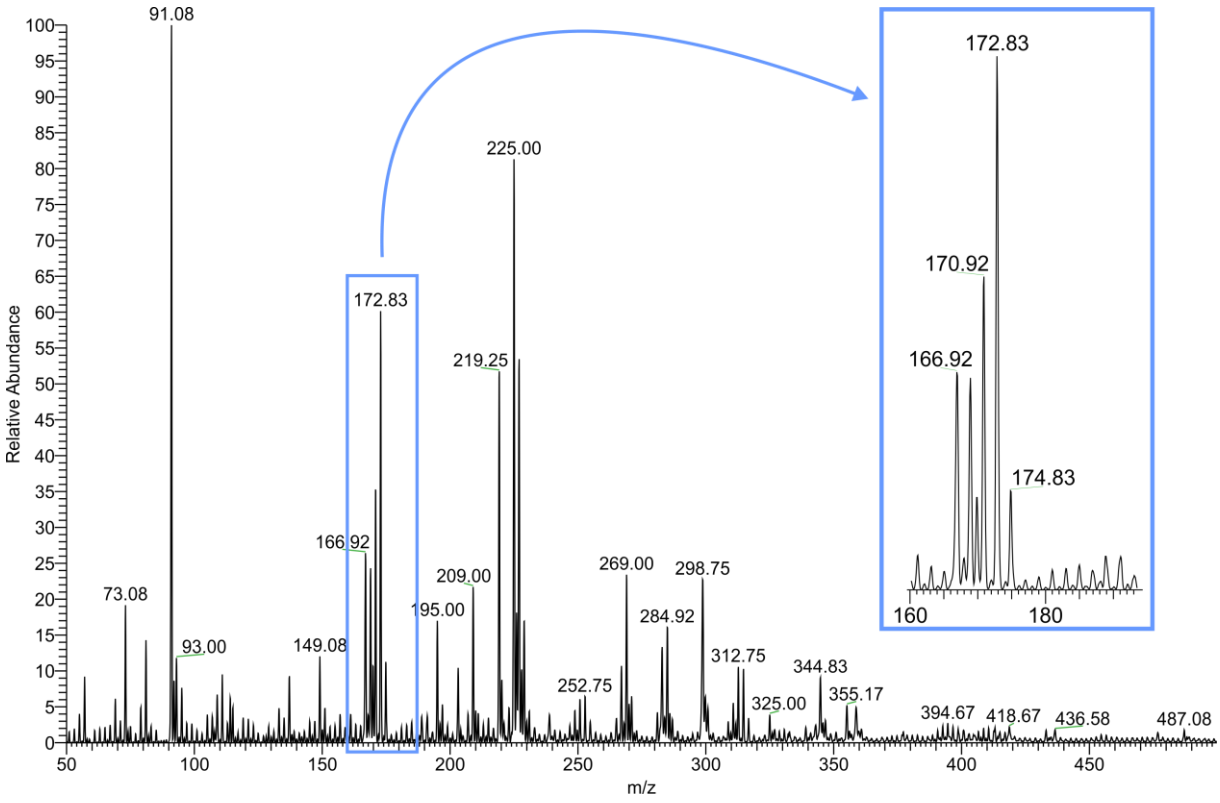

Figure S 68 ESI mass spectrum of a sample of **4** in *o*-dfb. The blue inset shows the region where signals of $[P_3Se]^+$ and unknown impurities overlap.

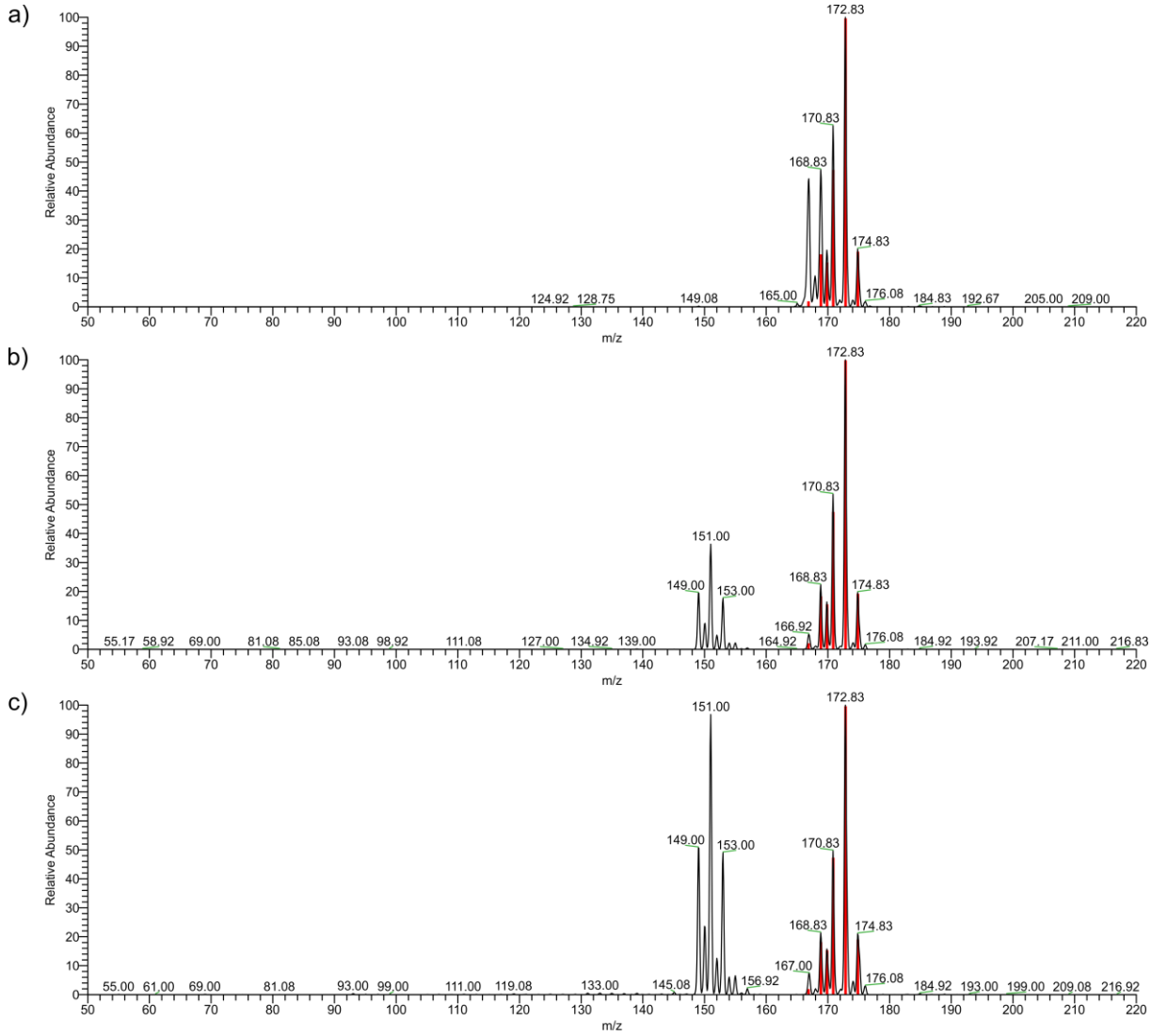

Figure S 69 CID experiments of mass-selected ions in a region between m/z 165 and m/z 176. The experiments have been performed at different normalized collision energies (increasing from a via b to c). The red bars illustrate the isotopic pattern expected for $[P_3Se]^+$.

3.4.3.3. Typical reaction with $TeCl_3[A]$ ($[A]^- = [Al(OR^F)_4]^-$ and $[F(Al(OR^F)_3)_2]^-$)

The experimental procedure on the scale of an NMR-tube reaction and on a bigger scale is already given in chapter 3.1. The sextet at a ^{125}Te chemical shift of 67.4 ppm has a coupling constant J(^{125}Te, ^{31}P) of 62 Hz, that can also be found in the ^{125}Te satellites of the singlet resonance at 9.8 ppm in the ^{31}P spectrum including the ^{123}Te with the corresponding coupling constant of 51 Hz. These satellites integrate to 24.0 % of the total signal intensity, indicating 3 chemical equivalent Te atoms, coupling to 5 chemical equivalent P atoms. The nature of the second pair of satellite peaks with a coupling constant of 125 Hz that integrate to an intensity of 1 % of the total signal intensity could not be clarified during our studies.

Table S 9 Typical product distribution obtained from the reaction of $TeCl_3$[A] with P_4.

Product	**Integral**	**Product Ratio**	**Ratio $[P_3Te]^+$ vs. $[P_5Cl_2]^+$**
$[P_3Te]^+$	0.4	13 %	0.3
$[P_5Cl_2]^+$	1.0	32 %	
PCl_3	0.7	15 %	
Unknown "P_5Te_3"	1.2	44 %	

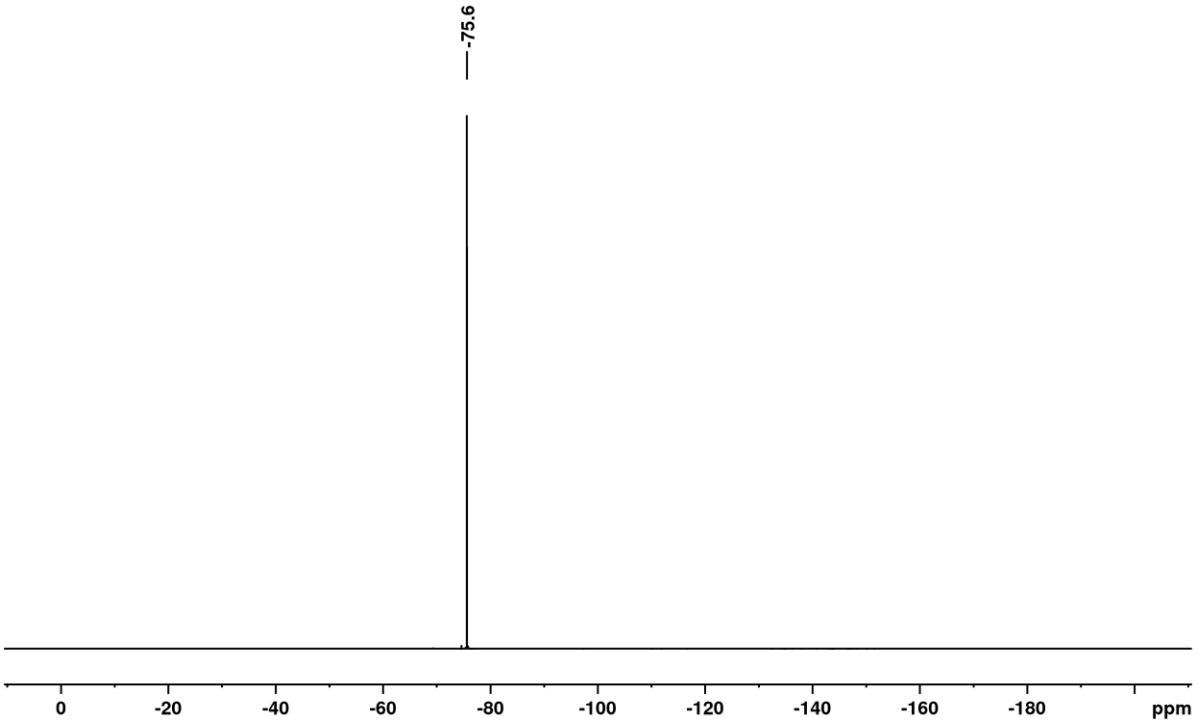

Figure S 70 ^{19}F-NMR spectrum (356.4 MHz, CD_2Cl_2, RT) of the product obtained by the reaction of **2a** with P_4.

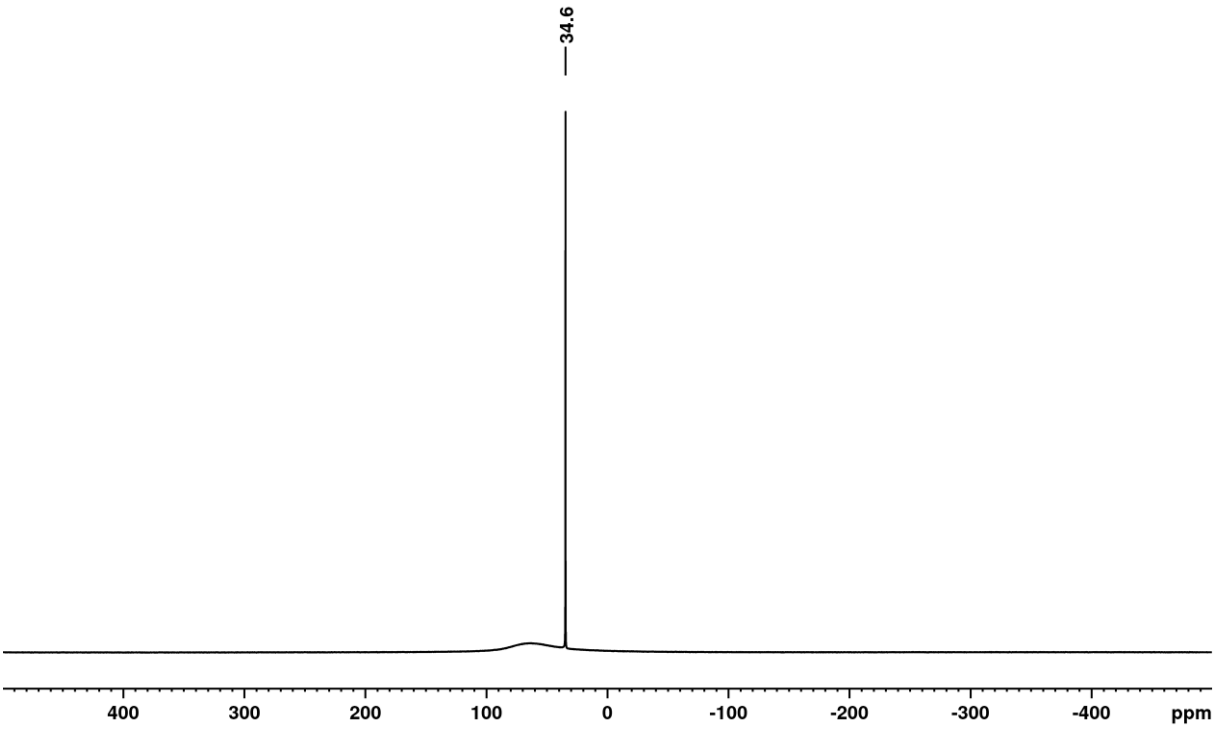

Figure S 71 ^{27}Al-NMR spectrum (104.3 MHz, CD_2Cl_2, RT) of the product obtained by the reaction of **2a** with P_4. The broad resonance at 70 ppm stems from the probe head.

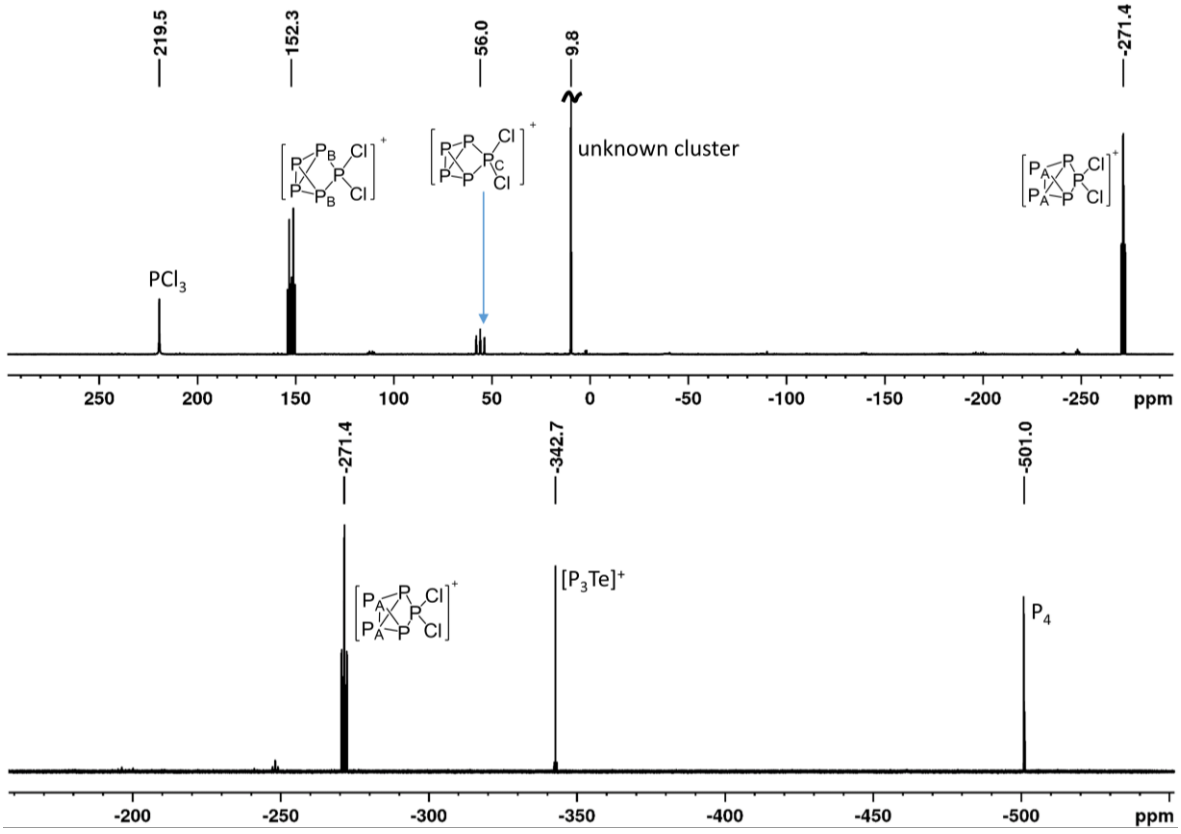

Figure S 72 Combined view of the ^{31}P-NMR spectra (162.0 MHz, CD_2Cl_2, RT) of the product obtained by the reaction of **2a** with P_4 over the whole spectral range. From 300 to −300 ppm (top) and from −150 to −550 ppm (bottom).

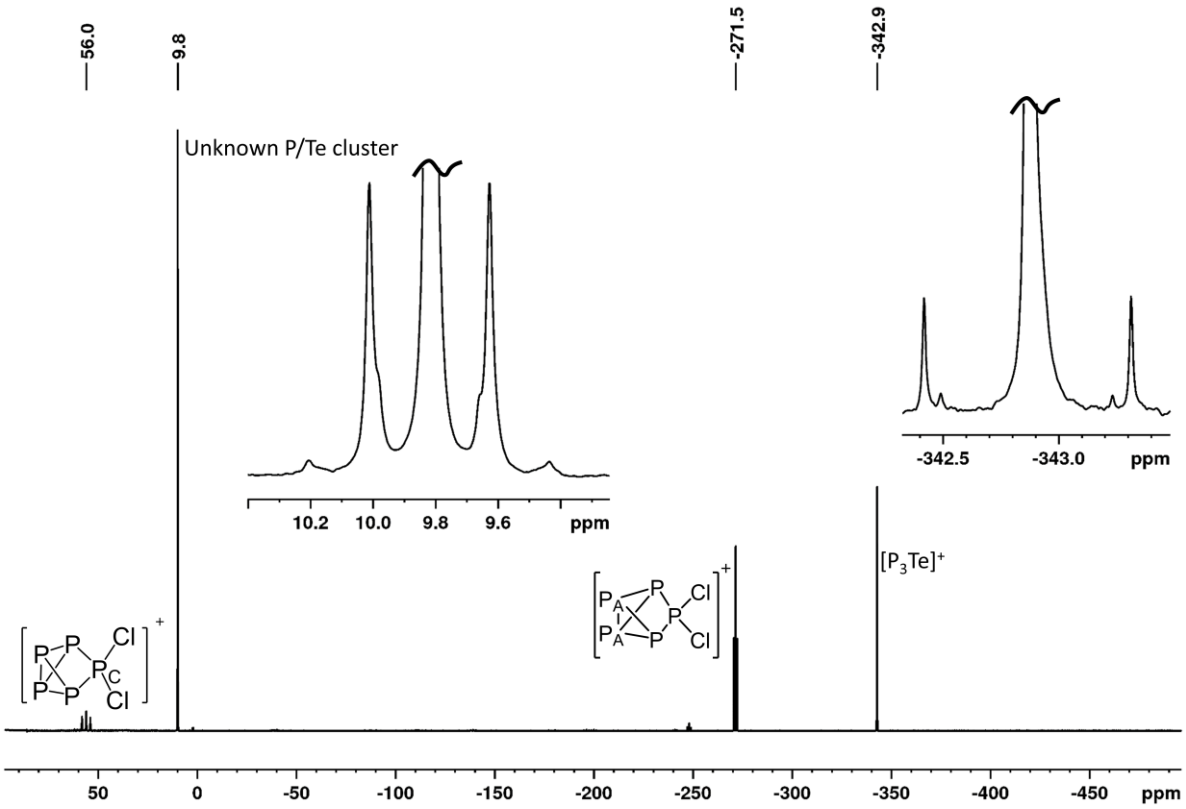

Figure S 73 Close-up view of the ^{31}P-NMR spectrum (162.0 MHz, CD_2Cl_2, RT) of the product obtained by the reaction of **2a** with P_4 in the region with both resonance showing ^{123}Te and ^{125}Te satellites.

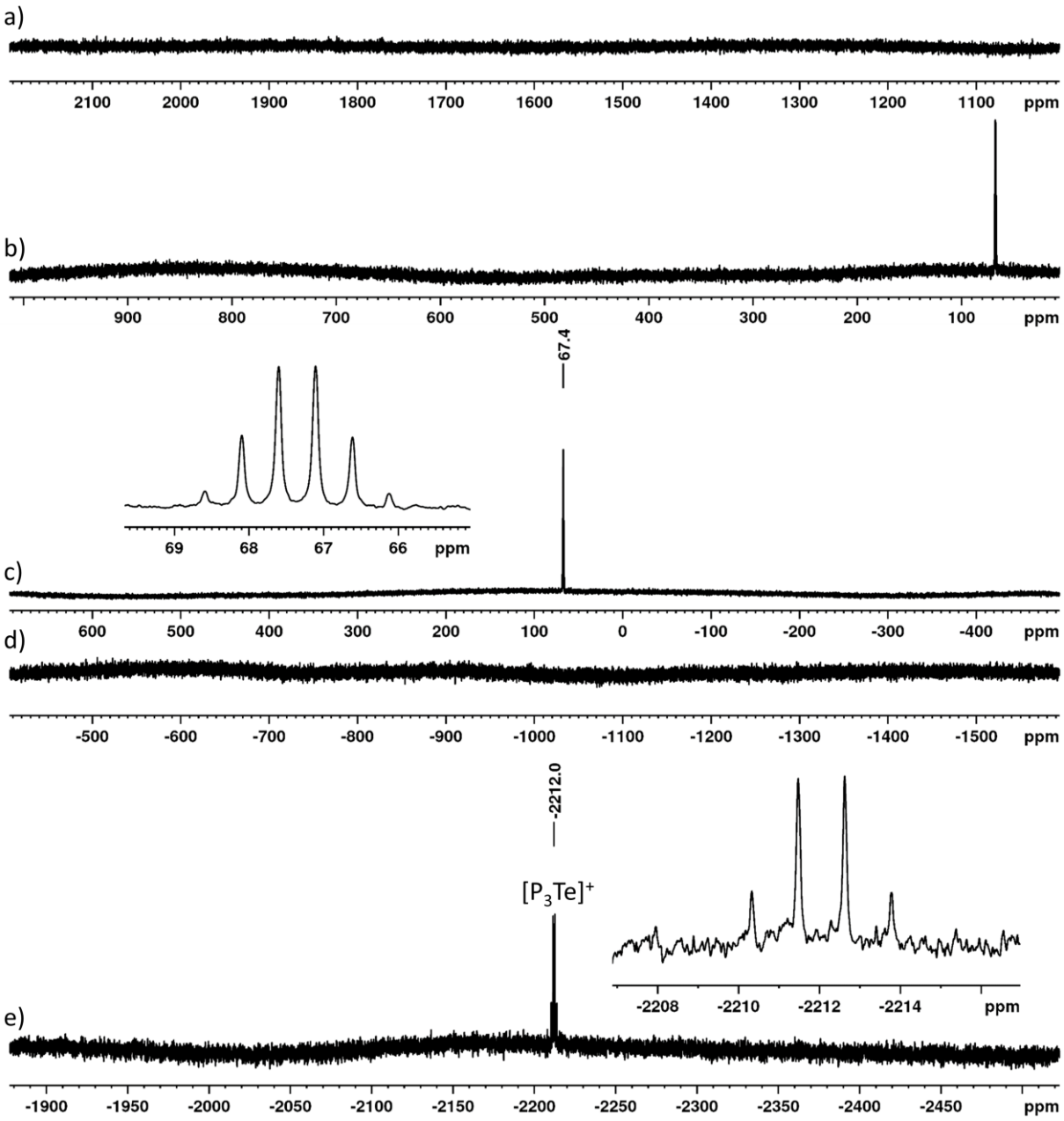

Figure S 74 Combined view of the ^{125}Te-NMR spectra (126.3 MHz, CD_2Cl_2, RT) of the product obtained by the reaction of **2a** with P_4 over the whole spectral range. From 2200 to 1000 ppm (a), 1000 to 0 ppm (b), 700 to −400 ppm (c), −400 to −1600 (d) and −1800 to −2600 ppm (e). The marked peak without label is from unknown origin.

3.4.3.4. Typical reaction with $SCl_3[F(Al(OR^F)_3)_2]$

The experimental procedure on the scale of an NMR-tube reaction and on a bigger scale is already given in chapter 3.1.

Table S 10 Typical product distribution obtained from the reaction of $SCl_3[F(Al(OR^F)_3)_2]$ with P_4.

Product	Integral	Product Ratio	Ratio $[P_3S]^+$ vs. $[P_5Cl_2]^+$
$[P_3S]^+$	0.4	5 %	0.3
$[P_5Cl_2]^+$	1.0	20 %	
PCl_3	1.9	75 %	

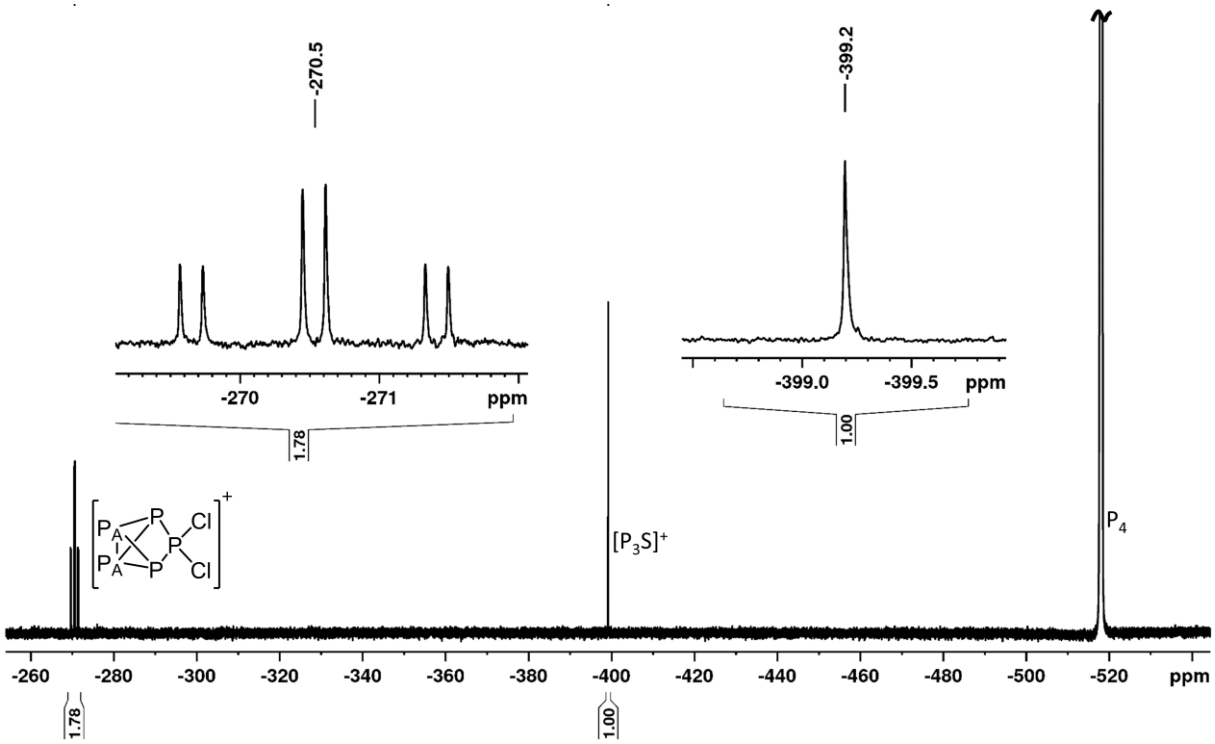

Figure S 75 Close up view of the ^{31}P-NMR spectrum (162.0 MHz, CD_2Cl_2, RT) of the product obtained by the reaction of **3** with P_4 from −250 to −550 ppm.

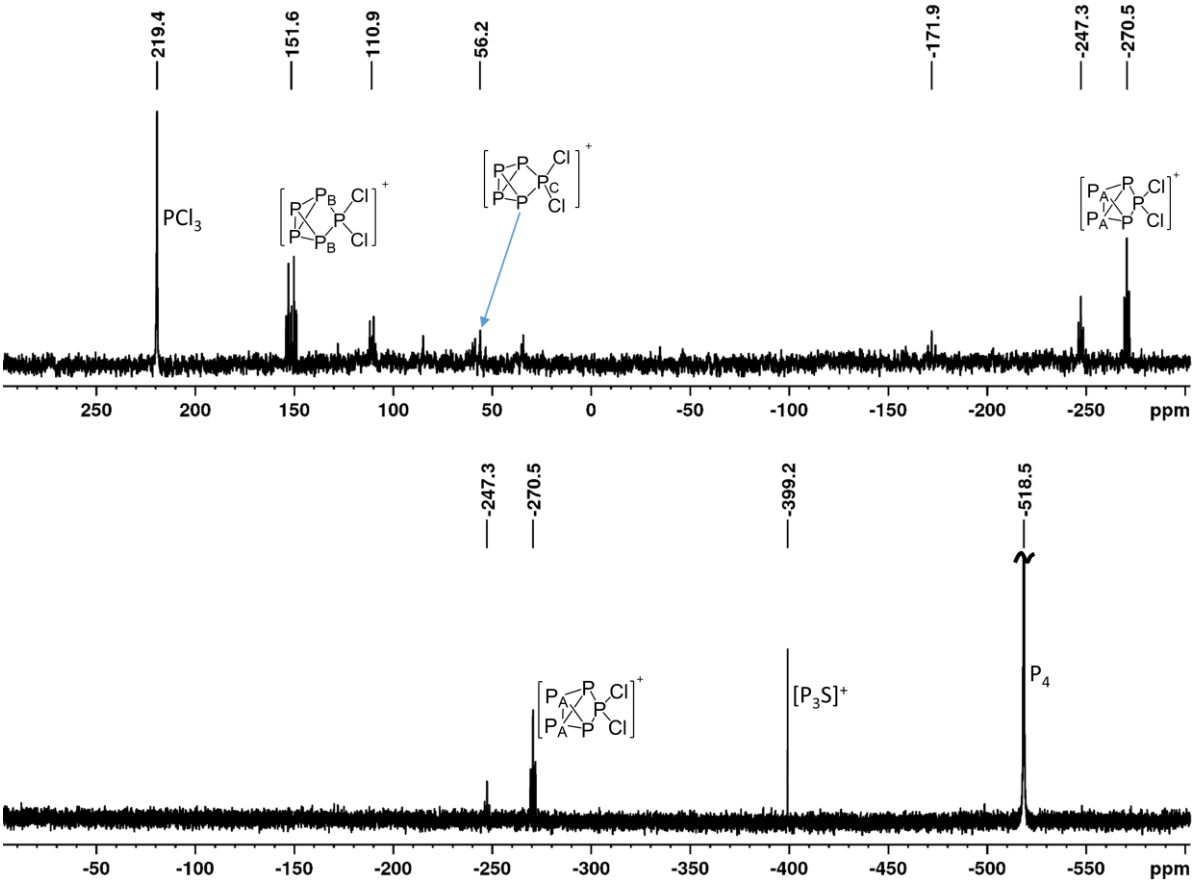

Figure S 76 Combined view of the ^{31}P-NMR spectra (121.5 MHz, CD_2Cl_2, RT) of the product obtained by the reaction of **3** with P_4 over the whole spectral range. From 300 to −300 ppm (top) and from 0 to −600 ppm (bottom). The marked peaks without labels are from unknown origin.

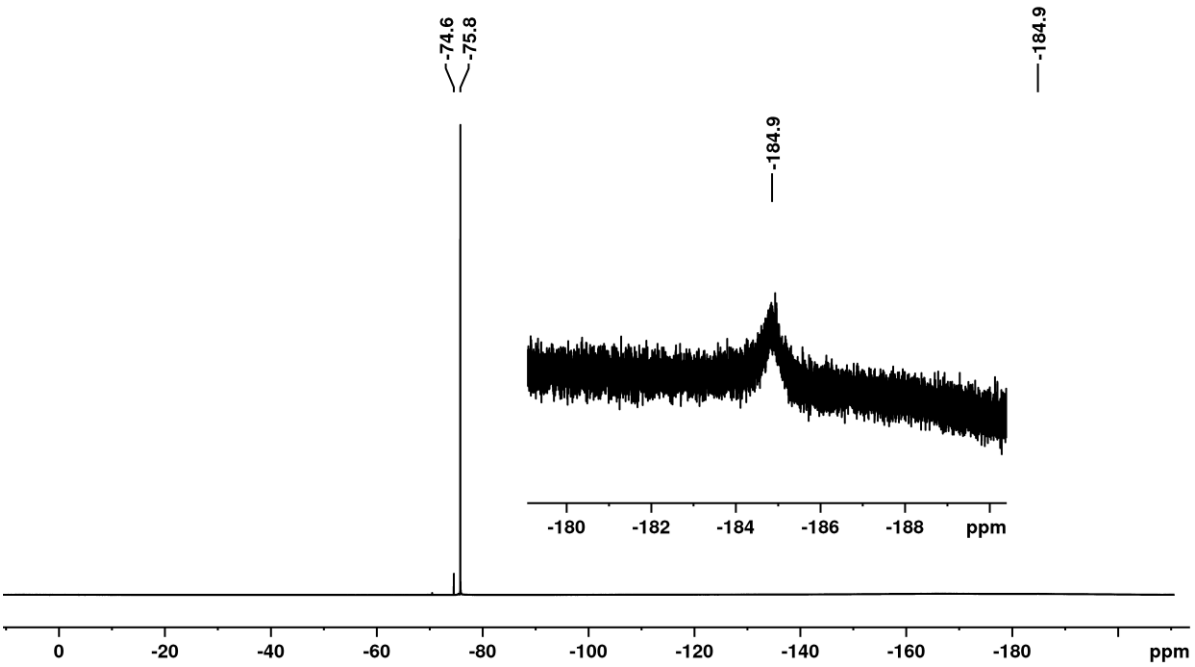

Figure S 77 ^{19}F-NMR spectrum (282.5 MHz, CD_2Cl_2, RT) of the product obtained by the reaction of **3** with P_4. The small resonance at −74.6 ppm stems from free alcohol $HOC(CF_3)_3$.

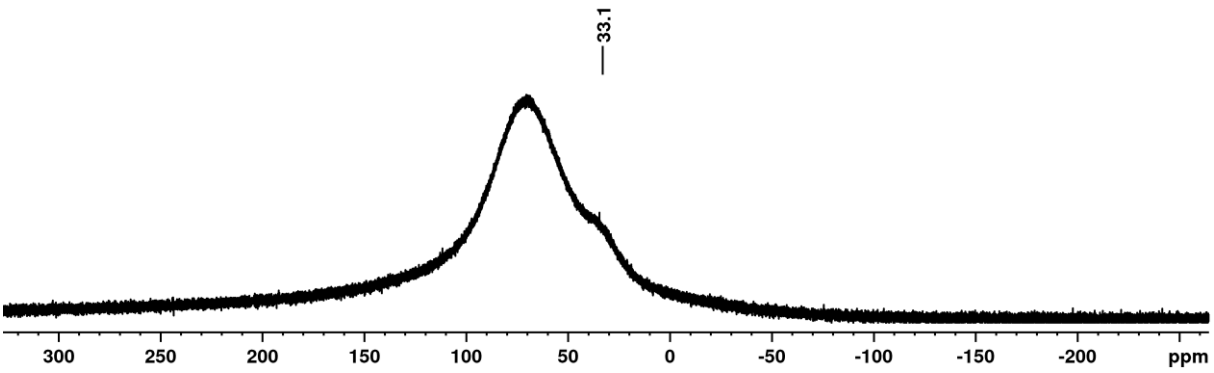

Figure S 78 ^{27}Al-NMR spectrum (78.2 MHz, CD_2Cl_2, RT) of the product obtained by the reaction of **3** with P_4. The broad resonance at 70 ppm stems from the probe head, the broad resonance at 33 ppm stems from the $[F(Al(OR^F)_3)_2]^-$ anion.

3.5. Other tested Reactions

Tested Access to $SeCl_3[Al(OR^F)_4]$ from $SeCl_4$ and $Li[Al(OR^F)_4]$

$Li[Al(OR^F)_4]$ (974 mg, 1.00 mmol, 1 eq.) and finely ground $SeCl_4$ (222 mg, 1.00 mmol, 1 eq.) were weighed into one bulb of a two bulb vessel separated by a glass frit. CH_2Cl_2 (5 ml) was condensed onto the solids and the mixture was sonicated for 2 d at room temperature which resulted in a pale yellow solution over a colorless precipitate. The solution was then filtered through the glass frit and the solvent was removed under vacuum. The initial precipitate was shown to be $SeCl_4$ by Raman spectroscopy. The precipitate obtained by drying the filtered solution has shown to be unreacted $Li[Al(OR^F)_4]$, contaminated with little $SeCl_4$ by Raman spectroscopy.

The same reaction was repeated on a smaller scale ($Li[Al(OR^F)_4]$ (300 mg, 0.31 mmol, 1 eq.); $SeCl_4$ (68 mg, 0.31 mmol, 1 eq.)) with SO_2 (0.8 mL) as a solvent due to the enhanced solubility of the Li-salt compared to CH_2Cl_2 yielded the same results after stirring the reaction mixture for 3 d.

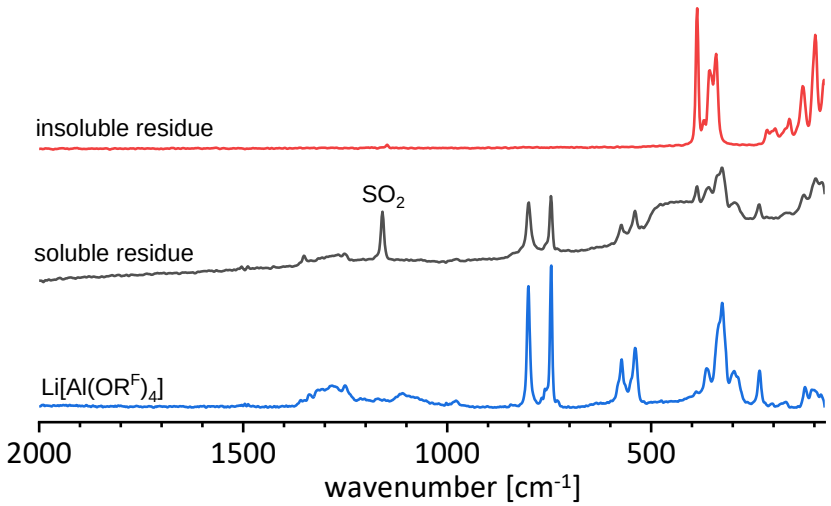

Figure S 79 Raman spectra between 2000 and 70 cm^{-1} of the isolated products from the attempted reaction of $SeCl_4$ with $Li[Al(OR^F)_4]$ in SO_2 (top and middle trace) compared to the Raman spectrum of neat $Li[Al(OR^F)_4]$.

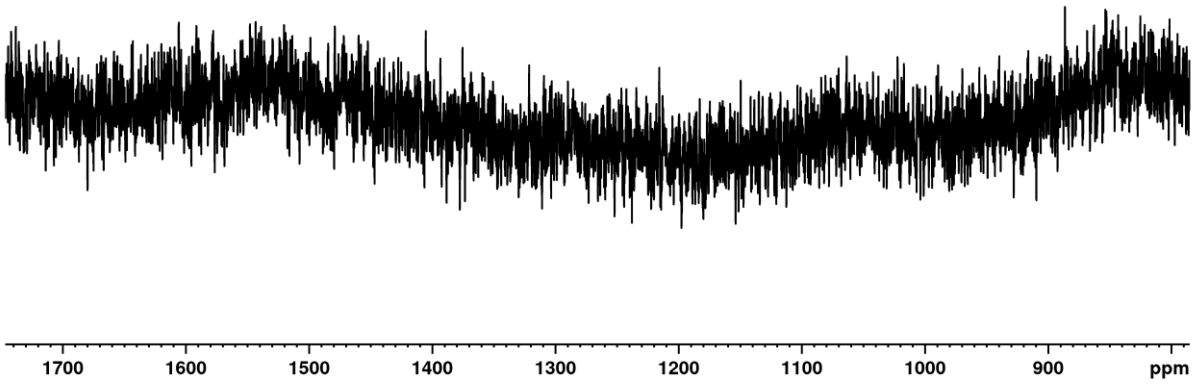

Figure S 80 ^{77}Se-NMR spectrum (57.2 MHz, SO_2, RT) of the product obtained by the reaction of $Li[Al(OR^F)_4]$ with $SeCl_4$ in SO_2 at room temperature.

Tested Access to $SeCl_3[Al(OR^F)_4]$ from $SeCl_3[AlCl_4]$ and $Li[Al(OR^F)_4]$

$Li[Al(OR^F)_4]$ (195 mg, 0.20 mmol, 1.0 eq.) and $SeCl_3[AlCl_4]$ (71 mg, 0.20 mmol, 1.0 eq.) were weighed into one bulb of a two bulb vessel separated by a glass frit. CH_2Cl_2 (5 ml) was condensed onto the solids and the mixture was sonicated for 2 d at room temperature which resulted in a pale yellowish solution over a colorless precipitate. The solution was then filtered through the glass frit and the solvent was removed under vacuum. The initial precipitate was shown to be $SeCl_3[AlCl_4]$ by Raman spectroscopy. The precipitate obtained by drying the filtered solution has shown to be unreacted $Li[Al(OR^F)_4]$ contaminated with little $SeCl_3[AlCl_4]$ by Raman spectroscopy.

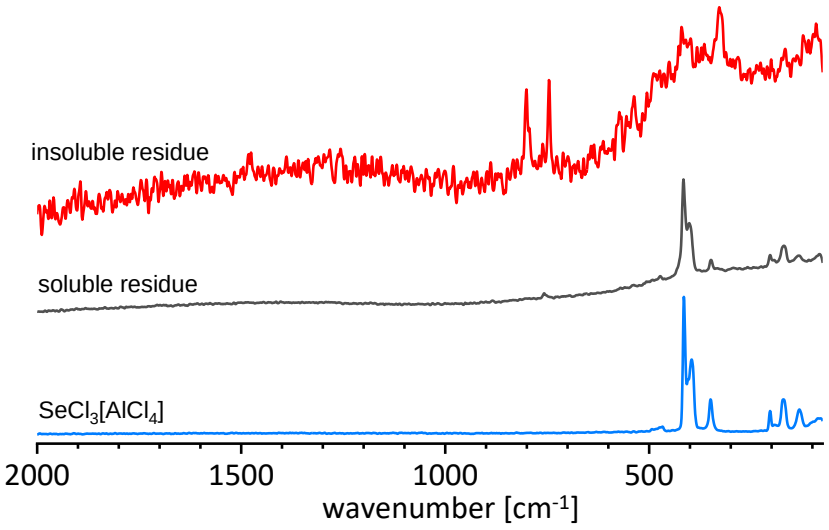

Figure S 81 Raman spectra between 2000 and 70 cm^{-1} of the isolated products from the attempted reaction of $SeCl_3[AlCl_4]$ with $Li[Al(OR^F)_4]$ in CH_2Cl_2 (top and middle trace) compared to the Raman spectrum of neat $SeCl_3[AlCl_4]$.

Tested Access to $SF_3[Al(OR^F)_4]$ from $Li[Al(OR^F)_4]$ and SF_4

Due to $Li[F(Al(OR^F)_3)_2]$ not being accessible[34], only the synthesis of $[SF_3]^+$ cations was considered due to the high FIA of $[SeF_3]^+$ and $[TeF_3]^+$ of 941 and 962 kJmol^{-1}.

$Li[Al(OR^F)_4]$ (300 mg, 0.31 mmol, 1.0 eq.) was weighed into one bulb of a two bulb vessel separated by a glass frit. C_6F_{14} (3 mL) was condensed onto the solids and the mixture was. An atmosphere of SF_4 was condensed onto the solution. The solution was allowed to stir for 18 h. Afterwards, all volatiles were removed under vacuum and the obtained powder was analyzed via NMR spectroscopy in CH_2Cl_2. **NMR:** ^{19}F-NMR (282.5 MHz, CH_2Cl_2, RT): δ = 74.9 (s., unknown), −72.0 (br., unknown), −74.5 (s, 9 F, $HOC(C\mathbf{F}_3)_3$), −75.7 (s, 36 F, $[Al(OC(C\mathbf{F}_3)_3)_4]^-$) ppm. ^{27}Al-NMR (78.2 MHz, CH_2Cl_2, RT): δ = 34.9 (s., 1 Al, $[\mathbf{Al}(OR^F)_4]^-$). ^{7}Li-NMR (116.7 MHz, CH_2Cl_2, RT): δ = −1.0 (s., $Li[Al(OR^F)_4]$) ppm.

The NMR spectra have shown anion decomposition and two small signals at around 70 to 80 ppm that could be caused by sulfur bound F atoms. However, the overall intensity of these signals is well below 1 % of the overall intensity of the residual $[Al(OR^F)_4]^-$ anion.

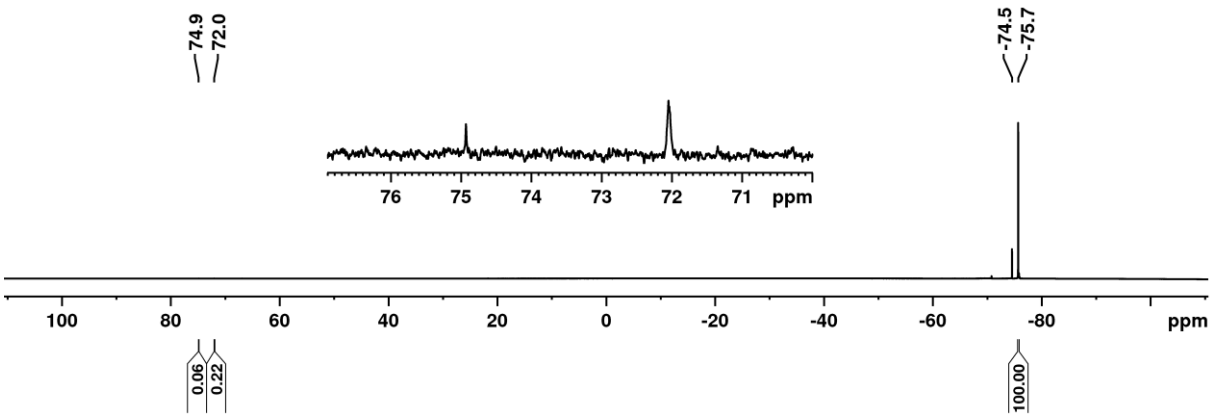

Figure S 82 ^{19}F-NMR spectrum (282.5 MHz, CH_2Cl_2, RT) of the product obtained from the reaction of SF_4 with $Li[Al(OR^F)_4]$ in C_6F_{14}. The small resonance at −74.6 ppm stems from free alcohol $HOC(CF_3)_3$.

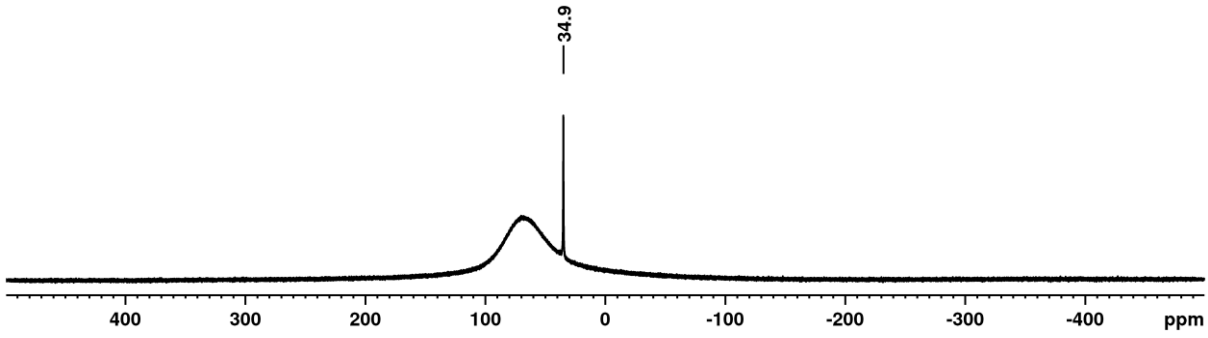

Figure S 83 ^{27}Al-NMR spectrum (78.2 MHz, CD_2Cl_2, RT) of the product obtained from the reaction of SF_4 with $Li[Al(OR^F)_4]$ in C_6F_{14}. The broad resonance at 70 ppm stems from the probe head.

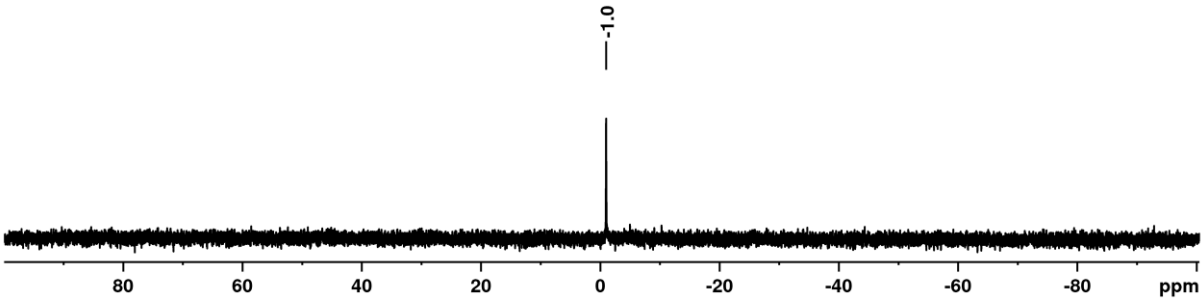

Figure S 84 ^{7}Li-NMR spectrum (116.7 MHz, CH_2Cl_2, RT) of the product obtained from the reaction of SF_4 with $Li[Al(OR^F)_4]$ in C_6F_{14}. The small resonance at −74.6 ppm stems from free alcohol $HOC(CF_3)_3$.

Tested Reaction of $Tl[Al(OR^F)_4]$ with PCl_3

$Tl[Al(OR^F)_4]$ (100 mg, 0.09 mmol, 1 eq.) was weighed in an NMR tube with a J. Young valve and dissolved in CD_2Cl_2 (0.7 mL). Freshly distilled PCl_3 (0.1 mL, approx. 160 mg, approx. 1.2 mmol, approx. 14 eq.) was added with a syringe and the resulting colorless solution was heavily shaken and then analyzed via NMR spectroscopy. The identical reaction with $Ag[Al(OR^F)_4]$ leads to a precipitation of AgCl and the decomposition of the anion.[39] **NMR:** ^{19}F-NMR (282.5 MHz, CH_2Cl_2, RT): δ = −75.6 (s, 36 F, $[Al(OC(C\mathbf{F}_3)_3)_4]^-$) ppm. ^{27}Al-NMR (78.2 MHz, CH_2Cl_2, RT): δ = 34.6 (s, 1 Al, $[\mathbf{Al}(OC(CF_3)_3)_4]^-$) ppm. ^{31}P-NMR (121.5 MHz, CH_2Cl_2, RT): δ = −219.5 (br., PCl_3) ppm.

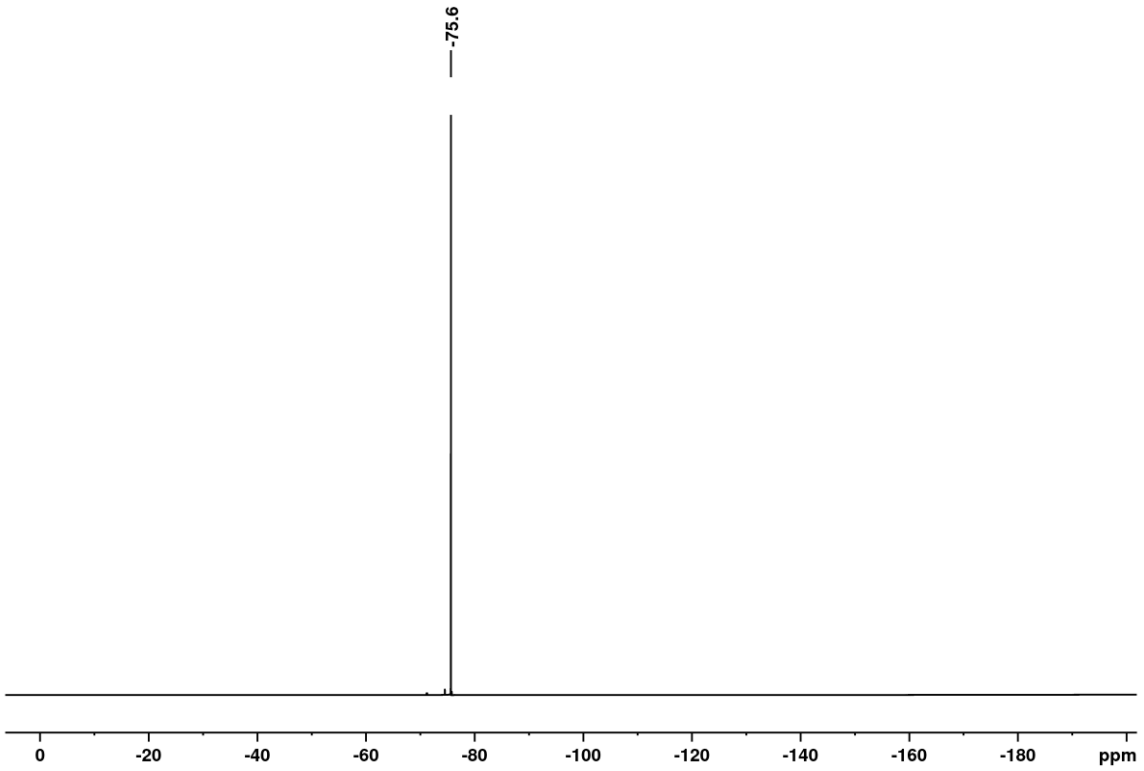

Figure S 85 ^{19}F-NMR spectrum (282.5 MHz, CD_2Cl_2, RT) of the tested reaction of PCl_3 with $Tl[Al(OR^F)_4]$.

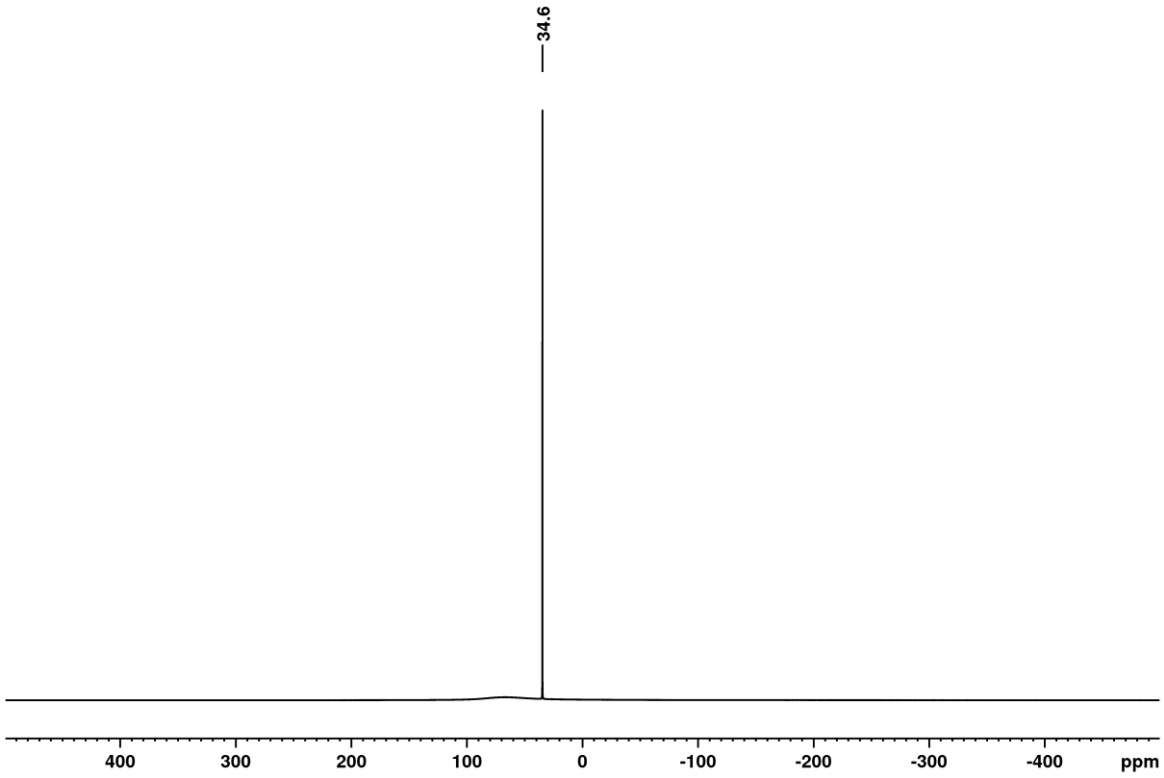

Figure S 86 ^{27}Al-NMR spectrum (78.2 MHz, CD_2Cl_2, RT) of the tested reaction of PCl_3 with $Tl[Al(OR^F)_4]$. The broad resonance from 50 to 100 ppm stems from the probe head.

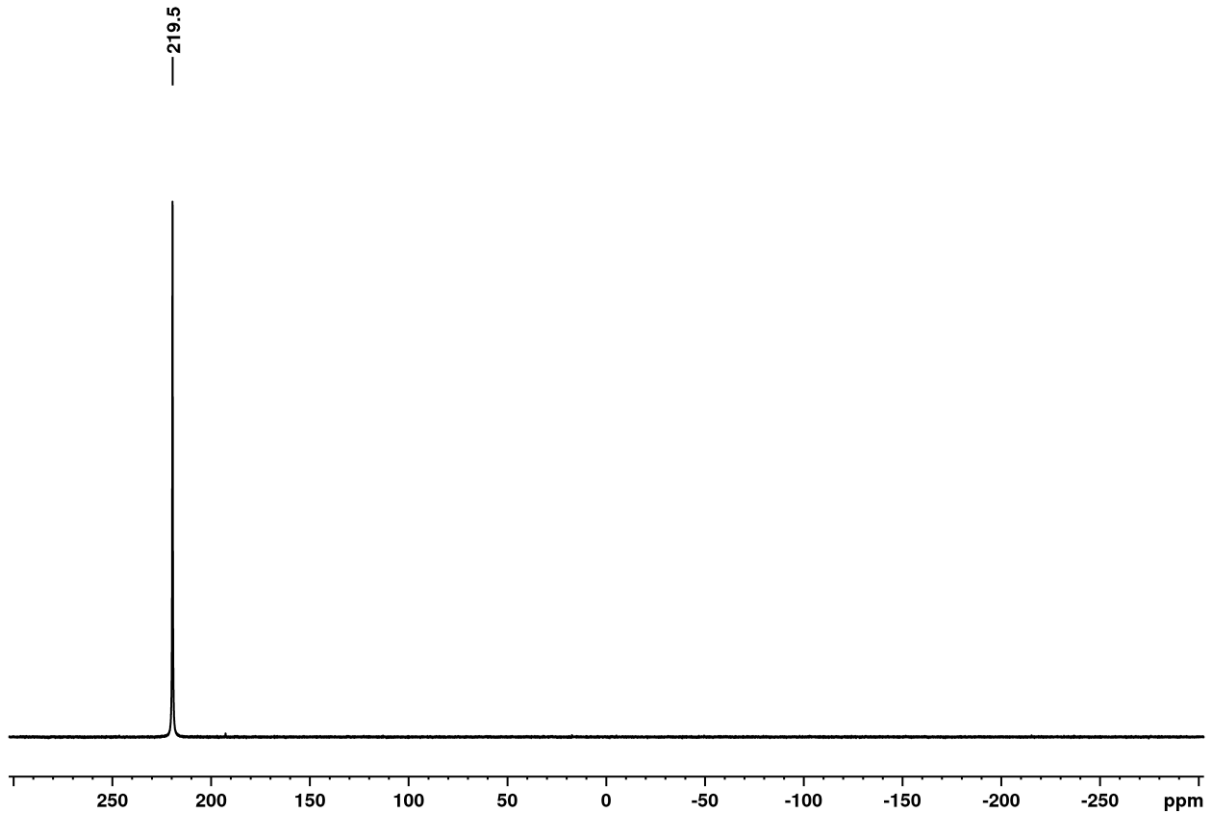

Figure S 87 ^{31}P-NMR spectrum (121.5 MHz, CD_2Cl_2, RT) of the tested reaction of PCl_3 with $Tl[Al(OR^F)_4]$.

Tested Reaction of $Tl[Al(OR^F)_4]$ with P_4

To check the possibility of a $Tl(P_4)_n[Al(OR^F)_4]$ complex to form $Tl[Al(OR^F)_4]$ (100 mg, 0.09 mmol, 1 eq.) and P_4 (21 mg, 0.18 mmol, 2 eq.) were weighed into one bulb of a two bulb vessel separated by a glass frit. CH_2Cl_2 (2 ml) was condensed onto the solids and the mixture was stirred for 1 h at room temperature until all the phosphorus was dissolved. The other side of the reaction vessel was then loaded with pentane and the solution was kept at room temperature for 5 days until colorless crystals had grown. scXRD experiments have shown the colorless crystals to be naked $Tl[Al(OR^F)_4]$.

Molecular Structure of $Tl[Al(OR^F)_4]$

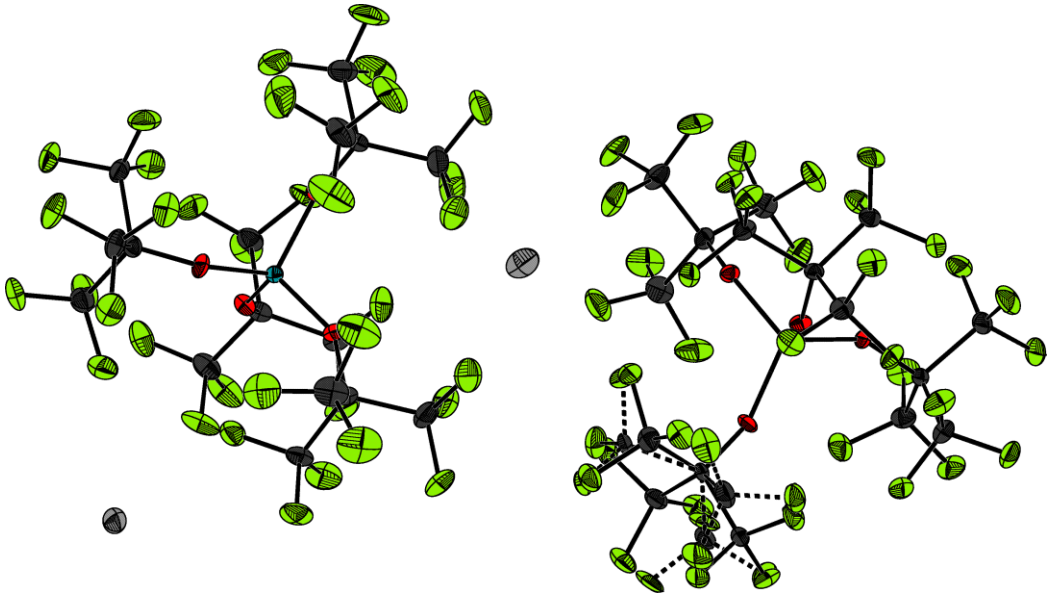

Figure S 88 Close up view of the molecular structure of the two crystallographically independent $Tl[Al(OR^F)_4]$ units in the crystal structure of $Tl[Al(OR^F)_4]$. All thermal ellipsoids are shown at 50 % probability. The stippled bonds indicate disordered parts of the structure.

4. Details to the Quantum Chemical Calculations

4.1. Calculated MO Diagrams

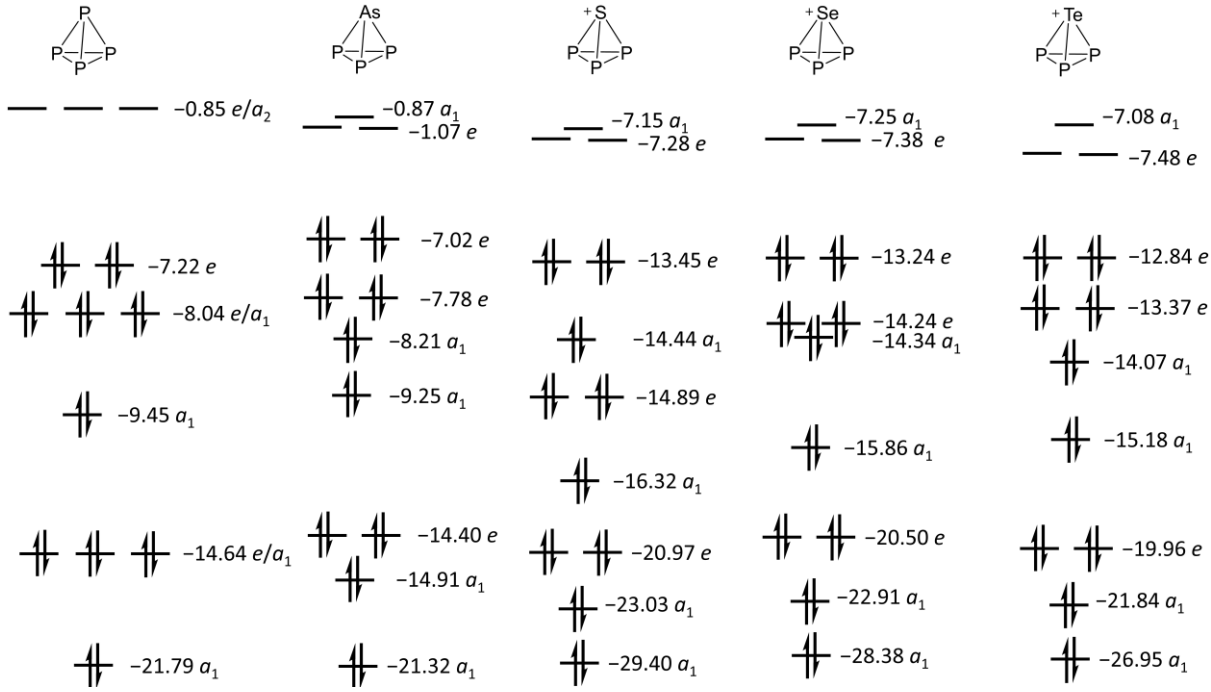

Figure S 89 Summary of the calculated MO diagrams of P_4, AsP_3, $[P_3S]^+$, $[P_3Se]^+$ and $[P_3Te]^+$. The diagram of P_4 was calculated using C_{3v} symmetry. The diagrams were calculated at the (RIJ)B3-LYP/def2-TZVPP level.

4.2. Aim Analyses and Laplacian of the Electron Density

Contour plots of the Laplacian of the electron density at the P_3 vertexes show a similar situation for all $[EP_3]^+$ cations. They are closely related to the neutral molecules AsP_3 and P_4. The contour plots of the P_2E vertexes show that $[P_3S]^+$ is very similar to P_4 and that $[P_3Se]^+$ and $[P_3Te]^+$ are more similar to AsP_3. The contour plots of the plane through a P–E bond and an opposite *bond critical point* (BCP) again show the similarity of the P–S bond to the P–P bond in P_4, whereas the heavier homologues show similarities to AsP_3. The contour plots of the plane through a P–P bond and an opposite BCP show a *local charge concentration* (LCC) slightly outside the middle of the P–P bonds and no lone pair for all tetrahedra. This is in accordance with the findings from the protonation of P_4[40] and the complexes $[M(P_4)_n]^{+}$[41] (M = Cu, Ag, Au), where simple positively charged ions coordinate side-on to the P_4 tetrahedron. Exohedral lone pairs of the clusters are absent for any of the tetrahedra, which confirms the nature of the tetrahedra as delocalized clusters rather than electron precise molecules.

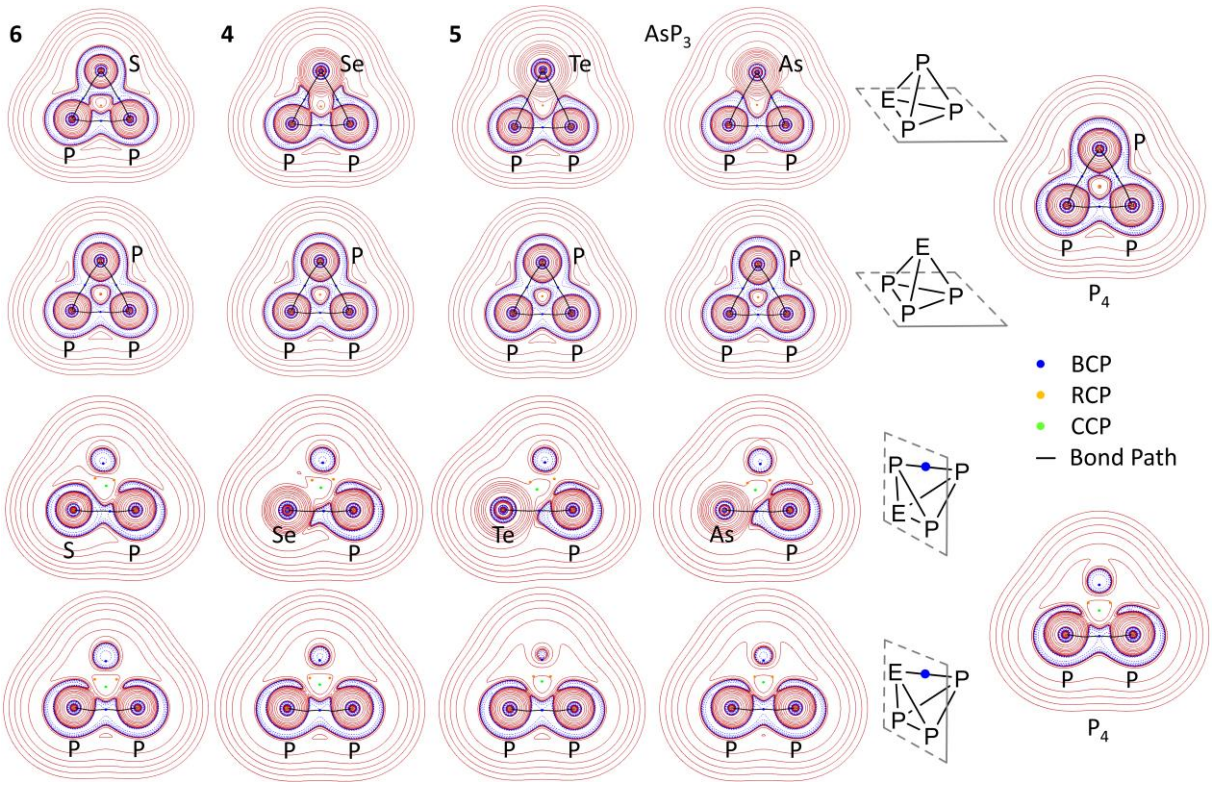

Figure S 90 Contour plots of the Laplacian of the electron density ρ of the $[EP_3]^+$ (E = S, Se, Te) cations, as well as P_4 and AsP_3 compared. The EP_2 planes (top row), P_3 planes (second row) as well as cross-sections through the E-P bond and the opposite BCP (third row) and through the P-P bond and the opposite BCP (bottom row) are shown. The red continuous contour lines indicate positive values and the blue dashed lines indicate negative values.

The electron density (ρ_{XCP}) at the critical points XCP (X = R (ring), C (cluster), B (bond)) of the $[EP_3]^+$ cations have similar values to P_4 and AsP_3. ρ_{RCP} of the P_3 ring is generally lower in P_4 than in the binary counterparts. ρ_{RCP} of the P_2E rings is the highest for $[SP_3]^+$ and the lowest for $[TeP_3]^+$, this trend is also reflected in ρ_{CCP}. ρ_{BCP}(P–P) is higher in the binary tetrahedra than in P_4, indicating stronger P–P bonds in the binary compounds. ρ_{BCP}(P–E) is highest in $[SP_3]^+$ and lowest in $[TeP_3]^+$ indicating stronger P–S bonds compared to P–Te bonds. The ellipticities of the electron density at the BCP of the P–P bonds (ε_{BCP}(P–P)) is higher for the binary compounds and ε_{BCP}(P–E) is the lowest for $[SP_3]$ and again highest for $[TeP_3]^+$ (Table S 11).

Table S 11 Summary of the AIM analysis ((RIJ)MP2/def2-QZVPP) of the $[EP_3]^+$ cations as well as AsP_3 and P_4. All electron densities (ρ) at the critical points XCP (X = R (ring), C (cluster), B (bond)) are given in eÅ^{-3}. The ellipticities of the electron density at a given critical point are denoted with ε_{XCP}.

Compound	$\rho_{CCP}(EP_3)$	$\rho_{RCP}(P_3)$	$\rho_{RCP}(P_2E)$	ρ_{BCP}(P–P)	ε_{BCP}(P–P)	ρ_{BCP}(P–E)	ε_{BCP}(P–E)
P_4	0.53	0.57	—	0.71	0.110	—	—
AsP_3	0.52	0.62	0.53	0.73	0.156	0.63	0.163
$[SP_3]^+$	0.57	0.60	0.61	0.74	0.149	0.76	0.078
$[SeP_3]^+$	0.53	0.60	0.55	0.75	0.203	0.67	0.151
$[TeP_3]^+$	0.47	0.60	0.48	0.74	0.230	0.55	0.189

4.3. Calculated NMR parameters

The calculated ^{31}P chemical shifts of the $[EP_3]^+$ cations were calculated using ORCA 4.1.1 based on previously calculated (RIJ)MP2/def2-QZVPP structures with (RIJK)B3-LYP/cc-pVQZ single points using a relativistic DKH2 operator with a fully decontracted basis set. The obtained chemical shifts were referenced against the chemical shift of P_4 in CH_2Cl_2 solution. To benchmark the obtained chemical shifts, the known molecules AsP_3 and SbP_3 were calculated using the same method. The obtained chemical shifts are given in Table S 12.

Table S 12 Calculated ^{31}P chemical shifts of P_4, AsP_3, SbP_3, $[P_3S]^+$, $[P_3Se]^+$ and $[P_3Te]^+$.

Compound	Diamagnetic Contribution [ppm]	Paramagnetic Contribution [ppm]	Shielding Tensor (calc.) [ppm]	Corrected [ppm][a)]	Observed [ppm]	NICS[b)]	NICS(P_3)[c)]	NICS(P_2E)[d)]
P_4	972.265	−107.891	864.374	−520	−520	−61.9	−60.4	–
AsP_3	972.285	−143.787	828.498	−484	−484	−61.3	−60.5	−59.5
SbP_3	972.939	−177.039	795.900	−452	−462	−58.6	−60.0	−56.1
$[P_3S]^+$	969.744	−219.103	750.641	−406	−399.3	−60.6	−54.9	−60.2
$[P_3Se]^+$	969.852	−263.374	706.478	−362	−360.6	−60.3	−55.0	−59.7
$[P_3Te]^+$	970.377	−286.972	683.405	−339	−342.9	−59.4	−55.9	−58.3

a) vs. diluted solution of P_4 in CH_2Cl_2 at −520 ppm. b) NICS values are calculated at the cage center. c) Calculated at the center of the P_3 trigons. d) Calculated at the center of the P_2E trigons.

This method was also tested for the prediction of the ^{77}Se- and ^{125}Te-NMR shifts. To test, if the method is valid and able to describe ^{77}Se- and ^{125}Te-NMR shifts over a broad spectral range, a set of several molecules (all in different regions of the spectral range) was calculated using this method and referenced. It is noticeable, that the trends in chemical shifts are described accurately over the whole spectral range (with $[ECl_3]^+$ and $[EP_3]^+$ spanning an experimental range of 2300 ppm (Se) and 5000 ppm (Te)). The exact values of the chemical shifts however differ and accurate results are only obtained if the chosen standard has a chemical shift near to the desired sample. Hence the chosen standard for the prediction of the chemical shift of $[EP_3]^+$, which lies in an atypical region for E(IV) compounds, is $EPMe_3$ (E = Se, Te).

Table S 13 Calculated ^{77}Se chemical shifts of $[P_3Se]^+$ and various other known compounds.

Compound	Diamagnetic Contribution [ppm]	Paramagnetic Contribution [ppm]	Shielding Tensor (calc.) [ppm]	Observed [ppm]	Corrected [ppm][a)]	Corrected [ppm][b)]
Me_2Se	3091.485	−1411.727	1679.758	0	0	184
$[SeCl_3]^+$	3083.022	−3032.079	50.943	1384 – 1407[c)]	1629	1813
$[SeMeCl_2]^+$	3084.928	−2701.957	382.971	1119[1]	1297	1481
$Se(CF_3)_2$	3099.365	−2152.248	947.117	717[42]	733	917
MeSeCN	3092.294	−1493.848	1598.446	125[42]	81	265
H_2Se	3093.27	−990.195	2103.075	−226[42]	−423	−239
$SePMe_3$	3099.359	−1000.634	2098.725	−235[42]	−419	−235
$Se(SiH_3)_2$	3097.054	−673.408	2423.646	−666[42]	−744	−560
$[P_3Se]^+$	3094.294	−218.928	2875.366	−894[c)]	−1196	−1012

a) vs. Me_2Se b) vs. $SePMe_3$ c) This work.

Table S 14 Calculated ^{125}Te chemical shifts of $[P_3Te]^+$ and various other known compounds.

Compound	Diamagnetic Contribution [ppm]	Paramagnetic Contribution [ppm]	Shielding Tensor (calc.) [ppm]	Observed [ppm]	Corrected [ppm][a)]	Corrected [ppm][b)]
Me_2Te	5749.458	−3200.978	2548.48	0	0	418
$[Te_4]^{2+}$	5748.237	−7555.736	−1807.499	2811[42]	4356	4774
$[TeCl_3]^+$	5743.331	−5411.198	332.133	1952[c)]	2216	2634
$TePMe_3$	5752.981	−2273.653	3479.328	−513[42]	−931	−513
$[P_3Te]^+$	5749.847	−195.196	5554.651	−2212[c)]	−3006	−2588

a) vs. Me_2Te b) vs. $TePMe_3$ c) This work.

4.4. Summary of the ab initio Reaction Enthalpies and Free Reaction Energies

Table S 15 Ab initio reaction enthalpies and free reaction energies for the formation of $[P_3E]^+$ from P_4 and $[EX_3]^+$ (E = S, Se, Te; X = F, Cl, Br, I) [$^{kJ}/_{mol}$].

reaction	theory [a]	basis set	level n	$\Delta_r H^{298}$(g)[b]	$\Delta_r G^{298}$(g)[b]	$\Delta_r G^{298}$(solv, CH_2Cl_2)[c]	$\Delta_r G^{298}$(solv, o–DFB)[c]	$\Delta_r G^{298}$(solv, SO_2)[c]
$P_4 + [EF_3]^+ \rightarrow [P_3E]^+ + PF_3$	DFT(BP86)	def2-TZVPP	T	−515, (−519), [−378]	−519, (−522), [−380]	−477, (−468), [−319]	−475, (−464), [−315]	−474, (−463), [−314]
E = S, Se (in parentheses), Te (in brackets)	MP2	aug-cc-pVnZ (F, Se)	T	−547, (−548), [−415]	−551, (−551), [−417]			
		aug-cc-pV(n+d)Z (P, S)	Q	−546, (−548), [−421]	−550, (−551), [−423]			
		aug-cc-pwCVnZ (Te,)	5	−545, (−549), [−423]	−549, (−552), [−425]			
	CCSD(T)		T	−552, (−559), [−398]	−557, (−562), [−399]			
			∞(CBS)[d]	−550, (−560), [−407]	−554, (−563), [−408]			
$P_4 + [ECl_3]^+ \rightarrow [P_3E]^+ + PCl_3$	DFT(BP86)	def2-TZVPP	T	−315, (−267), [−151]	−319, (−270), [−154]	−324, (−269), [−143]	−325, (−268), [−143]	−325, (−268), [−142]
E = S, Se (in parentheses), Te (in brackets)	MP2	aug-cc-pVnZ (Se)	T	−339, (−291), [−182]	−344, (−295), [−185]			
		aug-cc-pV(n+d)Z (P, S, Cl)	Q	−338, (−292), [−183]	−343, (−295), [−185]			
		aug-cc-pwCVnZ (Te)	5	−338, (−292), [−183]	−342, (−295), [−186]			
	CCSD(T)		T	−341, (−291), [−166]	−345, (−295), [−166]			
			∞(CBS)[d]	−339, (−291), [−167]	−343, (−295), [−170]			
$P_4 + [EBr_3]^+ \rightarrow [P_3E]^+ + PBr_3$	DFT(BP86)	def2-TZVPP	T	−249, (−192), [−88]	−253 , (−196), [−91]	−271, (−209), [−96]	−272, (−210), [−97]	−273, (−210), [−97]
E = S, Se (in parentheses), Te (in brackets)	MP2	aug-cc-pVnZ (Se, Br)	T	−260, (−206), [−111]	−264, (−210), [−113]			
		aug-cc-pV(n+d)Z (P, S)	Q	−258, (−204), [−107]	−262, (−207), [−110]			
		aug-cc-pwCVnZ (Te)	5	−258, (−203), [−106]	−262, (−207), [−109]			
	CCSD(T)		T	−265, (−210), [−102]	−269, (−213), [−104]			
			∞(CBS)[d]	−263, (−206), [−97]	−267, (−210), [−99]			
$P_4 + [EI_3]^+ \rightarrow [P_3E]^+ + PI_3$	DFT(BP86)	def2-TZVPP	T	−148, (−95), [−14]	−151, (−98), [−16]	−184, (−127), [−39]	−186, (−129), [−41]	−187, (−129), [−41]
E = S, Se (in parentheses), Te (in brackets)	MP2	aug-cc-pVnZ (Se)	T	−166, (−120), [−43]	−170, (−123), [−45]			
		aug-cc-pV(n+d)Z (P, S)	Q	−169, (−121), [−41]	−173, (−123), [−43]			
		aug-cc-pwCVnZ (Te, I)	5	−170, (−121), [−40]	−174, (−124), [−42]			
	CCSD(T)		T	−160, (−113), [−33]	−164, (−116), [−35]			
			∞(CBS)[d]	−165, (−115), [−29]	−168, (−118), [−32]			
$5/4\ P_4 + [SeCl_3]^+ \rightarrow [P_5Cl_2]^+ + ½\ Se_2Cl_2$	DFT(BP86)	def2-TZVPP	T	−273, (−231), [−132]	−242, (−200), [−101]	−227, (−182), [−84]	−225, (−181), [−82]	−225, (−180), [−82]
	MP2	aug-cc-pVnZ (Se)	T	−300, (−259), [−160]	−270, (−228), [−130]			
		aug-cc-pV(n+d)Z (P, S, Cl)	Q	−300, (−260), [−162]	−270, (−229), [−131]			
		aug-cc-pwCVnZ (Te)	5	−300, (−260), [−163]	−270, (−230), [−132]			
	CCSD(T)		T	−297, (−254), [−149]	−267, (−224), [−118]			
			∞(CBS)[d]	−297, (−256), [−152]	−267, (−226), [−121]			

[a] Start geometries from (RIJ)MP2/def2-QZVPP calculations, except for the BP86/def2-TZVPP calculations. [b] Thermodynamics (enthalpy, entropy, chem. pot.) taken from BP86/def2-TZVPP calculations. [c] COSMO[18] energies optimized at BP86/def2-TZVPP level and with ε_r = 8.93, 13.38 and 16.3 (CH_2Cl_2, *o*-dfb and $SO_{2(l)}$). [d] SCF energies calculated on CCSD(T)/aug-cc-pVnZ (n → ∞, extrapolation of MP2/aug-cc-pVnZ energies (n = 3, 5)), corrected by the difference MP2/aug-cc-pvnZ - MP2/aug-cc-pvnZ (n = T). [f] Calculations with Se, Br, I and Te include a *frozen core approximation*.

4.5. Summary of the Calculated FIAs

Table S 16 Ab initio FIAs of $[P_3E]^+$ (E = S, Se, Te) and EX_3 (E = S, Se, Te and X = F, Cl, Br, I) [$^{kJ}/_{mol}$]. The FIAs at DFT level were calculated relative to TMS^+/TMS-F. The MP2 and CCSD(T) FIAs were calculated against F^-**.** The FIAs at the BP86/def2-TZVPP level were calculated against BF_3/$[BF_4]^-$.

	theory [a]	basis set	level n	FIA	
$[EF_3]^+$	DFT(BP86)	def2-TZVPP	T	902, (929), [936]	
E = S, Se (in parentheses), Te (in brackets)	MP2	aug-cc-pVnZ (F, Se)	T	904, (935), [952]	
		aug-cc-pV(n+d)Z (P, S)	Q	905, (937), [955]	
		aug-cc-pwCVnZ (Te,)	5	904, (937), [955]	
	CCSD(T)		T	909, (939), [958]	
			∞(CBS)[b]	909, (941), [962]	
$[ECl_3]^+$	DFT(BP86)	def2-TZVPP	T	772, (796), [825]	
E = S, Se (in parentheses), Te (in brackets)	MP2	aug-cc-pVnZ (F, Se)	T	774, (803), [839]	
		aug-cc-pV(n+d)Z (P, S)	Q	775, (806), [842]	
		aug-cc-pwCVnZ (Te,)	5	776, (806), [842]	
	CCSD(T)		T	773, (800), [842]	
			∞(CBS)[b]	775, (803), [844]	
$[EBr_3]^+$	DFT(BP86)	def2-TZVPP	T	738, (759), [790]	
E = S, Se (in parentheses), Te (in brackets)	MP2	aug-cc-pVnZ (F, Se)	T	734, (762), [799]	
		aug-cc-pV(n+d)Z (P, S)	Q	736, (764), [801]	
		aug-cc-pwCVnZ (Te,)	5	737, (764), [801]	
	CCSD(T)		T	732, (759), [803]	
			∞(CBS)[b]	735, (762), [805]	
$[EI_3]^+$	DFT(BP86)	def2-TZVPP	T	680, (702), [736]	
E = S, Se (in parentheses), Te (in brackets)	MP2	aug-cc-pVnZ (F, Se)	T	678, (707), [748]	
		aug-cc-pV(n+d)Z (P, S)	Q	682, (711), [751]	
		aug-cc-pwCVnZ (Te, I)	5	683, (712), [752]	
	CCSD(T)		T	669, (699), [749]	
			∞(CBS)[b]	675, (704), [753]	
				F bound to *E*	F bound to P
$[EP_3]^+$	DFT(BP86)	def2-TZVPP	T	675, (696), [725]	828, (820), [798]
E = S, Se (in parentheses), Te (in brackets)	MP2	aug-cc-pVnZ (F, Se)	T	650, (682), [713]	806, (796), [775]
		aug-cc-pV(n+d)Z (P, S)	Q	652, (683), [714]	810, (800), [779]
		aug-cc-pwCVnZ (Te)	5	652, (683), [714]	811, (801), [779]
	CCSD(T)		T	629, (662), [695]	823, (813), [793]
			∞(CBS)[b]	630, (663), [697]	828, (819), [798]

[a] Start geometries from (RIJ)MP2/def2-QZVPP calculations. Thermodynamics (enthalpy, entropy, chem. pot.) taken from BP86/def2-TZVPP calculations. [b] SCF energies calculated on CCSD(T)/aug-cc-pVnZ (n → ∞, extrapolation of MP2/aug-cc-pVnZ energies (n = 4,5), corrected by the difference CCSD(T)/aug-cc-pvnZ - MP2/aug-cc-pvnZ (n = T). [c] Calculations with Se, Br, I and Te include a *frozen core approximation*.

4.5. Calculated Structures

P_4

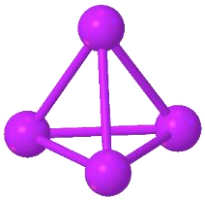

```
Symmetry: td
Method: (RIJ)MP2/def2-QZVPP

P          0.77533       -0.77533        0.77533
P         -0.77533        0.77533        0.77533
P          0.77533        0.77533       -0.77533
P         -0.77533       -0.77533       -0.77533
SCF energy GEOOPT =  -1363.067078418
MP2 energy =  -1363.7029056839
```

AsP_3

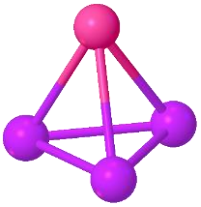

```
Symmetry: c3v
Method: (RIJ)MP2/def2-QZVPP

P          0.63345        1.09717        0.48116
As         0.00000        0.00000       -1.44348
P          0.63345       -1.09717        0.48116
P         -1.26691        0.00000        0.48116
SCF energy GEOOPT =  -3256.563884965
MP2 energy =  -3257.5884789784
```

SbP_3

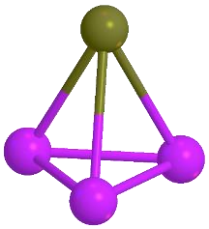

```
Symmetry: c3v
Method: (RIJ)MP2/def2-QZVPP

P          0.63461        1.09918        0.53856
Sb        -0.00000        0.00000       -1.61568
P          0.63461       -1.09918        0.53856
P         -1.26922        0.00000        0.53856
SCF energy GEOOPT =  -1261.582143520
MP2 energy =  -1262.6538589001
```

$[P_3S]^+$

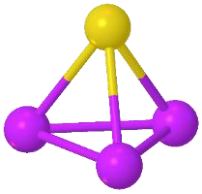

```
Symmetry: c3v
Method: (RIJ)MP2/def2-QZVPP

P          0.63555        1.10081        0.43279
S         -0.00000        0.00000       -1.29836
P          0.63555       -1.10081        0.43279
P         -1.27111        0.00000        0.43279
SCF energy GEOOPT =  -1419.596182330
MP2 energy =  -1420.2404138005
```

$[P_3Se]^+$

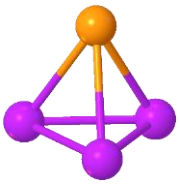

```
Symmetry: c3v
Method: (RIJ)MP2/def2-QZVPP

P          0.63656        1.10255        0.47323
Se        -0.00000        0.00000       -1.41970
P          0.63656       -1.10255        0.47323
P         -1.27311        0.00000        0.47323
SCF energy GEOOPT =  -3421.942402114
MP2 energy =  -3422.9730481223
```

$[P_3Te]^+$

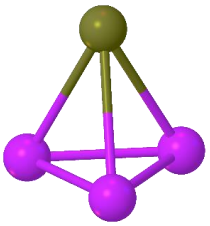

```
Symmetry: c3v
Method: (RIJ)MP2/def2-QZVPP

P          0.63764        1.10443        0.52853
Te         0.00000        0.00000       -1.58559
P          0.63764       -1.10443        0.52853
P         -1.27529        0.00000        0.52853
SCF energy GEOOPT =  -1289.063170096
MP2 energy =  -1290.1524017732
```

PF_3

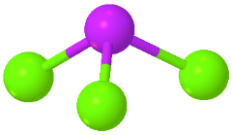

```
Symmetry: c3v
Method: (RIJ)MP2/def2-QZVPP

P          0.00000        0.00000        0.58047
F         -0.68228        1.18175       -0.19349
F         -0.68228       -1.18175       -0.19349
F          1.36456        0.00000       -0.19349
SCF energy GEOOPT =  -639.3445880081
```

MP2 energy = -640.3188433989

PCl_3

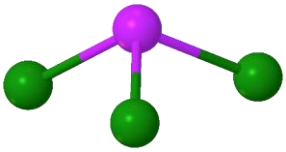

Symmetry: c3v
Method: (RIJ)MP2/def2-QZVPP

P	0.00000	0.00000	0.70994
Cl	-0.90213	1.56254	-0.23665
Cl	-0.90213	-1.56254	-0.23665
Cl	1.80426	0.00000	-0.23665

SCF energy GEOOPT = -1719.402222907
MP2 energy = -1720.1886694738

PBr_3

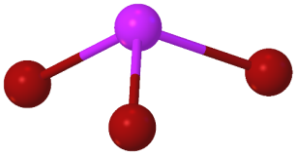

Symmetry: c3v
Method: (RIJ)MP2/def2-QZVPP

P	-0.00000	0.00000	0.75608
Br	-0.98597	1.70776	-0.25203
Br	-0.98597	-1.70776	-0.25203
Br	1.97195	0.00000	-0.25203

SCF energy GEOOPT = -8058.220453760
MP2 energy = -8058.9183991847

PI_3

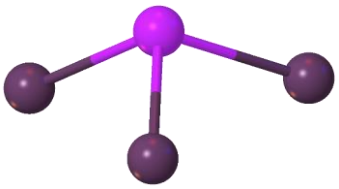

Symmetry: c3v
Method: (RIJ)MP2/def2-QZVPP

P	0.00000	0.00000	0.81269
I	-1.08337	1.87646	-0.27093
I	-1.08337	-1.87646	-0.27093
I	2.16674	0.00000	-0.27093

SCF energy GEOOPT = -1230.799755261
MP2 energy = -1232.9698343736

$[SF_3]^+$

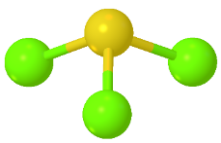

Symmetry: c3v
Method: (RIJ)MP2/def2-QZVPP

S	0.00000	0.00000	-0.52667
F	-0.66201	-1.14663	0.17555
F	-0.66201	1.14663	0.17555
F	1.32402	0.00000	0.17555

SCF energy GEOOPT = -695.6471730545
MP2 energy = -696.6496574985

$[SCl_3]^+$

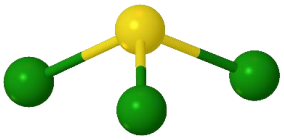

Symmetry: c3v
Method: (RIJ)MP2/def2-QZVPP

S	-0.00000	0.00000	-0.61569
Cl	-0.88744	-1.53709	0.20525
Cl	-0.88744	1.53709	0.20525
Cl	1.77487	0.00000	0.20525

SCF energy GEOOPT = -1775.783065302
MP2 energy = -1776.5976948753

$[SBr_3]^+$

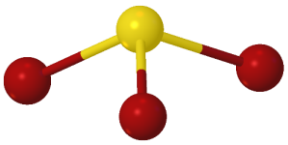

Symmetry: c3v
Method: (RIJ)MP2/def2-QZVPP

S	-0.00000	0.00000	-0.65443
Br	-0.97021	-1.68045	0.21816
Br	-0.97021	1.68045	0.21816
Br	1.94042	0.00000	0.21816

SCF energy GEOOPT = -8114.628041487
MP2 energy = -8116.5946026567

$[SI_3]^+$

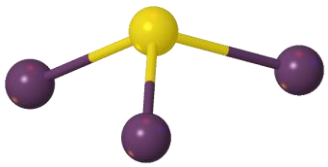

Symmetry: c3v
Method: (RIJ)MP2/def2-QZVPP

S	-0.00000	0.00000	-0.70194
I	-1.07972	-1.87013	0.23400
I	-1.07972	1.87013	0.23400
I	2.15944	0.00000	0.23400

SCF energy GEOOPT = -1287.255436542
MP2 energy = -1289.4427905296

$[SeF_3]^+$

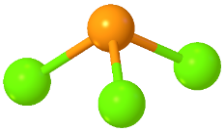

Symmetry: c3v
Method: (RIJ)MP2/def2-QZVPP

Se	0.00000	0.00000	-0.61160
F	-0.71340	-1.23565	0.20387
F	-0.71340	1.23565	0.20387
F	1.42680	0.00000	0.20387

SCF energy GEOOPT = -2697.985265572
MP2 energy = -2699.3735999986

$[SeCl_3]^+$

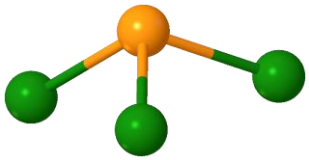

Symmetry: c3v
Method: (RIJ)MP2/def2-QZVPP

Se	-0.00000	0.00000	0.70201
Cl	0.92968	1.61025	-0.23400
Cl	0.92968	-1.61025	-0.23400
Cl	-1.85936	0.00000	-0.23400

SCF energy GEOOPT = -3778.152916852
MP2 energy = -3779.3450663577

$[SeBr_3]^+$

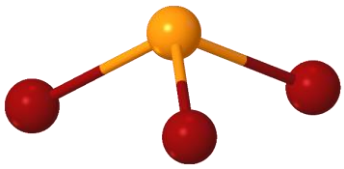

Symmetry: c3v
Method: (RIJ)MP2/def2-QZVPP

Se	0.00000	0.00000	0.73929
Br	1.00845	1.74668	-0.24643
Br	1.00845	-1.74668	-0.24643
Br	-2.01690	0.00000	-0.24643

SCF energy GEOOPT = -10117.00146557
MP2 energy = -10119.3455455125

$[SeI_3]^+$

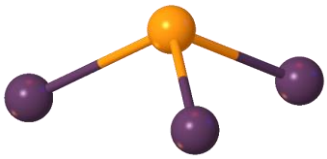

Symmetry: c3v
Method: (RIJ)MP2/def2-QZVPP

Se	-0.00000	0.00000	0.78966
I	1.11421	1.92988	-0.26321
I	1.11421	-1.92988	-0.26321
I	-2.22843	0.00000	-0.26321

SCF energy GEOOPT = -3289.625419316
MP2 energy = -3292.1930414921

$[TeF_3]^+$

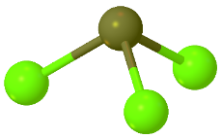

Symmetry: c3v
Method: (RIJ)MP2/def2-QZVPP

Te	0.00000	0.00000	-0.70531
F	-0.77048	-1.33452	0.23510
F	-0.77048	1.33452	0.23510
F	1.54097	0.00000	0.23510

SCF energy GEOOPT = -565.1705287044
MP2 energy = -566.6086084124

$[TeCl_3]^+$

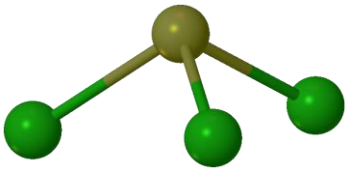

Symmetry: c3v
Method: (RIJ)MP2/def2-QZVPP

Te	-0.00000	0.00000	0.80716
Cl	0.98197	1.70082	-0.26906
Cl	0.98197	-1.70082	-0.26906
Cl	-1.96394	0.00000	-0.26906

SCF energy GEOOPT = -1645.332485487
MP2 energy = -1646.5706539690

$[TeBr_3]^+$

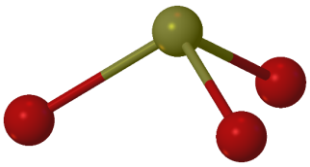

Symmetry: c3v
Method: (RIJ)MP2/def2-QZVPP

Te	-0.00000	0.00000	0.84307
Br	1.05919	1.83458	-0.28102
Br	1.05919	-1.83458	-0.28102
Br	-2.11839	0.00000	-0.28102

SCF energy GEOOPT = -7984.175909954
MP2 energy = -7986.5674067110

$[TeI_3]^+$

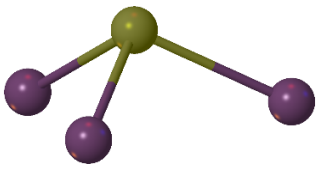

Symmetry: c3v
Method: (RIJ)MP2/def2-QZVPP

Te	0.00000	0.00000	0.89615
I	1.16300	2.01438	-0.29871
I	1.16300	-2.01438	-0.29871
I	-2.32600	0.00000	-0.29871

SCF energy GEOOPT = -1156.786949206
MP2 energy = -1159.4051524298

SF_4

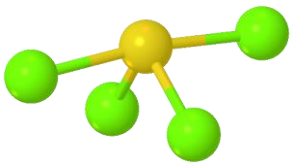

Symmetry: c2v
Method: (RIJ)MP2/def2-QZVPP

S	0.00000	0.00000	0.43428
F	0.00000	1.64436	0.32706
F	0.00000	-1.64436	0.32706
F	-1.19955	0.00000	-0.54358
F	1.19955	0.00000	-0.54358

SCF energy GEOOPT = -795.4251765166
MP2 energy = -796.7480862434

SCl_3F

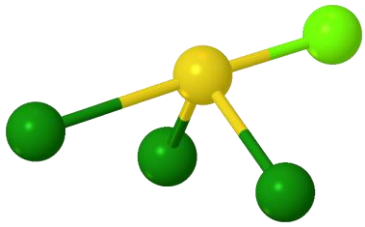

Symmetry: cs
Method: (RIJ)MP2/def2-QZVPP

S	0.17176	-0.47012	0.00000
Cl	-0.46339	0.55982	1.58949
Cl	2.05599	0.66368	0.00000
Cl	-0.46339	0.55982	-1.58949
F	-1.30098	-1.31321	0.00000

SCF energy GEOOPT = -1875.507308586
MP2 energy = -1876.6474607386

SBr_3F

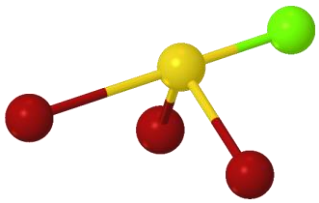

Symmetry: cs
Method: (RIJ)MP2/def2-QZVPP

S	0.16265	-0.50779	0.00000
Br	-0.53198	0.59928	1.74003
Br	2.23004	0.67807	0.00000
Br	-0.53198	0.59928	-1.74003
F	-1.32873	-1.36884	0.00000

SCF energy GEOOPT = -8214.337105155
MP2 energy = -8215.3897428261

SI_3F

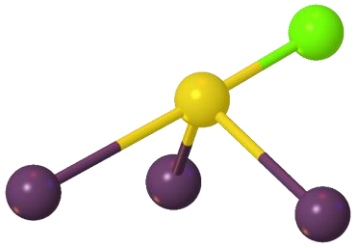

Symmetry: cs
Method: (RIJ)MP2/def2-QZVPP

S	0.16224	-0.54552	0.00000
I	-0.61424	0.64145	1.90305
I	2.42900	0.71091	0.00000
I	-0.61424	0.64145	-1.90305
F	-1.36275	-1.44831	0.00000

SCF energy GEOOPT = -1386.934803357
MP2 energy = -1389.4570682528

SeF_4

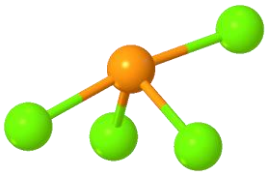

Symmetry: c2v
Method: (RIJ)MP2/def2-QZVPP

Se	0.00000	0.00000	0.49782
F	0.00000	1.75777	0.32735
F	1.29191	0.00000	-0.57626
F	-1.29191	0.00000	-0.57626
F	0.00000	-1.75777	0.32735

SCF energy GEOOPT = -2797.782316891
MP2 energy = -2799.4854201337

$SeCl_3F$

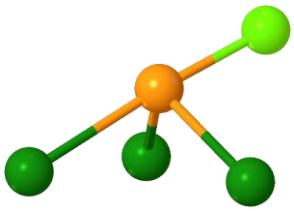

Symmetry: cs
Method: (RIJ)MP2/def2-QZVPP

Se	0.21279	-0.51567	0.00000
Cl	-0.48746	0.59519	1.65968
Cl	2.14469	0.70648	0.00000
Cl	-0.48746	0.59519	-1.65968
F	-1.38255	-1.38119	0.00000

SCF energy GEOOPT = -3877.892323228
MP2 energy = -3879.4043423624

$SeBr_3F$

Symmetry: cs
Method: (RIJ)MP2/def2-QZVPP

Se	0.20106	-0.55098	0.00000
Br	-0.55704	0.63590	1.80249
Br	2.31903	0.71684	0.00000
Br	-0.55704	0.63590	-1.80249
F	-1.40601	-1.43766	0.00000

SCF energy GEOOPT = -10216.72510273
MP2 energy = -10218.1486367568

SeI_3F

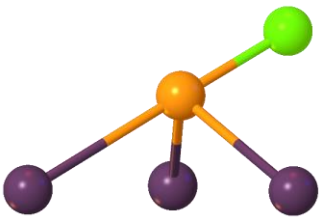

Symmetry: cs

Method: (RIJ)MP2/def2-QZVPP

```
Se          0.19696       -0.59245        0.00000
I          -0.64074        0.67949        1.96197
I           2.51604        0.74729        0.00000
I          -0.64074        0.67949       -1.96197
F          -1.43151       -1.51381        0.00000
SCF energy GEOOPT =  -3389.321247102
MP2 energy =  -3392.2153983778
```

TeF_4

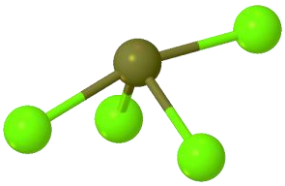

Symmetry: c2v
Method: (RIJ)MP2/def2-QZVPP

```
Te          0.00000        0.00000        0.57926
F           0.00000        1.88591        0.31455
F           0.00000       -1.88591        0.31455
F           1.40191        0.00000       -0.60418
F          -1.40191        0.00000       -0.60418
SCF energy GEOOPT =  -664.9799163922
MP2 energy =   -666.7279052716
```

$TeCl_3F$

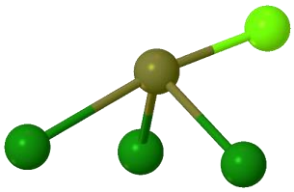

Symmetry: cs
Method: (RIJ)MP2/def2-QZVPP

```
Te          0.25786       -0.59099        0.00000
Cl         -0.50665        0.62921        1.75839
Cl          2.23958        0.77060        0.00000
Cl         -0.50665        0.62921       -1.75839
F          -1.48413       -1.43803        0.00000
SCF energy GEOOPT =  -1745.094796313
MP2 energy =  -1746.6469959305
```

$TeBr_3F$

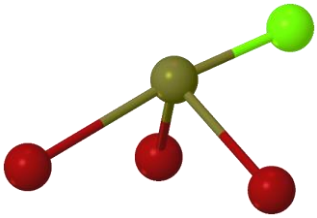

Symmetry: cs
Method: (RIJ)MP2/def2-QZVPP

```
Te          0.24469       -0.62582        0.00000
Br         -0.57742        0.66911        1.89883
Br          2.41126        0.78225        0.00000
Br         -0.57742        0.66911       -1.89883
F          -1.50111       -1.49465        0.00000
SCF energy GEOOPT =  -8083.924647844
MP2 energy =  -8085.3876401495
```

TeI_3F

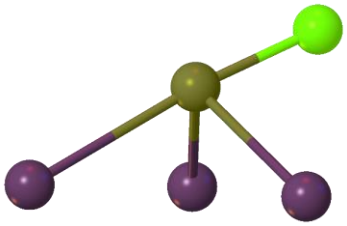

Symmetry: cs
Method: (RIJ)MP2/def2-QZVPP

```
Te          0.53130       -0.47530        0.00000
F           2.02439        0.81193        0.00000
I          -0.40735        0.88268       -2.05984
I          -1.74100       -2.10198        0.00000
I          -0.40735        0.88268        2.05984
SCF energy GEOOPT =  -1256.511764713
MP2 energy =  -1259.4470591743
```

P_3SF (via S)

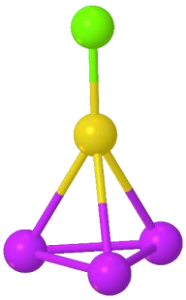

Symmetry: c3v
Method: (RIJ)MP2/def2-QZVPP

```
P          -0.61958        1.07314       -1.13138
P          -0.61958       -1.07314       -1.13138
S          -0.00000        0.00000        0.82794
P           1.23915        0.00000       -1.13138
F           0.00000        0.00000        2.56621
SCF energy GEOOPT =  -1519.240357574
MP2 energy =  -1520.2412320833
```

P_3SF (via P)

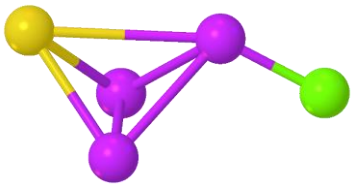

Symmetry: cs
Method: (RIJ)MP2/def2-QZVPP

```
P           0.52160       -0.90473        0.00000
P          -0.53421        0.71091       -1.08689
S           1.03148        1.66214        0.00000
P          -0.53421        0.71091        1.08689
F          -0.48466       -2.17924        0.00000
SCF energy GEOOPT =  -1519.364222372
MP2 energy =  -1520.3047858058
```

P_3SeF (via Se)

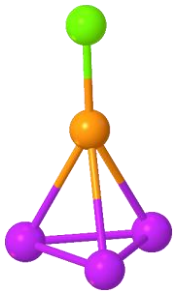

Symmetry: c3v
Method: (RIJ)MP2/def2-QZVPP

P	-0.62186	1.07708	-1.21041
P	-0.62186	-1.07708	-1.21041
Se	-0.00000	0.00000	0.88748
P	1.24371	0.00000	-1.21041
F	0.00000	0.00000	2.74378

SCF energy GEOOPT = -3521.604558461
MP2 energy = -3522.9841975536

P_3SeF (via P)

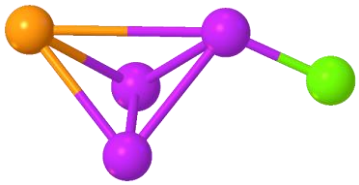

Symmetry: cs
Method: (RIJ)MP2/def2-QZVPP

P	0.51911	-0.91922	0.00000
P	-0.56274	0.67786	-1.09074
Se	1.10634	1.74917	0.00000
P	-0.56274	0.67786	1.09074
F	-0.49996	-2.18568	0.00000

SCF energy GEOOPT = -3521.708616269
MP2 energy = -3523.0346824740

P_3TeF (via Te)

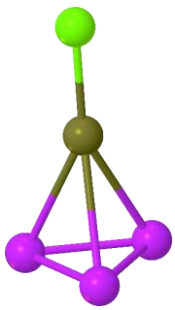

Symmetry: c3v
Method: (RIJ)MP2/def2-QZVPP

P	-0.62533	1.08310	-1.31131
P	-0.62533	-1.08310	-1.31131
Te	-0.00000	0.00000	0.96934
P	1.25066	0.00000	-1.31131
F	0.00000	0.00000	2.96458

SCF energy GEOOPT = -1388.748483864
MP2 energy = -1390.1797269530

P_3TeF (via P)

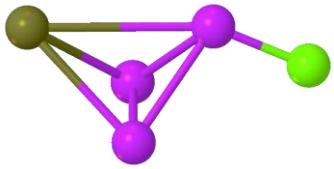

Symmetry: cs
Method: (RIJ)MP2/def2-QZVPP

P	0.50926	-0.93597	0.00000
P	-0.60704	0.63569	-1.09510
Te	1.21581	1.86894	0.00000
P	-0.60704	0.63569	1.09510
F	-0.51100	-2.20435	0.00000

SCF energy GEOOPT = -1388.822205146
MP2 energy = -1390.2040261481

Me_2Se

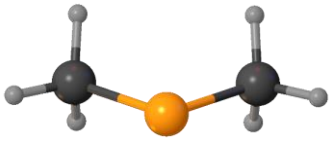

Symmetry: c2v
Method: (RIJ)MP2/def2-QZVPP

Se	0.00000	0.00000	-1.30131
C	0.00000	1.42945	-0.00814
C	0.00000	-1.42945	-0.00814
H	0.00000	-2.36469	-0.55894
H	-0.89130	-1.37472	0.60887
H	0.89130	-1.37472	0.60887
H	0.00000	2.36469	-0.55894
H	0.89130	1.37472	0.60887
H	-0.89130	1.37472	0.60887

SCF energy GEOOPT = -2479.150007494
MP2 energy = -2480.1129483396

$SeMeCl_2^+$

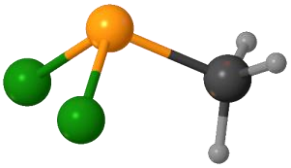

Symmetry: cs
Method: (RIJ)MP2/def2-QZVPP

Se	-1.08512	-0.48871	0.00000
C	0.81274	-0.26526	0.00000
Cl	-1.54712	0.73617	-1.62925
Cl	-1.54712	0.73617	1.62925
H	1.17286	-0.75926	-0.89982
H	1.17286	-0.75926	0.89982
H	1.02091	0.80013	0.00000

SCF energy GEOOPT = -3358.289163782
MP2 energy = -3359.4620268721

$Se(CF_3)_2$

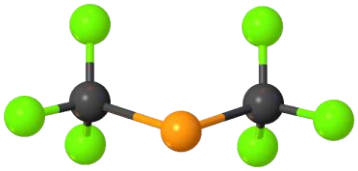

Symmetry: c2v
Method: (RIJ)MP2/def2-QZVPP
Energy =

Se	0.0000000	0.0000000	-1.3468095
C	0.0000000	-1.4503982	-0.0469281
C	0.0000000	1.4503982	-0.0469281
F	1.0731612	-1.4410846	0.7356622
F	0.0000000	-2.5832303	-0.7509916
F	-1.0731612	-1.4410846	0.7356622

```
F     1.0731612    1.4410846    0.7356622
F    -1.0731612    1.4410846    0.7356622
F     0.0000000    2.5832303   -0.7509916
SCF energy GEOOPT =  -3072.569736896
MP2 energy =  -3075.1050476034
```

MeSeCN

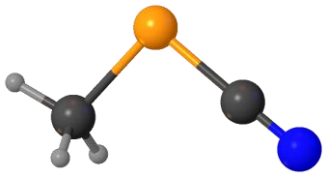

```
Symmetry: cs
Method: /def2-QZVPP

Se         -0.41323       -1.29717        0.00000
C           1.01147        0.01465        0.00000
H           0.94715        0.62044       -0.89502
H           1.93274       -0.55935        0.00000
H           0.94715        0.62044        0.89502
C          -1.77038       -0.08525        0.00000
N          -2.65491        0.68624        0.00000
SCF energy GEOOPT =  -2531.854678147
MP2 energy =  -2532.9790266701
```

H_2Se

```
Symmetry: c2v
Method: (RIJ)MP2/def2-QZVPP

Se          0.00000        0.00000       -0.67652
H           1.03391        0.00000        0.33826
H          -1.03391        0.00000        0.33826
SCF energy GEOOPT =  -2401.052160098
MP2 energy =  -2401.6429487139
```

$SePMe_3$

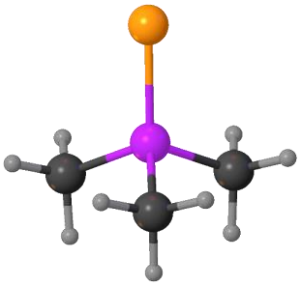

```
Symmetry: c3v
Method: (RIJ)MP2/def2-QZVPP

C    -0.8228295    1.4251825   -0.1679190
P     0.0000000    0.0000000    0.5805672
C    -0.8228295   -1.4251825   -0.1679190
C     1.6456590    0.0000000   -0.1679190
Se    0.0000000    0.0000000    2.6537352
H    -0.7911668   -1.3703411   -1.2549108
H    -1.8550720   -1.4480027    0.1723645
H    -0.3264711   -2.3305408    0.1723645
H    -0.7911668    1.3703411   -1.2549108
H    -0.3264711    2.3305408    0.1723645
H    -1.8550720    1.4480027    0.1723645
H     1.5823336    0.0000000   -1.2549108
H     2.1815431   -0.8825382    0.1723645
H     2.1815431    0.8825382    0.1723645
SCF energy GEOOPT =  -2859.600951659
MP2 energy =  -2860.9170464809
```

$Se(SiH_3)_2$

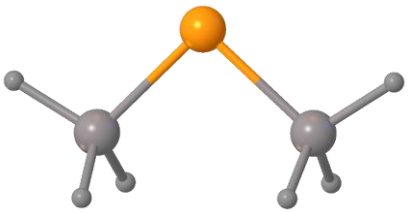

```
Symmetry: c2v
Method: (RIJ)MP2/def2-QZVPP

Se          0.00000        0.00000       -1.57261
Si          0.00000        1.66537       -0.03989
Si          0.00000       -1.66537       -0.03989
H           0.00000       -2.92556       -0.79935
H          -1.19947       -1.58300        0.81277
H           1.19947       -1.58300        0.81277
H           0.00000        2.92556       -0.79935
H           1.19947        1.58300        0.81277
H          -1.19947        1.58300        0.81277
SCF energy GEOOPT =  -2981.335228354
MP2 energy =  -2982.1907236972
```

Me_2Te

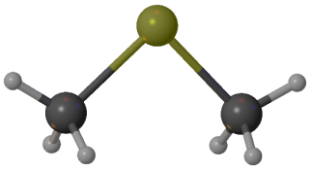

```
Symmetry: c2v
Method: (RIJ)MP2/def2-QZVPP

Te          0.00000        0.00000       -1.45151
C           0.00000        1.53725        0.00641
C           0.00000       -1.53725        0.00641
H           0.00000       -2.48829       -0.51720
H          -0.89215       -1.45970        0.61827
H           0.89215       -1.45970        0.61827
H           0.00000        2.48829       -0.51720
H           0.89215        1.45970        0.61827
H          -0.89215        1.45970        0.61827
SCF energy GEOOPT =  -346.2578073340
MP2 energy =  -347.2726194206
```

$[Te_4]^{2+}$

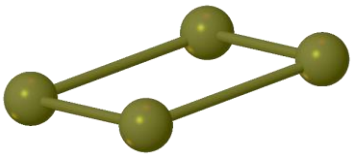

```
Symmetry: d4h
Method: (RIJ)MP2/def2-QZVPP

Te         -1.36499        1.36499        0.00000
Te         -1.36499       -1.36499        0.00000
Te          1.36499       -1.36499        0.00000
Te          1.36499        1.36499        0.00000
SCF energy GEOOPT =  -1068.092609019
MP2 energy =  -1070.5670094398
```

$TePMe_3$

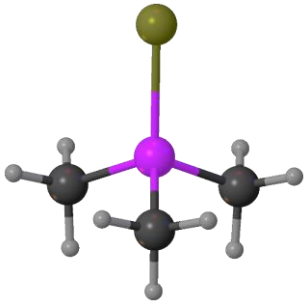

Symmetry: c3v
Method: (RIJ)MP2/def2-QZVPP

C	-0.82306	1.42558	-0.18540
P	0.00000	0.00000	0.56614
C	-0.82306	-1.42558	-0.18540
C	1.64612	0.00000	-0.18540
Te	0.00000	0.00000	2.86309
H	-0.78845	-1.36563	-1.27249
H	-1.85575	-1.44934	0.15326
H	-0.32729	-2.33180	0.15326
H	-0.78845	1.36563	-1.27249
H	-0.32729	2.33180	0.15326
H	-1.85575	1.44934	0.15326
H	1.57690	0.00000	-1.27249
H	2.18304	-0.88246	0.15326
H	2.18304	0.88246	0.15326

SCF energy GEOOPT = -726.7071294447
MP2 energy = -728.0734716541

S_2Cl_2

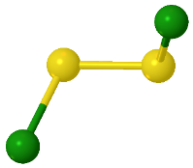

Symmetry: c2
Method: (RIJ)MP2/def2-QZVPP

S	-0.81805	-0.52299	-0.71842
S	0.81805	0.52299	-0.71842
Cl	-0.62072	-1.96494	0.71842
Cl	0.62072	1.96494	0.71842

SCF energy GEOOPT = -1714.143827253
MP2 energy = -1714.9424733878

Se_2Cl_2

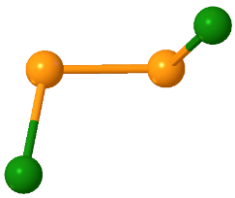

Symmetry: c2
Method: (RIJ)MP2/def2-QZVPP

Se	-0.94280	-0.58338	-0.76409
Se	0.94280	0.58338	-0.76409
Cl	-0.65261	-2.08667	0.76409
Cl	0.65261	2.08667	0.76409

SCF energy GEOOPT = -5718.850709283
MP2 energy = -5720.4105670680

Te_2Cl_2

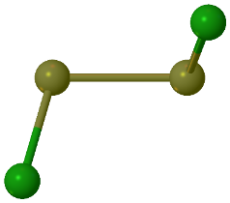

Symmetry: c2
Method: (RIJ)MP2/def2-QZVPP

Te	-1.09853	-0.67491	-0.81994
Te	1.09853	0.67491	-0.81994
Cl	-0.71070	-2.29274	0.81994
Cl	0.71070	2.29274	0.81994

SCF energy GEOOPT = -1453.121652427
MP2 energy = -1454.7785110059

$[P_5Cl_2]^+$

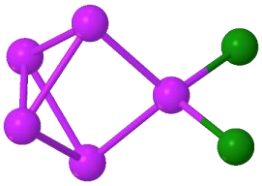

Symmetry: c2v
Method: (RIJ)MP2/def2-QZVPP

P	0.00000	-1.56593	0.63671
P	1.10005	0.00000	1.81483
P	-1.10005	0.00000	1.81483
P	0.00000	1.56593	0.63671
P	0.00000	0.00000	-0.82321
Cl	-1.56134	0.00000	-2.03994
Cl	1.56134	0.00000	-2.03994

SCF energy GEOOPT = -2622.664846296
MP2 energy = -2623.8698308909

$[P_3Se_4]^+$

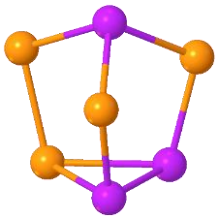

Symmetry: cs
Method: (rij)b-p/def2-TZVPP

Se	0.95278	-0.74219	-1.78153
Se	-2.02771	-0.85849	0.00000
P	0.01379	-1.83351	0.00000
Se	0.95278	-0.74219	1.78153
Se	-1.39215	1.42571	0.00000
P	0.75026	1.37533	1.12480
P	0.75026	1.37533	-1.12480

SCF energy GEOOPT = -10631.50269417

References to the Supporting Information

References

1 P. Weis, H. Scherer and I. Krossing, *Z. Anorg. Allg. Chem.*, 2019, **645**, 64.

2 T. A. Engesser, P. Hrobárik, N. Trapp, P. Eiden, H. Scherer, M. Kaupp and I. Krossing, *ChemPlusChem*, 2012, **77**, 643.

3 M. Gonsior, I. Krossing and N. Mitzel, *Z. anorg. allg. Chem.*, 2002, **628**, 1821.

4 G. R. Fulmer, A. J. M. Miller, N. H. Sherden, H. E. Gottlieb, A. Nudelman, B. M. Stoltz, J. E. Bercaw and K. I. Goldberg, *Organometallics*, 2010, **29**, 2176.

5 R. K. Harris, E. D. Becker, S. M. Cabral de Menezes, R. Goodfellow and P. Granger, *Pure Appl. Chem.*, 2001, **73**, 1795.

6 G. M. Sheldrick, *Acta Crystallogr., Sect. A: Found. Crystallogr.*, 2015, **71**, 3.

7 G. M. Sheldrick, *Acta Crystallogr., Sect. C: Cryst. Struct. Commun.*, 2015, **71**, 3.

8 C. B. Hübschle, G. M. Sheldrick and B. Dittrich, *J. Appl. Crystallogr.*, 2011, **44**, 1281.

9 a) D. Kratzert, J. J. Holstein and I. Krossing, *J. Appl. Crystallogr.*, 2015, **48**, 933; b) D. Kratzert and I. Krossing, *J. Appl. Crystallogr.*, 2018, **51**, 928;

10 L. J. Bourhis, O. V. Dolomanov, R. J. Gildea, J. A. K. Howard and H. Puschmann, *Acta Crystallogr., Sect. A: Found. Crystallogr.*, 2015, **71**, 59.

11 a) R. Ahlrichs, M. Bär, M. Häser, H. Horn and C. Kölmel, *Chem. Phys. Lett.*, 1989, **162**, 165; b) O. Treutler and R. Ahlrichs, *J. Chem. Phys.*, 1995, **102**, 346;

12 a) F. Neese, *WIREs Comput Mol Sci*, 2012, **2**, 73; b) F. Neese, *WIREs Comput Mol Sci*, 2018, **8**, e1327;

13 a) A. D. Becke, *J. Chem. Phys.*, 1993, **98**, 5648; b) C. Lee, W. Yang and R. G. Parr, *Phys. Rev. B*, 1988, **37**, 785; c) S. H. Vosko, L. Wilk and M. Nusair, *Can. J. Phys.*, 1980, **58**, 1200; d) P. J. Stephens, F. J. Devlin, C. F. Chabalowski and M. J. Frisch, *J. Phys. Chem.*, 1994, **98**, 11623;

14 a) R. Ahlrichs, *PCCP*, 2004, **6**, 5119; b) M. Sierka, A. Hogekamp and R. Ahlrichs, *J. Chem. Phys.*, 2003, **118**, 9136;

15 a) F. Weigend and R. Ahlrichs, *PCCP*, 2005, **7**, 3297; b) F. Weigend, *PCCP*, 2006, **8**, 1057;

16 A. Hellweg, C. Hättig, S. Höfener and W. Klopper, *Theor. Chem. Acc.*, 2007, **117**, 587.

17 a) P. Deglmann and F. Furche, *J. Chem. Phys.*, 2002, **117**, 9535; b) P. Deglmann, F. Furche and R. Ahlrichs, *Chem. Phys. Lett.*, 2002, **362**, 511; c) P. Deglmann, K. May, F. Furche and R. Ahlrichs, *Chem. Phys. Lett.*, 2004, **384**, 103;

18 A. Klamt and G. Schüürmann, *J. Chem. Soc., Perkin Trans. 2*, 1993, 799.

19 D. R. Lide, *CRC Handbook of Chemistry and Physics*, Taylor and Francis Group LLC, 87th edn., 2007.

20 A. E. Reed, R. B. Weinstock and F. Weinhold, *J. Chem. Phys.*, 1985, **83**, 735.

21 C. Ehrhardt and R. Ahlrichs, *Theoret. Chim. Acta*, 1985, **68**, 231.

22 R. F. W. Bader, *Acc. Chem. Res.*, 1985, **18**, 9.

23 M. Head-Gordon, J. A. Pople and M. J. Frisch, *Chem. Phys. Lett.*, 1988, **153**, 503.

24 a) F. Weigend, *Phys. Chem. Chem. Phys.*, 2006, **8**, 1057; b) F. Weigend and R. Ahlrichs, *Phys. Chem. Chem. Phys.*, 2005, **7**, 3297;

25 a) T. H. Dunning, *J. Chem. Phys.*, 1989, **90**, 1007; b) R. A. Kendall, T. H. Dunning and R. J. Harrison, *J. Chem. Phys.*, 1992, **96**, 6796; c) K. A. Peterson, D. E. Woon and T. H. Dunning, *J. Chem. Phys.*, 1994, **100**, 7410; d) A. K. Wilson, T. van Mourik and T. H. Dunning, *J. Mol. Struc. - THEOCHEM*, 1996, **388**, 339; e) D. E. Woon and T. H. Dunning, *J. Chem. Phys.*, 1993, **98**, 1358;

26 a) F. Weigend, A. Köhn and C. Hättig, *J. Chem. Phys.*, 2002, **116**, 3175; b) C. Hättig, *Phys. Chem. Chem. Phys.*, 2005, **7**, 59;

27 K. A. Peterson, *J. Chem. Phys.*, 2003, **119**, 11099.

28 C. Hättig, G. Schmitz and J. Kossmann, *PCCP*, 2012, **14**, 6549.

29 A. J. Austin, M. J. Frisch, J. A. Montgomery and G. A. Petersson, *Theor. Chem. Acc.*, 2002, **107**, 180.

30 T. Lu and F. Chen, *J. Comput. Chem.*, 2012, **33**, 580.

31 K. Wolinski, J. F. Hinton and P. Pulay, *J. Am. Chem. Soc.*, 1990, **112**, 8251.

32 a) T. Nakajima and K. Hirao, *Chem. Rev.*, 2012, **112**, 385; b) M. Reiher and A. Wolf, *J. Chem. Phys.*, 2004, **121**, 2037;

33 a) W. A. de Jong, R. J. Harrison and D. A. Dixon, *J. Chem. Phys.*, 2001, **114**, 48; b) D. H. Bross and K. A. Peterson, *Theoret. Chim. Acta*, 2013, **133**, 1434;

34 A. Martens, P. Weis, M. C. Krummer, M. Kreuzer, A. Meierhöfer, S. C. Meier, J. Bohnenberger, H. Scherer, I. Riddlestone and I. Krossing, *Chem. Sci.*, 2018, **45**, 789.

35 W. Sawodny and K. Dehnicke, *Z. Anorg. Allg. Chem.*, 1967, **349**, 169.

36 C.-W. Hsu, Y.-C. Tsai, B. M. Cossairt, C. Camp, J. Arnold and C. C. Cummins, in *Inorganic syntheses*. *Volume 37*, ed. P. P. Power, John Wiley and Sons Inc, Hoboken, NJ, 2018, vol. 49, pp. 123–134.

37 B. M. Cossairt, M.-C. Diawara and C. C. Cummins, *Science*, 2009, **323**, 602.

38 S. G. Frankiss, *J. Mol. Struct.*, 1968, **2**, 271.

39 A. Bihlmeier, M. Gonsior, I. Raabe, N. Trapp and I. Krossing, *Chem. Eur. J.*, 2004, **10**, 5041.

40 A. Wiesner, S. Steinhauer, H. Beckers, C. Müller and S. Riedel, *Chem. Sci.*, 2018, **9**, 7169.

41 a) I. Krossing and L. van Wüllen, *Chem. Eur. J.*, 2002, **8**, 700; b) I. Krossing, *J. Am. Chem. Soc.*, 2001, **123**, 4603; c) L. C. Forfar, T. J. Clark, M. Green, S. M. Mansell, C. A. Russell, R. A.

Sanguramath and J. M. Slattery, *Chem. Commun.*, 2012, **48**, 1970; d) G. Santiso-Quiñones, A. Reisinger, J. Slattery and I. Krossing, *Chem. Commun.*, 2007, 5046;

42 H. Duddeck, in *eMagRes*, ed. R. K. Harris, Wiley, S.l., 2007, vol. 19, p. 1.